

Comparative analysis of worker head anatomy of *Formica* and *Brachyponera* (Hymenoptera: Formicidae)

ADRIAN RICHTER^{1,2,*}, FRANCISCO HITA GARCIA², ROBERTO A. KELLER^{2,3},
JOHAN BILLEN⁴, EVAN P. ECONOMO^{2,#} & ROLF GEORG BEUTEL^{1,#}

¹ Institut für Zoologie and Evolutionsforschung, FSU Jena, 07743 Jena, Germany; Adrian Richter [adrian.richter@uni-jena.de]; Rolf Georg Beutel [rolf.beutel@uni-jena.de] — ² Biodiversity and Biocomplexity Unit, Okinawa Institute of Science and Technology Graduate University, Onna-son, Okinawa, 904-0495, Japan; Francisco Hita Garcia [fhitagarcia@gmail.com]; Evan P. Economo [evaneconomo@gmail.com] — ³ Museu Nacional de Historia Natural e da Ciência and Centre for Ecology, Evolution and Environmental Changes, Universidade de Lisboa, 1749-016 Lisbon, Portugal; Roberto A. Keller [roberto.kellerperez@gmail.com] — ⁴ Ecological Networks, Zoological Institute KU Leuven, 3000 Leuven, Belgium; Johan Billen [johan.billen@kuleuven.be] — * Corresponding author; # joint supervision

Accepted on May 8, 2020.

Published online at www.senckenberg.de/arthropod-systematics on May 26, 2020.

Editor in charge: Klaus-Dieter Klass

Abstract. An organism's morphology plays a crucial role in its interactions with its environment. Therefore, comparative anatomical analysis is a critical basis to understanding the ecology, behavior, and evolution. While our knowledge of ant internal anatomy has considerably improved in recent years, it is still highly fragmentary, and many evolutionary questions remain unsolved. The current work is a contribution of a series of studies with the larger goal to increase our knowledge of ant head morphology and reconstruct the evolution of this tagma across the ant phylogeny. We investigated the head anatomy of “generalized” ant species from phylogenetically distant clades to establish a very solid basis for future works on the formicid head and its transformations. To achieve a multifaceted documentation, we used a broad array of techniques, including microphotography, scanning electron microscopy, μ CT-scan based 3D-reconstructions, and histological sections. This enabled us to show many anatomical features in unprecedented clarity and detail. Our results outline considerable conservation of the main structural features across the ant tree of life, but they also reveal many details that could prove phylogenetically informative and/or functionally important. The cephalic digestive tract with its sclerotization, associated musculature, and glands is more diverse than previously reported. More work will be necessary to clarify the functional and systematic significance of the observed differences. The cephalic endoskeleton, especially the tentorium and torular apodeme, is identified as a second structural complex of high potential. This previously neglected character system is apparently functionally important and very likely phylogenetically informative. Our results improve the basis for reconstructing the groundplan of the formicid head and evolutionary transformations in the stem group and crown group. Future studies focusing on functional aspects and evolutionary changes of different elements of the head will help to create a complete picture of the evolution of this highly successful group of insects.

Key words. Ants, head, anatomy, skeletomusculatur system, 3D-reconstruction, μ CT-scan, homology.

1. Introduction

Formicidae is one of the most dominant groups of insects in nearly all terrestrial ecosystems outside polar regions (e.g. LACH et al. 2010). Like other organisms, ants interact with their environment using morphological structures such as mouthparts or locomotor organs. Consequently, comprehensive knowledge of structure and function of the body parts of extant and extinct species is necessary to understand their success and the evolution on the phenotypic level. With the ant phylogeny resolving in ever-

increasing accuracy and resolution (e.g. BRANSTETTER et al. 2017; BOROWIEC et al. 2019), we have a basis to understand how the ant phenotype arose and was successively remodeled and diversified over time.

The current study presents a comparative analysis of head structures among two major subfamilies, extending a previous analysis of the cephalic morphology of workers from the subfamily Myrmicinae (RICHTER et al. 2019). These, combined with forthcoming studies on other sub-

families, will form a basis for a broad analysis of how the anatomy of the ant head has evolved across the phylogeny, facilitating or at least accompanying the stunning diversification of ant morphology, ecology, and behavior. As the head is the body region where sensory (acquisition, processing) and feeding functions are concentrated, it plays a central role in the way insects interact with their environment. Its morphology is apparently linked with the particular ecology and behavior displayed by the organism.

The external morphology of ants has been well studied within the framework of phylogenetic and taxonomic studies (e.g. BARONI URBANI et al. 1992; BOLTON 2003; KELLER 2011). However, with the exception of specific structures such as the glandular system (e.g. BILLEN 1993; BILLEN et al. 2013; BILLEN & AL-KHALIFA 2015; 2016), the richness of internal character systems remains to be evaluated in a phylogenetic context. Key aspects of internal ant morphology such as the head musculature, its endoskeleton, and the cephalic digestive tract have never been studied in detail and only documented for very few species (e.g. JANET 1923; LILICO-OUACHOUR et al. 2018), making it presently impossible to evaluate them in the context of the phylogeny of Formicidae, thus preventing the development of meaningful hypotheses on their evolution. The first complete description of the head of a formicid species with modern methods was done by RICHTER et al. (2019) for *Wasmannia affinis* Santschi, 1929 (Myrmicinae), revealing many novel aspects of ant anatomy including a modified dorsal mandibular articulation (secondary mandibular joint with respect to the groundplan of ectognathous insects), and the presence of a previously undescribed prepharyngeal muscle originating on a torular apodeme. That study also raised questions about the evolution of structures that have only rarely been documented in the literature, such as the cephalic digestive tract and cranial endoskeleton (see for instance KUBOTA et al. 2019 and YAMADA et al. 2020 on the tentorium). Our ultimate goal is thus to provide a detailed and systematic documentation of external and internal head structures across the whole family, incorporating most lineages and several representatives for larger clades to achieve a solid assessment of the character evolution based on current phylogenetic hypotheses.

The present work represents a further step towards this goal, documenting the cephalic anatomy of *Formica rufa* Linnaeus, 1761 (type species of Formicidae, Formicinae), and *Brachyponera luteipes* (Mayr, 1862) (Ponerinae). *Formica rufa* feeds mainly on honeydew of plant sucking arthropods and additionally uses species of different arthropod groups as prey (e.g. DOMISCH et al. 2009). In contrast, *Brachyponera luteipes* is primarily predacious, like most members of the subfamily Ponerinae (SCHMIDT & SHATTUCK 2014) but relies on seeds as additional food source (ZHOU et al. 2007). We also included in our anatomical investigation the closely related *Brachyponera chinensis* (EMERY 1895), an invasive species in North America from its native Asian range (GUÉNARD & DUNN 2010), which accepts a diverse array of different food

substrates, including sugar and lipids (Mo 2013). Both species are rather “generalized” forms, thus serving as good representatives of the two major ant clades formicoids and poneroids (informal ending -oid does not imply superfamily rank in studies on ants), an appropriate starting point to investigate the diversity of anatomical structures in ants as a whole. We chose generalized species to get an initial idea of the anatomical diversity across the ant phylogenetic tree, and to assess which structures may contain phylogenetic signal or may be of interest from a functional perspective, and thus provide new insights in the evolution of ants. While comparing the observed structures and discussing potential phylogenetic and functional implications, another aim is to provide the groundwork for the clarification of persisting homology problems. Well-established homology hypotheses are crucial for understanding the evolution on the phenotypic level of any group of organisms. However, this aspect has been rather neglected in ant morphology and taxonomy in recent decades, with few exceptions, such as Keller’s morphology-based phylogeny of ants (KELLER 2011), the detailed treatment of male genitalia by BOUDINOT (2013), or RICHTER et al. (2019) addressing the homology of sections of the cephalic digestive tract for the first time. Related to the problem of homology is the use of a consistent, ontologized terminology as the basis for comparative morphological work, as recently discussed by SILVA & FEITOSA (2019). Even though progress has been made, many issues of homology and terminology persist.

2. Material and methods

2.1. Material

Adult workers of *Formica rufa*, *Brachyponera chinensis*, and *Brachyponera luteipes* were used in this study. *Formica rufa* shows a slight worker size polymorphism that does not affect our qualitative anatomical results. We used workers with a head width (measured as maximum head width in full face view) ranging from ca. 1.2 mm to ca. 2.2 mm. *Brachyponera luteipes* workers are monomorphic with a representative head width of ca. 0.79–0.81 mm (n=3). For CT scanning specimens from the collection of OIST were chosen. The specimens of *F. rufa* with the CASENT numbers 0790267 and 0709411 were used, and of *B. luteipes* the individuals with the CASENT numbers 0709409 and 0709409. The specimens used for histological sectioning were collected in Belgium (*F. rufa*) and Taiwan (*B. chinensis* and *luteipes*). For the SEM images, specimens of *F. rufa* collected in Belgium and *B. luteipes* collected in Japan (Okinawa) were used.

2.2. Scanning electron microscopy

Workers of *F. rufa* were fixed in 70% ethanol. The head of several specimens was severed and after removal of

the antennae with forceps macerated in 10% KOH overnight. Afterwards, the maxillolabial complex was either already in an extended position, or extended by slight pressure onto the head. The mouthparts of some heads were dissected using Dumont forceps and minute needles attached to a hobby knife handle. All samples were transferred to 100% ethanol (70, 80, 90, 95, 100%) and dried at the critical point in liquid CO₂ with an Emitech K 850 Critical Point Dryer (Sample Preparation Division, Quorum Technologies Ltd., Ashford, England). The samples were glued on the tip of minute needles and sputter coated with gold using an Emitech K 500 (Sample Preparation Division, Quorum Technologies Ltd., Ashford, England). Using a rotatable specimen holder (POHL 2010), SEM micrographs were taken with a Philips ESEM XL30 (Philips, Amsterdam, Netherlands) equipped with Scandium FIVE software (Olympus, Münster, Germany).

Workers of *B. luteipes* with an extended maxillolabial complex were killed and fixed in 70% ethanol. The head of one specimen was slightly compressed with forceps to fully inflate the glossa (see Fig. 8). The elastic cuticle of the head was not damaged in this process. The head of several specimens was severed with Dumont No. 5 forceps and the antennae removed. Some of the heads were immersed in 10% KOH solution and macerated for six hours at room temperature. They were then washed in water twice for five minutes and subsequently transferred to 70% ethanol. The mouthparts were removed using Dumont forceps and minute needles attached to a hobby knife handle. All samples of *B. luteipes* (removed mouthparts, entire heads, heads without mouthparts, and heads without antennae) were dehydrated in a graded ethanol series (70, 80, 90, 95, 100%) and subsequently transferred to t-butyl (2 × for 10 minutes). In t-butyl, the samples were put into a Hitachi ES-2030 freeze dryer (Hitachi, Chiyoda, Japan) and vacuum dried overnight. The samples were then glued onto SEM stubs with double-sided adhesive tape, employing a dog hair glued to a glass pipette to manipulate and clean them. Samples were sputter coated with gold (Model: VE3030CVD of the OIST imaging section). SEM images were taken with a JEOL JSM-7900F (JEOL Ltd, Tokyo, Japan), using the manufacturer software. Two heads of *B. luteipes* without antennae and a few dissected mouthparts of this species were glued on minute needles and documented as described above for *Formica*.

2.3. Photomicrography

Before heads of *F. rufa* and *B. luteipes* were sputter coated with gold as described above, photos were taken with a Canon EOS 7 D Mark II equipped with a Canon MP-E65 macro lens, in combination with an adjustable extension bellows. The samples were illuminated by two flashes through a transparent plastic cylinder for soft light. Zerene Stacker (Zerene Systems LLC, Richland, USA) was used to combine image stacks with a different focus.

2.4. Histological section series

The heads were removed from the body with a transverse cut behind the compound eyes, thus creating a large posterior opening for the penetration of chemicals used during tissue processing. The heads were fixed in 2% cold glutaraldehyde in a buffer of 50 mM Na-cacodylate and 150 mM saccharose. Postfixation took place in 2% osmium tetroxide in the same buffer, and was followed by dehydration in a graded acetone series. Tissues were embedded in Araldite® and sectioned with a Leica EM UC6 ultramicrotome (Wetzlar, Germany). Transverse, longitudinal, and frontal serial semithin sections were made for both species with a thickness of 1 µm. A 0.1% solution of methylene blue and thionin was used for staining. Sections were viewed under an Olympus BX-51 microscope (Tokyo, Japan), equipped with an Olympus Camedia C-3040 Zoom digital camera (Tokyo, Japan). Pictures were taken at 10 µm intervals employing a 10 × objective and used for anatomical comparisons and descriptions. Some additional images of anatomical details were taken with a 40 × objective. Selected section images were mounted as image plates as described below.

2.5. Micro-computed tomography scanning

µCT-scanning was performed using a Zeiss Xradia 510 Versa 3D X-ray microscope operated with the Zeiss Scout-and-Scan Control System software (version 11.1.6411.17883) at the Okinawa Institute of Science and Technology Graduate University, Japan. Specimens fixed in 100% ethanol were immersed in a 2 M iodine solution for four days, except for one specimen of *F. rufa* (CASENT0709411) which was accidentally kept in the solution for several months. All specimens were washed in 100% ethanol for one hour before mounting them within a sealed pipette tip of appropriate size. 1601 projection images were taken for a full 360° rotation. Scan settings were selected in order to yield optimum scan quality. Specimens of *B. luteipes* were scanned at 40 kv and 3 W and voxel sizes of 1,1557 µm³ (CASENT0709409) and 1,2244 µm³ (CASENT0709419) were achieved. Specimens of *F. rufa* were scanned with the same energy values, and voxel sizes of 2,5527 µm³ (CASENT0709411) and 2,8337 µm³ (CASENT0790267) were achieved. 3D reconstructions of the resulting scan projection data were done with the Zeiss Scout-and-Scan Control System Reconstructor (version 11.1.6411.17883) and saved in DICOM file format.

2.6. 3D modelling and volume calculation

Scans of CASENT0790267 (*F. rufa*) and CASENT0709409 (*B. luteipes*) were segmented. As the *F. rufa* individual showed an abnormal muscle in the region of the mandibular musculature (see Results section), the mandibles and associated structures were also segmented for the

scan of CASENT0709411 (*F. rufa*). Segmentation was performed in Amira 6.5 (Visage Imaging GmbH, Berlin, Germany). Large structures (cuticle, mandibles, brain, large muscles, pharyngeal gland) were pre-segmented by manually segmenting every 30th slice, and subsequently semiautomatically segmented using the online application biomedisa (LÖSEL & HEUVELINE 2016) and the watershed function of Amira. The resulting segmentations were compared to assess the anatomical accuracy. The ones with less spilling of segmented materials into wrong structures were selected for post-processing (biomedisa for CASENT0709409 and CASENT0709411, watershed for CASENT0790267) and then cleaned up and completed by adding the remaining structures with the interpolation function of amira. Finally, segmented materials were exported with the plugin script “multiExport” (ENGELKES et al. 2018) in Amira 6.2 as Tiff image stacks. The image series were then imported in VG-Studio 3.2.5 (Volume Graphics GmbH, Heidelberg, Germany) to create volume renders (Phong) of individual structures. To calculate the volumina of different structures, a label analysis was run in Amira. To obtain the volume of the head capsule, it was labelled as one material. As the antennae were not completely present on the scans, only the scape was labelled. The volumes of individual materials from the label analysis were divided by the head volume in Microsoft Excel (2016) to assess the percentage of the volume compared to the entire head. It is important to note that only one specimen per species was investigated in this way. Only selected values are reported within the manuscript, but the whole table of volume measurements is available in the supplementary material (File 2).

2.7. Data availability

The μ CT scans used in this study are available at the online repository Zenodo as DICOM files under the DOI 10.5281/zenodo.3786977. Additionally, videos of 3D-volume renders of all the main anatomical structures are available there.

2.8. Image processing

Image plates were arranged in Adobe Photoshop® CS6 (Adobe System Incorporated, San Jose, USA). All images were subjected to limited levels adjustment and smart sharpen (30%). Labels for the image plates were created in Adobe Illustrator® CS6 (Adobe Systems Incorporated, San Jose, USA).

2.9. Terminology

The terminology largely follows RICHTER et al. (2019), but several adjustments were made. We recognize the increasing demand for morphological data, which are

computer-parsable and suitable for automated computation (see e.g. VOGT 2019). Even though it would not be possible to present our descriptions as “knowledge graph” without losing a lot of detailed information, we follow the suggestion of this author to link the used terms to the Hymenoptera Anatomy Ontology (HAO, YODER et al. 2010) wherever possible. This revealed many gaps in HAO concerning structures in ant morphology, without an established general designation. It is also apparent that some of the current definitions in HAO are not perfectly applicable to ants, for example if structures used in the definition are missing or the positional relationships are different. However, in many cases older alternative definitions, also deposited in HAO, reflect the meaning of the terms better when applied to Formicidae, making an assignment of HAO terms possible. For the musculature we do not use HAO terms, but instead follow the nomenclatures of v. KÉLER (1963) and WIPFLER et al. (2011), which are commonly used in entomology, and were also previously applied to ants (RICHTER et al. 2019) and other groups of Hymenoptera (e.g. ZIMMERMANN & VILHELMSSEN 2016). As separate regions of the head capsule, e.g. “frons”, “vertex” etc., are not separated by any sutures or other unambiguous markings, we refer to them instead as “frontal region”, “vertexal region” etc.

As indicated in RICHTER et al. (2019), M. 41a (0hy1a) (described for the first time by the authors) is reinterpreted as M. 47 / 0hy2 (v. KÉLER 1963; WIPFLER et al. 2011). The terminology of the processes/arms of the sitophore plate has been rather inconsistent in previous publications and no label exists for them in the HAO yet. Therefore, they will consistently be designated as “oral arms” following ZIMMERMANN & VILHELMSSEN (2016). “Torular apodeme” is introduced as a term to describe the “phragma of the antennal acetabulum” of RICHTER et al. (2019). The term torulus is used here as encompassing the whole sclerite forming the antennal insertion, including the acetabulum, external torular rims/lobes as well as the internal torular apodeme, following KELLER (2011).

We introduce here the term “atala” (plural, “atalae”) (áh-tah-lah, from the Arabic عتلة for crowbar) for the prominent process on the lateral side of the mandibular base between the dorsal and ventral articulations of the mandible. This process receives the tendon of the abductor muscle, and the distance of its tip from the axis of mandibular rotation mechanically facilitates the opening of the mandibles, comparable with the use of a crowbar, providing an elongated lever arm for improved force transduction. A mandibular atala is universally present across all ants. Previous names for this structure include abductor apodeme (KELLER 2011), abductor swelling (RICHTER et al. 2019), and lateral articular process of the mandible (SILVA & FEITOSA 2019). We prefer our new term because this structure is obviously of high functional (biomechanics of the abductor) and phylogenetic importance (with considerable variation in aculeate Hymenoptera, Keller unpubl. data), which justifies a specific term, instead of an ambiguous (abductor apodeme) or composite one.

3. Results

A full description is provided for each of the documented cephalic elements of *Formica rufa*, whereas the treatment of head structures of *Brachyponera luteipes* focuses on the differences. When structures are not mentioned explicitly, it is implied that they are very similar to what was described for *Formica*. A table summarizing structural congruities and differences between the two genera is presented in Supplementary File 3. The structural differences between the examined *Brachyponera luteipes* and *B. chinensis* are negligible.

3.1. Head capsule

Formica rufa

The prognathous head (HAO_0000397) (moderately declined in working posture, i.e. subprognathous in general insect terminology; e.g. BEUTEL et al. 2014) of workers is rectangular with rounded corners, appearing almost cubic in dorsal and ventral view (Figs. 1A,C, 2A,C) (heads of smaller specimens are slightly less wide anteriorly and more rounded) (Figs. 1A, 2A); it reaches its maximum width immediately behind the eyes (**ce**, Figs. 1B, 2B) (HAO_0000217); in lateral view it appears oval with a slightly flattened ventral side. The cervical articulation between the prothorax (HAO_0000874) and the margin of the posteroventrally located occipital foramen (HAO_0000347) is narrow; the area immediately surrounding it is countersunk into a concavity of the occipital region (HAO_0000658) (Figs. 1C, 2C); the strongly sclerotized postocciput (HAO_0000790) forms a collar-like enclosure of the foramen, which appears hourglass-shaped due to the presence of mesally directed postoccipital condyles (HAO_0000654). The fissure-shaped posterior tentorial pits (HAO_0000768) are visible at the lateral edge of the postocciput (**ptp**, Fig. 2C). The postgenal bridge (HAO_0000777) is extensive and each side of it is slightly convex (**pgb**, Figs. 1C, 2C); the internal postgenal ridge (HAO_0001104) is externally marked by a thin sulcus (**pgr**, Figs. 1C, 2C). The large clypeus (HAO_0000212) appears roughly diamond-shaped in dorsal view; its main middle portion is slightly raised above the surrounding areas, together with the anterior frontal region between the antennae (**cl**, Figs. 1A,B, 2A,B); its anterior margin is strongly inflected (**cli**, Fig. 5B) and the inflected portion is thickened. The epistomal sulcus (**es**, Figs. 1A, 2A) (HAO_0000306) runs from the dorsal mandibular articulation (**dma**, Figs. 1B, 2B) diagonally to the anterior tentorial pits (HAO_0000126) (**atp**, Figs. 1A, 2A), from where it forms an arch in front of the antennal articulations; from the posterior, almost straight portion at the level of the scapal base, a pair of diagonal lines run posteromesad, forming a triangular supra-clypeal area (HAO_0001821) (**sca**, Figs. 1A, 2A) with different cuticular sculpture; from the top corner of the triangle a thin frontal line is marked by a smoother

surface sculpture compared to the surrounding cuticle (**fl**, Figs. 1A, 2A). The frontal carinae (HAO_0001533) are short and do not form distinct “frontal lobes” (**frc**, Figs. 1A,B, 2A,B); the toruli, which are thus uncovered dorsally, face dorsolaterad due to the raised frontal region between them and have a relatively simple circular rim (HAO_0000103) (**to**, Figs. 1A,B, 2A,B); a small lobe emerges from the median arch but does not cover the bulb of the scape (**tol**, Fig. 3F). The compound eyes are well-developed (565 ommatidia in the smallest investigated worker), oval and located dorsolaterally on the posterior portion of the head. Additionally, three small ocelli (HAO_0000661) (**oc**, Figs. 1A, 2A) are located in shallow depressions on the vertexal region (HAO_0001077). The ventrally visible hypostoma (HAO_0000411) is the hypostomal carina (HAO_0000413) (**hysc**, Figs. 1C, 2C, 11A); it has a median indentation and a lateral inward twist (Fig. 11A); together with the main part of the hypostoma it forms the deep hypostomal cavity (HAO_0001316) (**hyc**, Fig. 11A), which contains the base of the maxillolabial complex; the hypostoma forms large triangular processes projecting into the oral foramen (**hysp**, Fig. 11A); the concave anterior surface of the processes (*, Fig. 11A) receives the lateral margin of the stipes (HAO_0000958), whereas their lateral margin encloses the mandibles (HAO_0000506) on the mesal side; a much smaller additional rounded projection (**white arrowhead**, Fig. 11A) is present mesad the socket (pleurostomal fossa HAO_0000732) (**vma**, Fig. 11A) that receives the ventral mandibular condyle (HAO_0000508); this rounded projection fits into a depression of the closed mandible (*, Fig. 4B). The cuticle is largely smooth, with a fine reticular microstructure and a short pubescence.

Brachyponera luteipes

The head is rectangular with rounded corners and distinctly longer than broad in dorsal view; the maximum width is reached in the middle region; in profile it appears also roughly rectangular but wedge-shaped anteriorly (Figs. 1D–F, 2D–F). The occipital region appears concave in ventral view; the occipital foramen is located further posterior and is narrower than in *Formica*; the concave area around it is more extended; a low carina delimits it along its dorsal edge (occipital carina HAO_0000653) (**oca**, Figs. 1F, 2F); the carina is almost completely flattened laterad the occipital region but continues into short distinct diagonal portions ventrally (**white arrowhead**, Figs. 1F, 2F). The postgenal bridge is raised in the middle region rather than depressed (**pgb**, Figs. 1F, 2F); the postgenal ridge is not externally marked by a different cuticular structure or a sulcus. The clypeus is posteriorly narrowed by the anteromesally shifted antennal insertions (**cl**, Figs. 1D,E, 2D,E); the area laterad the anterior tentorial pits is similarly shaped as in *Formica*, whereas rounded concavities for the antennal insertions are present mesad of them; the posterior median clypeal portion extends between the antennal insertions as a long, thin strip (**mcl**, Figs. 1A, 2A); it bears a mesal carina directly between the antennal sockets; the mesal clypeal

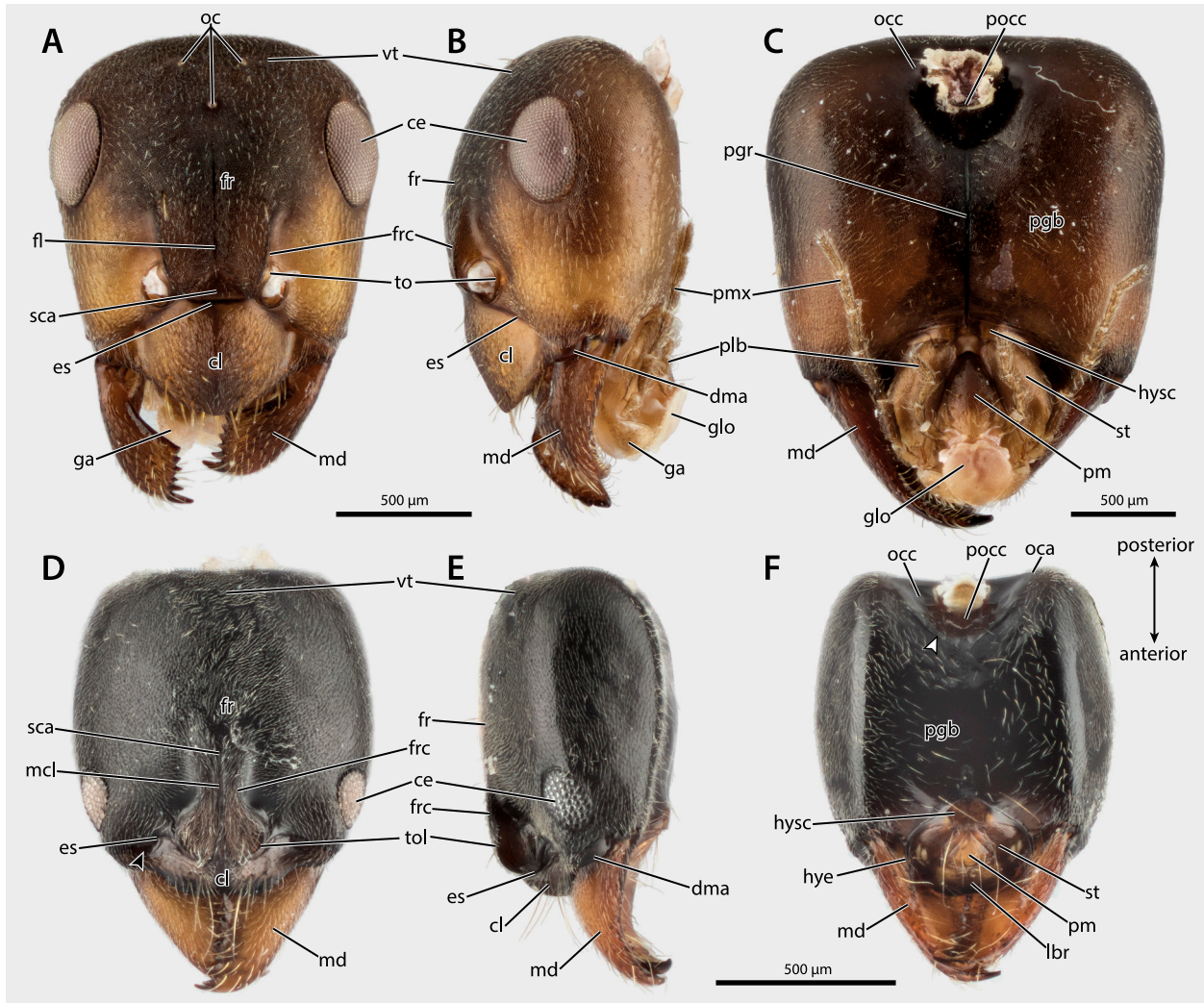


Fig. 1. Photomicrographs of heads of *Formica rufa* (A–C) and *Brachyponera luteipes* (D–F). Note the slight difference in shape between a small (A,B) and a larger head (C). A,D: Dorsal view. B,E: Lateral view. C,F: Ventral view. — **Abbreviations:** ce – compound eye; cl – clypeus; dma – dorsal mandibular articulation; es – epistomal sulcus; fr – frontal area; frc – frontal carina; fl – frontal line; ga – galea; glo – glossa; hysc – hypostomal carina; hyst – elongated tip of hypostomal carina; lbr – labrum; md – mandible; oc – ocelli; oca – occipital carina; occ – occipital region; pgb – postgenal bridge; pgr – postgenal ridge (visible through the head capsule); plb – labial palp; pmx – maxillary palp; pm – prementum; pocc – postocciput; sca – supraclypeal area; st – stipes; to – torulus; tol – torular lobe; vma – ventral mandibular articulation; vt – area of the vertex. — **Symbols:** white arrowhead – ventral carina on the postgena; black arrowhead – groove on lateral clypeus.

area including the region between the antennal sockets (which consists of the anterior frontal region in *Formica*) is raised much more steeply than in *Formica*, which results in an almost vertical orientation of the anterior clypeal portion (Figs. 1E, 2E); distinct clypeal grooves are present directly laterad the anterior tentorial pits (**black arrowhead**, Figs. 1D, 2D). The clypeal inflection (**cli**, Fig. 5D) is much shorter; its posterior edge bears a flat ridge on the dorsal and ventral side. The epistomal sulcus is represented by an external furrow that is deeper and narrower in the part mesad the anterior tentorial pit (**es**, Figs. 1D,E, 2D,E). A supraclypeal area is presented as a small, elongated oval depression directly posterad the clypeus (**sca**, Figs. 1D, 2D). The frontal carinae are more approximated due to the mesal shift of the antennal insertions, but they are also short (**frc**, Figs. 1D,E, 2D,E); as in *Formica*, the frontal carinae do not form “frontal lobes”; they are slightly curved and anteriorly end above the very

large torular lobes (**tol** Figs. 1D,E, 2D,E, 3E), which almost completely cover the torular acetabula (**ac**, Fig. 3E) in dorsal view. The lateral arch of the torulus (**trl**, Fig. 3E) is short and barrel-shaped, which results in a more horizontal orientation of the antennal base. The compound eye is slightly smaller than in *Formica* and has fewer ommatidia (63, n=1); it is also slightly less ovoid and located only a short distance behind the dorsal mandibular articulation, close to the anterior head margin. Ocelli are missing. The hypostomal carina (**hysc**, Figs. 1F, 2F) is broader than in *Formica* and straight, without a twist in its lateral part; its anterolateral edges are distinctly projecting above the mesal mandibular base (**hye**, Figs. 1F, 2F); the triangular processes are more rounded and thicker (**hysp**, Fig. 11B); they are not concave anteriorly and the lateral stipital margin consequently inserts along the edge between the process and the remaining hypostoma (*, Fig. 11B). An additional process forming

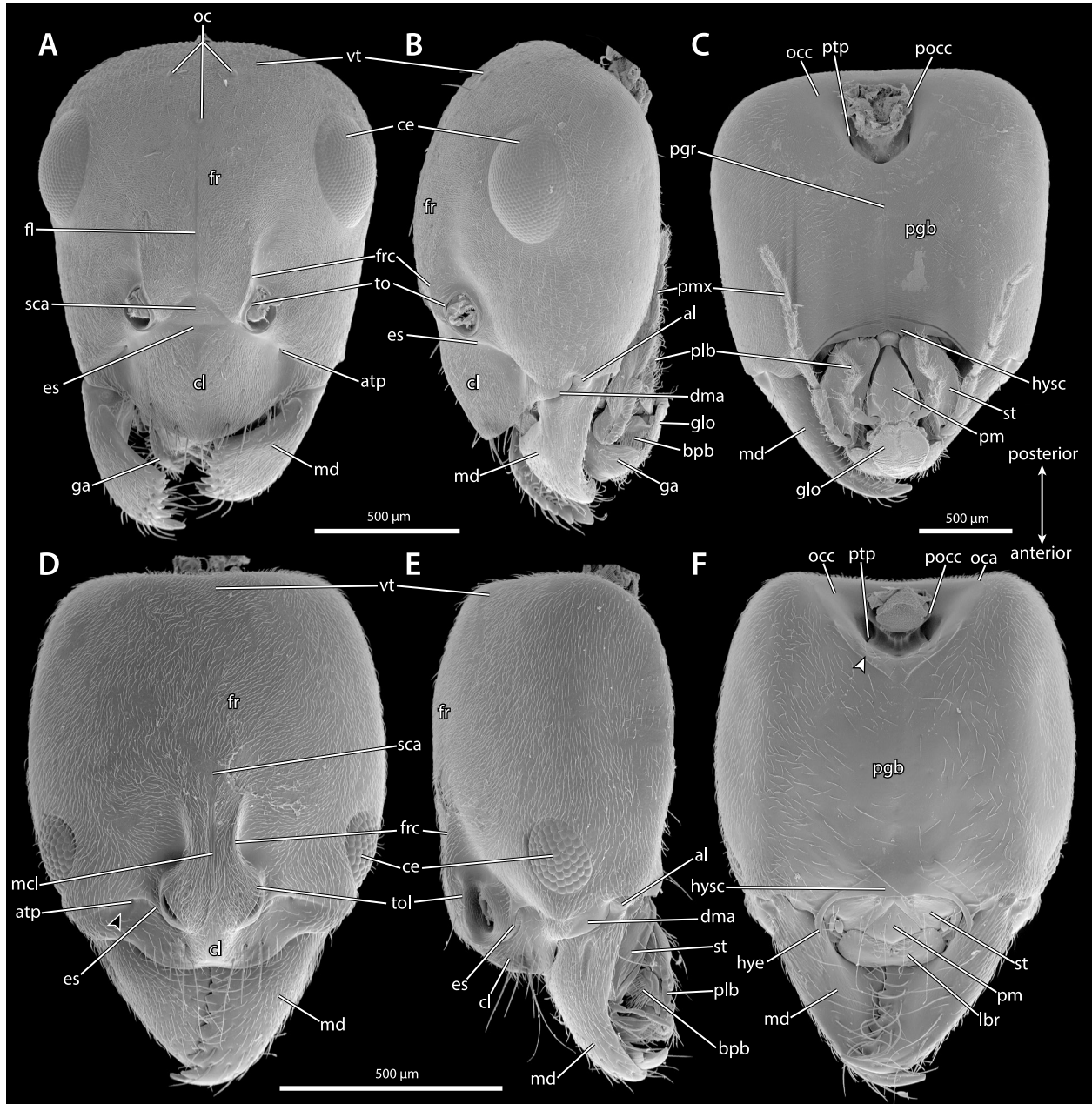


Fig. 2. SEM micrographs of heads of *Formica rufa* (A–C) and *Brachyponera luteipes* (D–F). Note the slight difference in shape between a small (A,B) and a larger head (C) in *Formica rufa*. A,D: Dorsal view. B,E: Lateral view. C,F: Ventral view. — **Abbreviations:** al – atala; atp – anterior tentorial pit; ce – compound eye; cl – clypeus; dma – dorsal mandibular articulation; es – epistomal sulcus; fr – frontal area; frc – frontal carina; fl – frontal line; ga – galea; glo – glossa; hyst – hypostomal carina; hyst – elongated tip of hypostomal carina; lbr – labrum; md – mandible; oc – ocelli; oca – occipital carina; occ – occipital region; pgb – postgenal bridge; pgr – postgenal ridge (visible as line of smooth cuticle); plb – labial palp; pmx – maxillary palp; pm – prementum; pocc – postocciput; sca – supraclypeal area; st – stipes; to – torulus; tol – torular lobe; vma – ventral mandibular articulation; vt – area of vertex. — **Symbols:** white arrowhead – ventral continuation of occipital carina; black arrowhead – groove on lateral clypeus.

the mesal arch of the pleurostomal fossa is missing (compare Fig. 11A,B). The cuticle is largely smooth but covered with small pores with minute setae inserted in them.

3.2. Endoskeleton

Formica rufa

The long, tube-like anterior tentorial arms (HAO_0001454) (ata, Figs. 5E,F, 9A,B, 11A, 13B) are oval to round in

cross section. They extend through the head with a diagonal orientation. The median lamellae form short broad lobes along the middle third of the anterior arms (ml, Figs. 5E,F, 9A,B, 11A); they appear slightly sinuate in sagittal view (Fig. 9B). Additional lateral lamellae are present between the proximal limit of the median lamellae and the anterior tentorial pits (ll, Figs. 9A,B, 13B); they are dorsally oriented at their posterior origin and ventrolaterally at their anterior end, forming a relatively even curve between these points. The posterior arms

(HAO_0001343) are very short (**pta**, Figs. 5E,F, 9A,B, 11A). The tentorial bridge (HAO_0000998), located shortly before the occipital foramen, is slightly curved upwards (**tb**, Figs. 5E,F, 9A,B, 11A); it bears a distinct anteromedian process (**tba**, Fig. 11A) (HAO_0002479) and a small anterior strengthening ridge. Dorsal tentorial arms (HAO_0000275) are present as thin outgrowths shortly anterad the posterior end of the lamellae (**dta**, Figs. 5E,F, 9A,B, 11A); they are anterodorsally orientated and do not reach the head capsule; the distal end is slightly inflated. A secondary tentorial bridge is missing. Posterior tentorial processes are present as short tubes in the lateroventral postoccipital region (**ppt**, Figs. 5B,F, 9B,F). The well-developed postgenal ridge extends along the entire ventral midline of the head; its inflated dorsal edge forms a rod-like margin (**pgr**, Figs. 5F, 9F); posteriorly it splits into two flat ridges, which extend towards the posterior tentorial pits without reaching them. The torulus bears a finger-like apodeme extending into the cephalic lumen (**toa**, Figs. 5B,F, S1A) (phragma of the antennal acetabulum of RICHTER et al. 2019/ torular apodeme). The epistomal ridge (HAO_0000305) is strongly developed internally (**esr**, Fig. 5B). Two short ridges originating at the posterior clypeal margin between the antennal foramina (see Fig. S1A) demarcate the triangular supraclypeal area.

Brachyponera luteipes

The posterior position of the occipital foramen and the elongate shape of the head result in a more horizontal orientation of the tentorium (Figs. 5G,H, 9C,D, 11B, 13H). The median lamellae are present along almost the entire length of the anterior arms (**ml**, Figs. 9C,D, 11B); a posteriorly deepening concavity forms the area of origin of the extrinsic antennal muscles (Fig. 5H). The lateral lamellae (**ll**, Fig. 9C,D) are much broader than in *Formica*; anteriorly they end only shortly before the median lamellae; they are dorsolaterally oriented over most of their length, twisting only slightly dorsad posteriorly and laterad anteriorly. The anterior arms are sharply bent dorsad at their posterior end; the vertical portion is fused to the posterior head capsule (**ata**, Figs. 5H, 9D); it is connected with the tentorial bridge (**tb**, Figs. 5G,H, 9C,D), which is shaped like a rounded arch and strengthened by a ridge on its ventral side. The posterior arms (**pta**, Figs. 9C,D, 11B) are very short and fused with the anterior arms, and thus almost unrecognizable as individual endoskeletal elements. The obsolete dorsal arms, minute short tubes originating at the posterior end of the median lamellae, run anteriorly directly ventrad the brain (not visible in μ CT-data; Fig. S2F). Tube-like posterior processes in the postoccipital region are missing. The torular apodeme, a long and flat cuticular extension, reaches into the head capsule; its distal part is bent towards the anterior cephalic margin (**toa**, Fig. 5C). The epistomal ridge is firmly connected with the closely approximated antennal sockets (**esr**, Fig. 5D); the left and right branches diverge posterior to the antennal foramina, before flattening and converging in the sagittal plane; in one specimen

of *B. chinensis* the left and right branches of the ridge fuse in front of the antennal insertions; the division of the two branches remains as a Y-shaped tip of the ridge (Fig. 14E); the base of the Y-shaped ridge shortens posterad, resulting in a new separation of the right and left branches, which then converge towards the midline before obliterating completely. The supraclypeal area is not marked by internal ridges.

3.3. Antennae

Formica rufa

The geniculate 12-segmented antennae (HAO_0000101) are inserted directly behind the clypeus; the distance between the foramina (HAO_0001022) is only slightly shorter than their distance to the lateral margin of the head (Figs. 1A, 2A). The semispherical bulbous (HAO_0000889, radicle) (**bb**, Fig. 3B) of the scapus (HAO_0000908) (**sc**, Fig. 3B) is almost completely visible as it rests on the shallow torular acetabulum (**ac**, Fig. 3F); its lateral margin articulates with a stout, peg-like antennifer (HAO_0001431). The bulbous is connected to the distal main part of the scape by a short, straight constriction (bulbous neck, **bbn**, Fig. 3B), located on its posterolateral surface. The scapus is almost half as long as the entire antenna. The cylindrical pedicel (HAO_0000706) (**pd**, Fig. 3B) is straight except for a basal angle resulting in the geniculate antennal shape. The straight and cylindrical flagellomeres (HAO_0000342) are longer than wide, and decrease in length towards the antennal apex. They bear a dense vestiture of thin articulated hairs interspersed with thicker setae (see WALTHER 1979 for a more detailed documentation). Short straight setae on the bulbous including its neck and the proximal pedicellar region, presumably proprioceptors, are only indistinctly visible (Fig. 3B).

Musculature (Figs. 5E,F, 12): The four extrinsic muscles are of similar size (smallest ca. 0.1% and largest ca. 0.15% of the head volume). All of them insert on thin tendons (the precise insertion sites are not shown in the 3D-reconstructions; the tendons were not recognizable in the data set but visible on histological sections, see Fig. 12E). **M. tentorioscapalis anterior (M. 1/ 0an1)**: origin (= O): dorsal surface of the anterior tentorial arm, lateral lamella and posteriorly also on mesal lamella; Insertion (= I): on a tendon originating anterolaterally on the bulbous. **M. tentorioscapalis posterior (M. 2/ 0an2)**: smallest of the four muscles, O: mesally on the mesal lamella, posterior to 0an4; I: on a tendon originating posteromesally on the bulbous. **M. tentorioscapalis lateralis (M. 3/ 0an3)**: largest of the four muscles, O: anterior tentorial arm, posterior to the other three muscles, partly on the posterior ends of the lateral and mesal lamellae; I: on a tendon originating laterally/ventrally (as the bulbous is more vertically than horizontally oriented) on the bulbous. **M. tentorioscapalis medialis (M. 4/ 0an4)**: O: anterior tentorial arm and on the anterior mesal and lateral lamellae, anteromesad 0an1; I: on a tendon originating mesal-

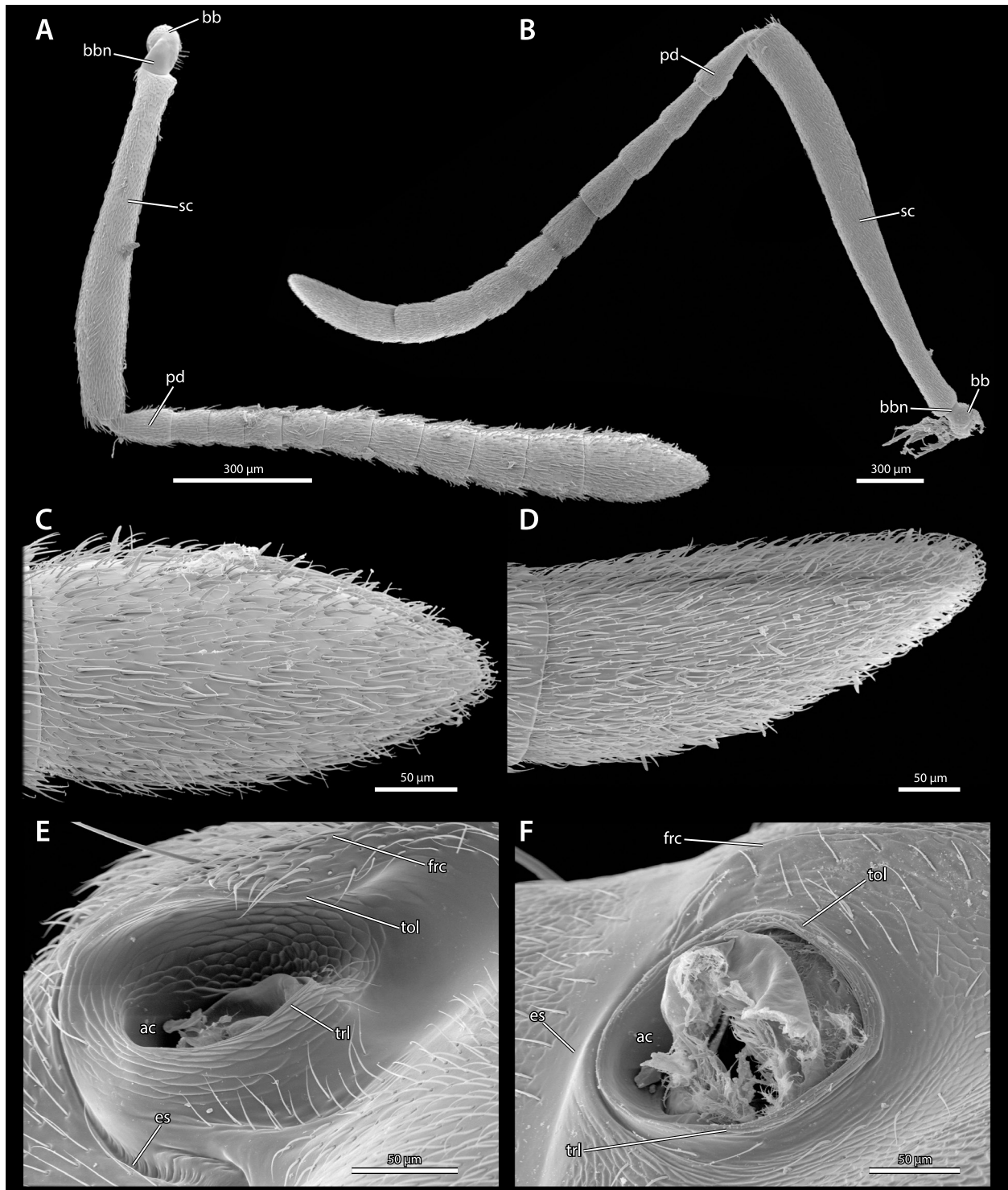


Fig. 3. SEM micrographs of the antennae and antennal sockets of *Formica rufa* (B,D,F) and *Brachyponera luteipes* (A,C,E). A–D: Dorsal view. E,F: Lateral view. — **Abbreviations:** ac – torular acetabulum; bb – bulb; bbn – bulb neck; es – epistomal sulcus; frc – frontal carina; pd – pedicellus; sc – scapus; tol – torular lobe; trl – lateral torular arch.

ly/dorsally on the anterior region of the bulb. Intrinsic muscles, one of them bipartite. *M. scapopedicellaris lateralis* (M. 5/ 0an6), O: laterodorsally on the scapus at the level of the distal bundle of 0an7; I: on a short tendon originating from the dorsolateral base of the pedicellus. *M. scapopedicellaris medialis* (M. 6/ 0an7): two distinct bundles O: mesoventrally on the distal half of the scapus;

I: on a long tendon originating from the mesoventral base of the pedicellus.

Brachyponera luteipes

The antennal sockets are closely approximated medially, and also closer to the anterior cephalic margin (Figs. 1D, 2D). The bulb is sunk into the deeper acetabulum of

the torulus and completely concealed dorsally by the medial torular lobe. The bulbus neck is shifted anteromesad compared to *Formica*; it is sharply bent posterad (Fig. 3A). The flagellomeres are about as long as wide and increase in size towards the antennal apex; the preapical flagellomere is wider than long, the apical one distinctly longer than wide. Like in *Formica* the vestiture is composed of fine and larger setae (see also SIDDQUI et al. 2010); the density of the latter increases towards the apical flagellomere; irregularly dispersed pores on the antenna are likely sockets of missing setae (Fig. 3C); a group of setae on the bulbus neck is much longer than any of the other proprioceptors (Fig. 3A).

Musculature (Figs. 5G,H, 12): The four extrinsic muscles differ distinctly in size (smallest ca. 0.1% and largest ca. 0.28% of the head volume). All of them insert with tendons (precise insertion sites not shown in 3D-reconstructions but visible in histological sections, see Fig. 12F). *M. tentorioscapalis anterior* (**M. 1/ 0an1**): O: dorsal surface of the anterior tentorial arm, mesal lamella and anteriorly on lateral lamella; I: anterolaterally on the bulbus. *M. tentorioscapalis posterior* (**M. 2/ 0an2**): O: very long area along the deep concavity of the mesal lamella; I: posteromesally on the bulbus. *M. tentorioscapalis lateralis* (**M. 3/ 0an3**): by far the largest extrinsic muscle, O: anterior arm and its lateral lamella, posterolaterad the other muscles; I: laterally/ventrally on the bulbus. *M. tentorioscapalis medialis* (**M. 4/ 0an4**): O: only mesally on the anterior region of the mesal lamella, mesad 0an1; I: mesally/dorsally on the anterior region of the bulbus. Intrinsic muscles both undivided. *M. scapopedicellaris lateralis* (**M. 5/ 0an6**), O: laterodorsally on the distal third of the scapus; I: with two short tendons on the laterodorsal pedicellar base. *M. scapopedicellaris medialis* (**M. 6/ 0an7**): single bundle, O: mesoventrally on the distal third of the scapus, slightly proximad 0an6; I: with a short tendon on the mesoventral base of the pedicellus.

3.4. Mandibles

Formica rufa

The large mandibles (HAO_0000506) are divided into a thick basal stem and a distal blade, the latter appearing roughly triangular in dorsal view (Fig. 4A,B). The blade is bent mesad and torqued relative to the stem; its masticatory margin forms an angle of approximately 45° with the main axis of mandibular movement; it bears a series of seven to eight teeth, a large apical one followed by a slightly smaller preapical tooth, then much smaller ones of about equal size; the basal margin is straight and forms an angle of almost 90° with the masticatory margin; the basal margin ends dorsally on the mesal side of the mandibular base; short carinae extend from the ventral/external mandibular margin to the apical and preapical tooth, respectively (**mdc**, Fig. 4B). An indistinct carina, subtended proximally by a row of sensilla, is present along the row of teeth following the preapical one (Fig. 4B).

The mandibular base forms the articulatory surfaces of the primary (ventral) and secondary (dorsal) joint; dorsally it bears the membranous mandalus (**ma**, Fig. 4A), which ends in the fissure-shaped opening of the mandibular gland (**mgo**, Fig. 4A); a minute cuticular process originating on the proximomesal edge of the mandalus extends above the mandibular gland duct; a flat, approximately crescent-shaped groove is present distad the mandalus (**white arrowhead**, Fig. 4A). The extensive, dorsoventrally elongated articulatory surface of the dorsal (secondary) mandibular joint (mandibular acetabulum, HAO_0001391) (**dma**, Fig. 4A) articulates with an elongated laterodistal clypeal condyle (**dma**, Figs. 1A, 2A, 11A); the surface of both elements of the joint is smooth. The ventral basal margin forms the condyle of the primary mandibular joint (HAO_0000508) (**vma**, Fig. 4B), which is in the form of a stout knob fitting into the small pleurostomal fossa (HAO_0000732) (**vma**, Fig. 11A); a distinct smooth depression mesad/ dorsad the condyle (*, Fig. 4B) fits with the small rounded projection of the hypostoma (see “head capsule”, **white arrowhead**, Fig. 11A). A flat depression with a wrinkled surface (**mmg**, Fig. 4B) is present on the mesal mandibular surface; the larger triangular hypostomal process contacts the ventral part of the mandibular base at the proximal margin of this depression. The atala, a process on the lateral side of the mandibular base of similar size as the ventral condyle, is located between the dorsal and ventral articulations (**al**, Fig. 4A); it fits into a lateral concavity of the oral foramen (**ala**, Fig. 11A); its distal surface displays a scale-like pattern, whereas the proximal surface contacting the head capsule is very smooth; the tendon of *M. craniomandibularis externus* inserts internally on the atala.

Musculature (Fig. 5A,B): *M. craniomandibularis internus* (**M. 11/ 0md1**): largest cephalic muscle, O: entire posterior cephalic area and most of the lateral internal surface, also on extensive dorsal and ventral regions; most of the attachment areas are connected, but a large ventral region is separated from extensive lateral and dorsal attachment sites enclosing the eye; a smaller, dorsomesal occipital bundle is also isolated from the rest; I: most fibers insert on thin cuticular fibrillae of the adductor tendon, the main part of which is a sclerotized, massive, rectangular plate (**mda**, Fig. 5A,B); the plate is connected to the mesal mandibular base with a less strongly sclerotized broad ligament; posteriorly, the sclerotized plate divides into two extensive sheet-like main branches (**mda_{lb}**, **mda_{cb}**, Fig. 5B) and a thin and short mesal branch (**mda_{mb}**, Fig. 5B); the proximal part of the lateral edge of the main central branch is bent upwards at about 90°, partly connecting the two main branches; a dorsal side branch originating from the central branch (**mda_{ab}**, Fig. 5B) receives the fibers of the dorsomesal isolated bundle; two fiber bundles connect directly to the main body of the apodeme and the mesal branch, one on the lateral side and one mesally. *M. craniomandibularis externus* (**M. 12/ 0md3**): distinctly smaller than 0md1 and appearing flattened in lateral view, O: ventrally on

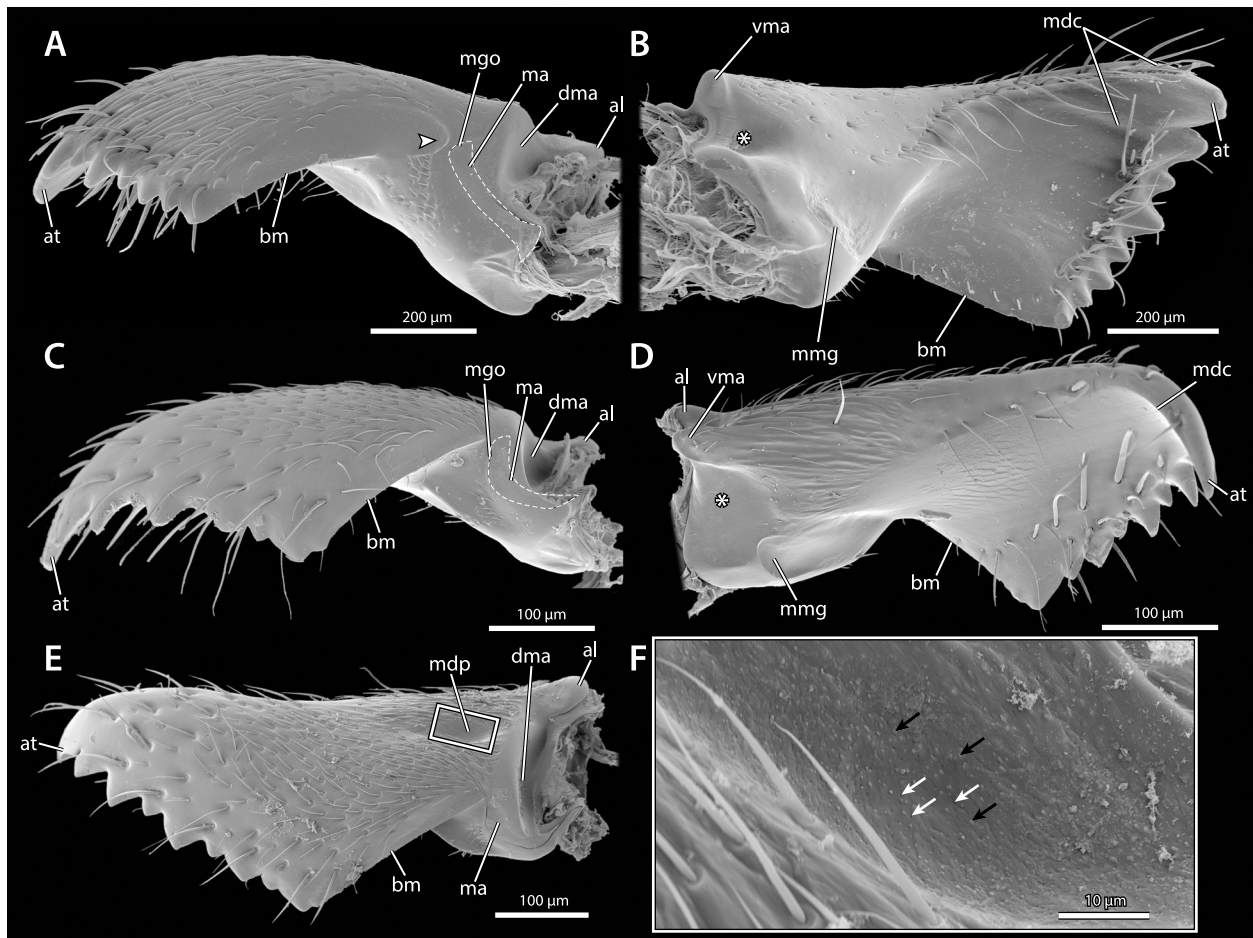


Fig. 4. SEM micrographs of the mandibles of *Formica rufa* (A,B) and *Brachyponera luteipes* (C–F). A,C: Dorsal view. B,D: Ventral view. E,F: Dorsolateral view. — **Abbreviations:** al – atala; at – apical tooth; bm – basal margin; dma – dorsal mandibular articulation; ma – mandalus; mdp – mandibular pit; mdc – mandibular carinae; mgo – mandibular gland opening; mmg – mesal mandibular groove. — **Symbols:** white arrowhead – groove distad mandalus; * – groove mesad/dorsad ventral mandibular articulation; black arrows – minute tubercles; white arrows – minute pores; white outlines – area of mandalus.

the anterior head capsule, reaching about half-way between the hypostoma and the occipital foramen, and on the anterior postgenal ridge. I: thin, short tendon originating from the atala. **M. hypopharyngo-mandibularis (M. 13) / M. tentorio-mandibularis medialis inferior (Omd8):** extremely thin, two fibers, O: ventrolaterally from the lateral lamella of the anterior tentorial arm next to the insertion of 0mx3; I: dorsomesally on the proximal inner surface of the mandible. **M. X (Fig. S1C):** an aberrant muscle only present in one side of the head of one of the scanned *Formica* individuals connects the dorsal and ventral walls of the posterior head capsule and displaces some of the fibers of 0md1 in that region (Fig. S1).

Brachyponera luteipes

The mandibles are longer and appear less curved than in *Formica* in dorsal view (Fig. 4C). The blade is longer and less strongly bent mesad, although the masticatory margin curves further apicomeresad; the masticatory margin is slightly closer to a horizontal orientation and forms an angle of ca. 30° with the mandibular axis of rotation. Nine teeth (“incisivi”) are present, with an alternating pattern of larger and smaller ones over the entire

length of the edge following the mandibular apex; the basal margin ends further laterally, at about mid-length of the dorsal side of the basal mandibular stem (Fig. 4C). The basal margin is in contact with a ventral projection of the internal clypeal edge (clf, Fig. 11B) over its entire length. A carina running from the basal tooth towards the preapical tooth is missing, whereas one extending towards the apical one is present (mdc, Fig. 4D). The very fine curved fissure of the mandalus extends around the dorsal articulatory surface (mgo, Fig. 4C). A shelf-like surface laterad the mandalus bears few small setae. The mandibular acetabulum is deeper than in *Formica* (dma, Fig. 5C). The ventral (primary) mandibular condyle appears more slender than in *Formica* (vma, Fig. 5D); the depression mesad/dorsad the condyle (*, Fig. 4D) is less concave. The surface of the flat depression on the mesal mandibular side is smooth, entirely lacking wrinkles (mmg, Fig. 4D); the surface of the atala is also smooth. A relatively flat pit on the proximolateral mandibular region displays small tubercles and minute pores on its surface (mdp, Fig. 4E,F).

Musculature (Fig. 5C,D): **M. craniomandibularis internus (M. 11/ Omd1):** largest muscle of the head, O:

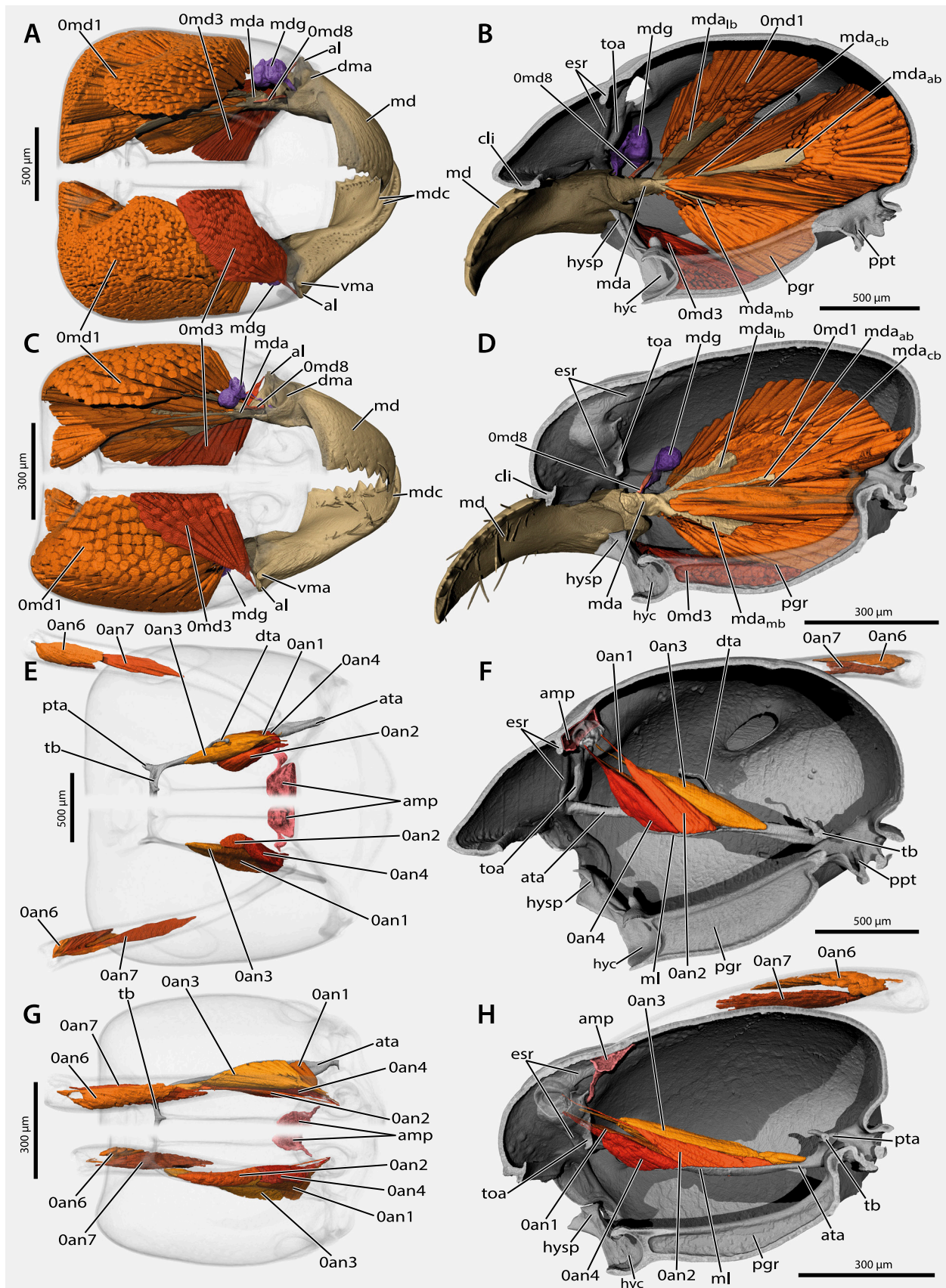


Fig. 5. Volume renderings of head of *Formica rufa* (CASENT0709411: **A,B**; CASENT0790267: **E,F**) and *Brachyponera luteipes* (CASENT0709409: **C,D,G,H**). **A,C,E,G**: Upper part dorsal view, lower part ventral view. **B,D,F,H**: Sagittal view. **A–D**: Mandibular musculature and mandibular gland. **E–H**: Antennal musculature, in **F** and **H** parts of antennal torulus transparent to show muscles and bulbous. — **Abbreviations**: **0an1** – *M. tentorioscapalis anterior*; **0an2** – *M. tentorioscapalis posterior*; **0an3** – *M. tentorioscapalis lateralis*; **0an4** – *M. tentorioscapalis medialis*; **0an6** – *M. scapopedicellaris lateralis*; **0an7** – *M. scapopedicellaris medialis*; **0md1** – *M. craniomandibularis internus*; **0md3** – *M. craniomandibularis externus*; **0md8** – *M. tentoriomandibularis*; **al** – atala; **amp** – antennal ampulla;

posterior bundles mainly on the occipital region, other parts on large areas of the lateral surface, the dorsolateral areas, and most of the surface of the ventral wall of the head capsule. As in *Formica*, a large lateral/dorsolateral area and a large ventral area are separated from each other, and a mesal bundle inserting above the occipital foramen is also isolated; I: most of the fibers attach directly on the apodeme; its main body (**mda**, Fig. 5C,D) divides into three parts of very similar size, a central (**mda_{cb}**, Fig. 5B), a dorsolateral (**mda_{lb}**, Fig. 5B) and a ventromesal (**mda_{mb}**, Fig. 5B) branch, all three extensive and sheet-like; the central one is straight, whereas the others are concave; a smaller branch divided from the mesal one (**mda_{ab}**, Fig. 5B) receives the isolated muscle bundle as in *Formica*; in addition to the fibers of the mesal and lateral bundle inserted close to the main body of the apodeme, almost all bundles of the posterior head regions are directly attached; only the portions of the muscle closest to lateral, mesal and anteroventral margins are attached by cuticular threads, which are shorter than those of *Formica*. **M. craniomandibularis externus (M. 12/ 0md3)**: very similar to that of *Formica*. **O**: more fibers on the postgenal ridge than on the ventral wall of the head capsule. **I**: upon a tendon that is shorter than in *Formica*. **M. hypopharyngo-mandibularis (M. 13)/ M. tentorio-mandibularis medialis inferior (0md8)**: similar to its homologue in *Formica*, but with its origin placed further anterad, at the anterior edge of the lateral lamella.

3.5. Maxillae

Formica rufa

The maxillae (HAO_0000513) are closely associated with the labium (HAO_0000453), both forming the maxillolabial complex (Figs. 1B,C, 2B,C). The cardines (HAO_0000187) are small elongated rods, T-shaped on their proximal end, with the lateral extension much longer than the mesal one (**cd**, Fig. 6A,B), which articulates with a small condyle of the head capsule (HAO_0002074) (**cc**, Fig. 11); a notch in the distal hypostomal margin, laterad the condyle, receives the lateral extension and the proximal cardinal shaft; the distal cardinal tip is strongly bent anterad/dorsad; a membrane at the V-shaped articulatory area connects it to the stipes (cardinostipital hinge, HAO_0002076); a stipital process extends beyond the distal cardinal margin internally, additionally reinforcing the cardinostipital articulation; ventrally, the cardo is covered with minute spines and also bears a number of short and thin setae (Fig. 6B). The cardo is largely enclosed in the hypostomal cavity, with only the tip vis-

ible externally, even in the fully extended position of the maxillolabial complex; in the retracted position it faces downward, whereas the stipes (HAO_0000958) is dorsally oriented with an angle of almost 90° relative to the longitudinal cephalic axis. The external surface of the stipes is sclerotized (external stipital sclerite, HAO_0002098) (**st**, Fig. 6A); in the retracted position it closes the oral foramen (HAO_0000670), together with the prementum (HAO_0000804) and the labrum (HAO_0000456); the stipes appears triangular in cross section and its mesal face is also sclerotized (HAO_0002096) (Fig. 13B), especially the proximal internal edge, which forms a stabilizing sclerite (**stis**, Fig. S2E); the mesal face bears an irregular row of setae on its distal two thirds (Fig. 6B); proximally, a membranous area adjacent with the stipes connects with the membrane closing the oral foramen; the internal sclerite is connected to the stipito-premental conjunctivum (HAO_0002125) (**spc**, Figs. 7B, S1D, S2D,E), a weakly sclerotized band of cuticle linking the stipes, the premental arm (HAO_0002155), and the hypopharynx at the lateroventral edges of the infrabuccal pouch (HAO_0001563); the external stipital face appears roughly rectangular, but with the distal end tapering towards the mesal side; a small and rounded proximomesal stipital lobe covers the membrane connecting the pre- and postmentum (HAO_0000785) (Figs. 1C, 2C). The lateral stipital edge is deeply inserted into the concave anterior surface of the triangular hypostomal process (Fig. 11A; **white arrowhead**, S2A); the mesal edge is in contact with the premental ditches (HAO_0002227) when the mouthparts are retracted. The six-segmented maxillary palp inserts distally on the mesal stipital edge (HAO_0000515) (**pmx**, Fig. 6A,B); palpomere 1 is short and stout, and its distal margin appears slanted; the following palpomeres are elongate and each of them is thinner than the preceding one; all palpomeres, especially the distal ones, are densely covered with setae; distinctly different types of hair-shaped sensilla are present, a subdecumbent pubescence and distinct sets of elongate, thicker setae on the dorsal side of palpomeres 1–5 and the ventral margins of the distal portions of palpomere 3–5. The galeolacinial complex, formed by the closely connected endite lobes (**ga**, Fig. 6A,B, HAO_0000368; **lc**, Fig. 6A,B, HAO_0000457), is broadly connected to the distal internal edge of the stipes; the entire structure is bent mesad above the labium and hypopharynx (Fig. 13A). The galea is sclerotized on its dorsal and ventral side; its anterior half is bent downwards in the retracted position, and bears a row of setae along the edge of its dorsal sclerotized area; additional setae are inserted along the entire dorsal surface of the inflected

ata – anterior tentorial arm; **cli** – clypeal inflection, ventral wall; **dta** – dorsal tentorial arm; **esr** – epistomal ridge; **hyc** – hypostomal cavity; **hysp** – hypostomal triangular process; **md** – mandible; **mda** – mandibular apodeme; **mda_{ab}** – mandibular apodeme, accessory branch; **mda_{cb}** – mandibular apodeme, central branch; **mda_{lb}** – mandibular apodeme, lateral branch; **mda_{mb}** – mandibular apodeme, mesal branch; **mdc** – mandibular carinae; **mdg** – mandibular gland; **ml** – mesal lamella; **pgr** – postgenal ridge; **ppt** – posterior process of tentorium; **pta** – posterior tentorial arm; **tb** – tentorial bridge; **toa** – torular apodeme; **vma** – ventral mandibular articulation. — **Colors: beige / brown** – mouthparts; **grey** – cuticle; **orange / red** – muscles; **pink** – antennal ampullae; **purple** – glands.

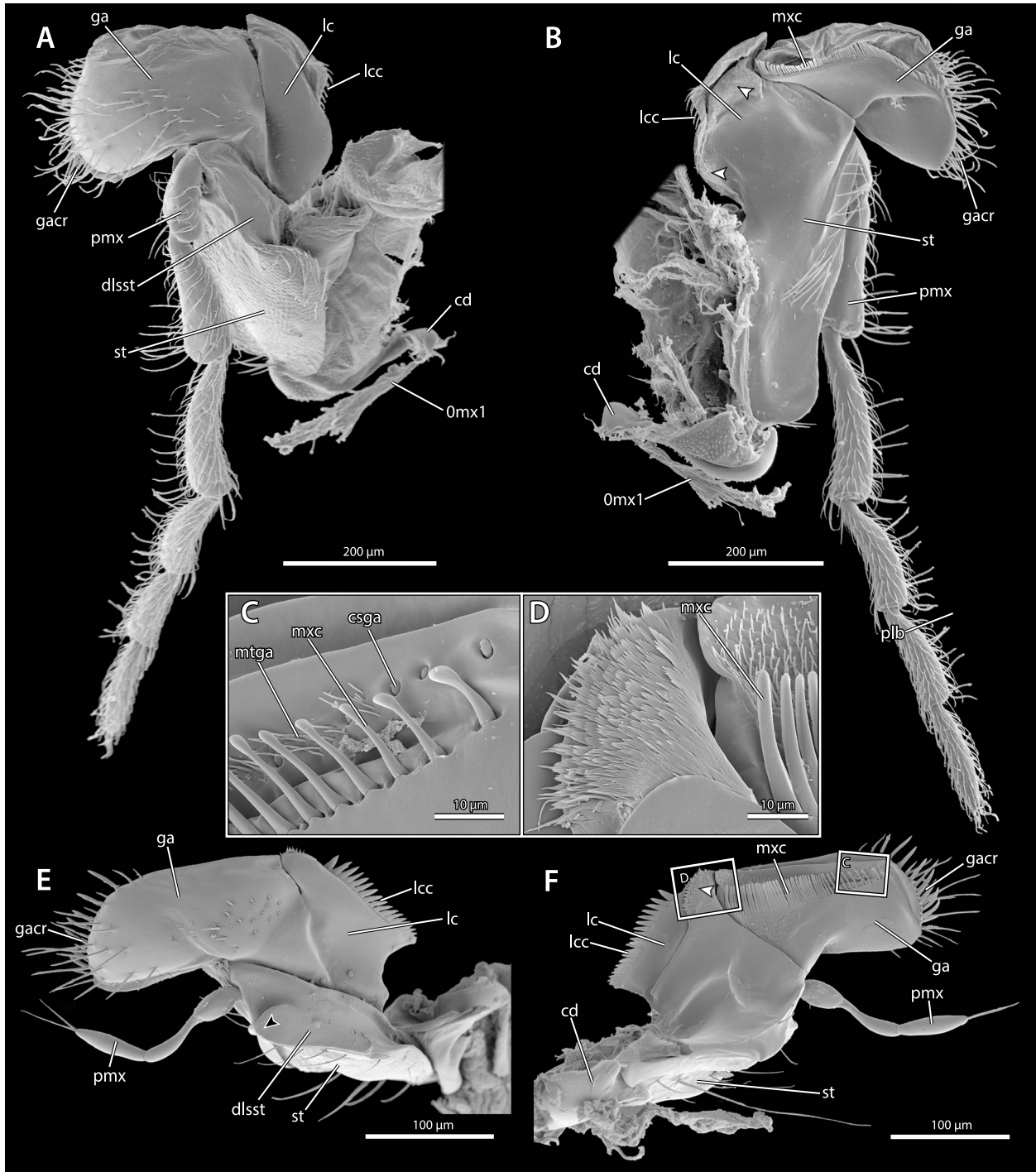


Fig. 6. SEM micrographs of the maxillae of *Formica rufa* (A,B) and *Brachyponera luteipes* (C–F). **A:** Dorsal view, slightly shifted frontolaterad. **B:** Mesoposterior view. **E,H:** Close view of the paraglossa. **C,D,F:** Ventral view. **E:** Dorsolateral view. — **Abbreviations:** **0mx1** – *M. craniocardinalis externus*; **cd** – cardo; **csga** – conical sensilla of galea; **dlsst** – distal lateral stipital surface; **ga** – galea; **gacr** – galeal crown; **lc** – lacinia; **lcc** – lacinial comb; **mtga** – galeal microtrichia; **mxc** – maxillary / galeal crown; **pmx** – palpus maxillaris; **st** – stipes. — **Symbols:** white arrowheads – fields of microtrichia on lacinia; black arrowheads – extended distal lateral edge of stipes.

part (galeal crown HAO_0002132) (**gacr**, Fig. 6A,B), and also on the straight part of the galea close to the stipes; ventrally, the galea bears a long comb of setae (galeal comb, HAO_0002243) (**mxc**, Fig. 6B) close to its outer margin; the area between the comb and the outer margin is densely covered with minute microtrichia. The lacinia also bears a row of setae along its edge (lacinial comb, HAO_0002124) (**lcc**, Fig. 6A,B); close to

the galea, its ventral side displays a large field of small scale-like combs of microtrichia; a smaller field of longer, hair-like microtrichia, originating in pairs or triplets from scale like bases, are visible on the posterior end of the lacinial lobe (**white arrowheads**, Fig. 6B); the basal lacinial sclerite (HAO_0002093) (**lcs**, Fig. S2A) is mesally connected to the stipes and well sclerotized; it is more or less continuous with the internal stipital scler-

rite, but can be recognized on cross sections as distinctly thickened region, where it receives the stipitolacinal muscle (0mx6).

Musculature (Fig. 9B,F): *M. craniocardinalis externus* (M. 15/ 0mx1): long muscle composed of many thin fibers; O: posteroventral head capsule anterad the depression around the occipital foramen, and partly on the posterior postgenal ridge; I: on a relatively short tendon originating on the lateral proximal extension of the cardo. *M. tentoriocardinalis* (M. 17/ 0mx3) or *M. tentoriostipitalis posterior* (0mx5): O: anteriorly on the anterior tentorial arm, partly on its lateral lamella (directly behind insertion of 0md8); I: on a thin tendon originating on an internal process of the base of the external stipital sclerite, which is part of the cardinostipital hinge. *M. tentoriostipitalis* (M.18)/ *M. tentoriostipitalis anterior* (0mx4): two distinct bundles; O: anterior bundle ventrally on the anterior tentorial arm directly behind 0mx3; posterior bundle ventrally on the lobe-like mesal lamella; I: on flat, merging tendons inserted on the mesal stipital wall (internal stipital sclerite) close to the stipito-premental conjunctivum. *M. stipitolacinalis* (M. 20/ 0mx6): very flat muscle; O: distally on the lateral stipital margin; I: on the basal lacinial sclerite. *M. stipitogalealis* (M. 21/ 0mx7): O: along almost the entire length of the internal surface of the external stipital sclerite; I: on a tendon attached to the inner base of the galea. *M. stipitopalpalis externus* (M. 22/ 0mx8): well-developed muscle, similar in size to 0mx7. O: external stipital sclerite laterad 0mx7; I: base of first palpomere. *M. palpopalpalis maxillae primus, secundus, tertius? quartus?* (M. 24, 25, 26, 27/ 0mx12, 13, 14, 15): intrinsic muscles of the maxillary palp; the two proximal ones (primus/secundus) are distinct, whereas the following muscles in the thin palpomeres are not clearly recognizable on μ CT images and histological sections. O: on the base of the palpomere; I: base of the following palpomere.

Brachyponera luteipes

The proximal end of the cardines appears rather L- than T-shaped, with a scarcely visible mesal extension (Fig. 6E,F); the V-shaped articulatory area formed with the stipes is deeper and narrow. In cross section the stipes appears more rectangular proximally and triangular distally. The external stipital sclerite is of similar shape, but with its distal margin tapering more towards its middle region, rather than mesally; the distal part of the lateral stipital margin forms a broad shoulder region (**dlst**, Fig. 6); it is distally expanded as a wedge-shaped tip of the external face (**black arrowhead**, Fig. 6), which is externally pressed against the lateral labral process in the retracted position; a notch is present posteromesad the extension (Fig. S1F); its mesal part receives the first palpomere in retracted position, providing space for the palpus to protrude from the retracted complex; furthermore, the lateral labral process reaches into the lateral part of the groove (Fig. S1F); the mesal stipital edge interacts more closely with the premental ditches than in *Formica*, almost over the entire length of the stipes;

the lateral stipital edge is in contact with the angle between the hypostoma and the hypostomal/ postgenal triangular process (*, Fig. 11B). The three-segmented maxillary palp inserts mesad the notch described above (**pmx**, Fig. 6E); palpomere 1 has a straight distal margin; the following two are both long and thin; palpomere 2 is narrowed proximally and widens distally, 3 appears slightly club-shaped; only palpomere 3 bears two setae apically; no other types of sensilla were identified. The maxillary endite lobes are of similar shape, but the posterior margin of the lacinia is more pointed (**lc**, Fig. 6E,F); the stout, apically pointed setae of the galeal crown are interspersed by few slightly shorter and thinner setae (**gacr**, Fig. 6E); the setae on the dorsal galeal surface are rather long and less dense than in *Formica*; a second field of much shorter setae is present on the posterior region of the galea, close to the lacinia (Fig. 6E); the maxillary comb is formed by very closely arranged blunt setae that decrease in length anteriorly (**mx**, Fig. 6C,D,F); a well-developed row of cone-like sensilla coeloconica is present distad the comb (**csga**, Fig. 6C), it is surrounded by small hair-like microtrichia (**mtga**, Fig. 6C); the posterior ventral galeal surface proximad the comb and close to the lacinia is scale-like (Fig. 6F); the lacinial comb is formed by a row of thick, spine-like cuticular extensions instead of setae (**lcc**, Fig. 6); a conspicuous longitudinal fold is present on the ventral surface of the lacinia (Fig. 6C,F); its surface is smooth, except for the area close to the anterior margin, which bears a small field of scale-like microtrichial combs with some surrounding individual hair-like microtrichia, similar to the structures found in *Formica* (**white arrowhead**, Fig. 6D,F). In contrast to *Formica* the basal lacinial sclerite is not thickened.

Musculature (Fig. 9C,D): *M. craniocardinalis externus* (M. 15/ 0mx1): relatively thin muscle; O: similar to the origin in *Formica*, but with less fibers on the ventral head capsule and more on the postgenal ridge; I: on a broad, anteriorly narrowing tendon attached to the lateral cardinal base. *M. tentoriocardinalis* (M. 17/ 0mx3) or *M. tentoriostipitalis posterior* (0mx5): O: similar to the origin in *Formica*, but partly on the mesal lamella instead of the lateral one; I: like in *Formica*, with the tendon running very close to the cardo. *M. tentoriostipitalis* (M.18)/ *M. tentoriostipitalis anterior* (0mx4): only one distinctly developed bundle; O: ventrally on the broadest part of the mesal lamella; I: with two merging tendons as in *Formica* and on the same insertion site. *M. stipitolacinalis* (M. 20/ 0mx6): slightly more compact but otherwise similar to its equivalent in *Formica*. *M. stipitogalealis* (M. 21/ 0mx7): O: further distad than in *Formica*; I: with a very short tendon on the inner base of the galea. *M. stipitopalpalis externus* (M. 22/ 0mx8): much smaller than 0mx7, otherwise similar to its equivalent in *Formica*. *M. palpopalpalis maxillae primus, secundus?* (M. 24, 25/ 0mx12, 13): intrinsic muscles of the maxillary palp; only the proximal one (primus) is clearly recognizable on μ CT images and histological sections. O: on the base palpomere 1; I: base of palpomere 2.

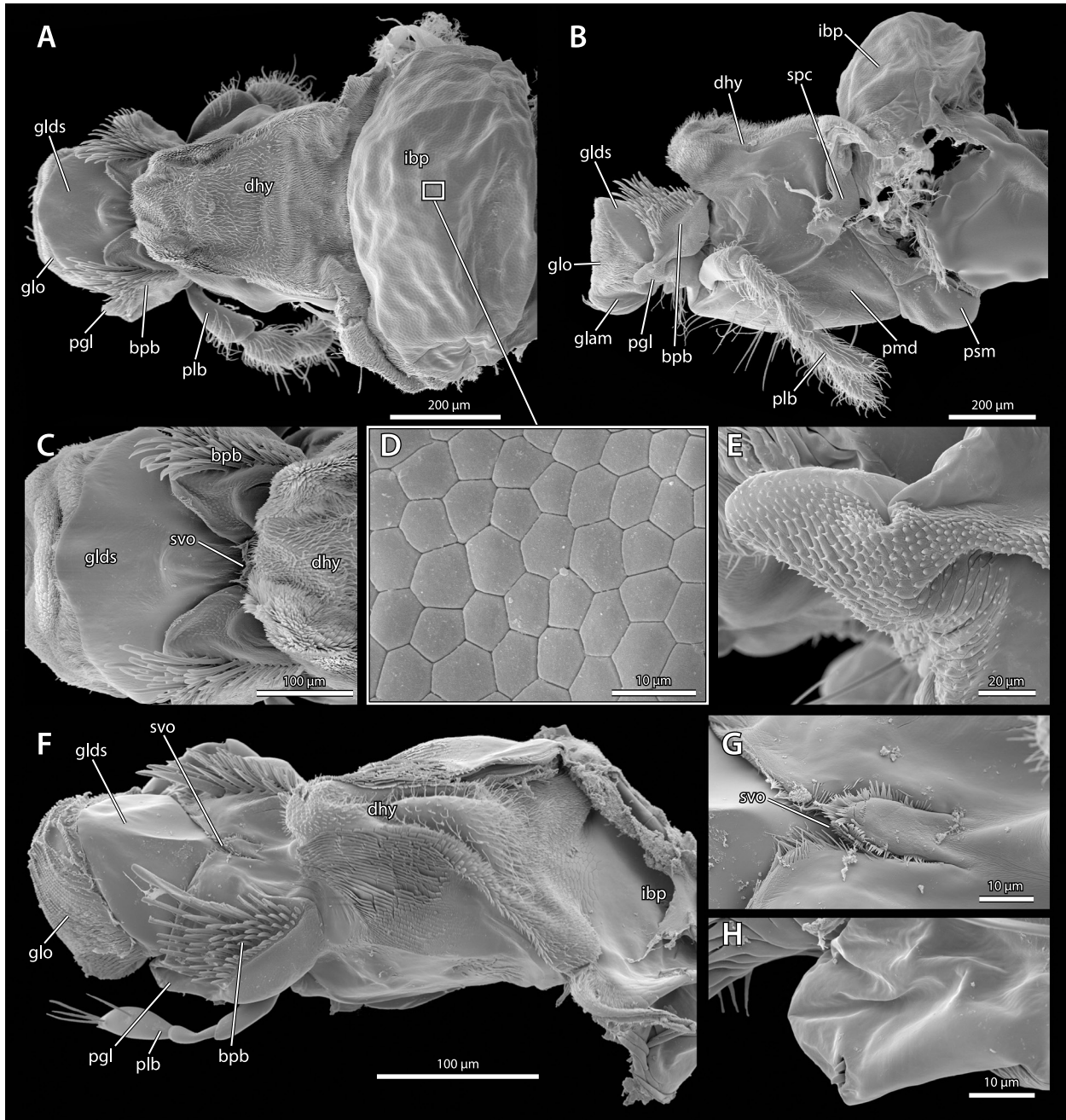


Fig. 7. SEM micrographs of the labium of *Formica rufa* (A–E) and *Brachyponera luteipes* (F–H). A,C,D: Dorsal view. B,E,H: Lateral view. F,G: Dorsolateral view. E,H: Close view of the paraglossa. — **Abbreviations:** bpb – basiparaglossal brush; dhy – distal hypopharynx; glam – anterior glossal margin; glds – dorsal glossal sclerite; glo – glossa; ibp – infrabuccal pouch; pgl – paraglossa; plb – palpus labialis; pmd – premental ditch; spc – stipito-premental conjunctivum; svo – salivary opening.

3.6. Labium and distal hypopharynx

Formica rufa

A membrane, which is folded inwards and thus not visible externally, connects the proximal part of the labium (HAO_0000453) with the maxillary base; the stipito-premental conjunctivum connects the entire maxillolabial complex with the infrabuccal pouch (HAO_0001563) (spc, Figs. 7B, S1D, S2D,E). The labium is also completely fused to the distal hypopharynx (HAO_0001575), which forms the dorsal surface of the proximal part of the entire structure (the labium and the distal hypopharynge-

al part including the infrabuccal pouch [hypopharyngeal wall, HAO_0000409] are described together here); the ventral labial surface is formed by the small postmentum (psm, Fig. 7B, HAO_0000785) and the large prementum (Fig. 7B, HAO_0000804); the anterior upper surface bears the fused glossae (simply referred to as “glossa” in the following, HAO_0000376) (glo, Fig. 7A–C) and paraglossae (HAO_0000686) (pgl, Fig. 7A,B,E). The postmentum, a relatively broad horseshoe-shaped sclerite, is connected to the prementum by a membrane; the distal region of the sclerite and the proximal membrane are covered with small, spine-like microtrichia. The pre-

mentum is strongly sclerotized; it is divided into a lateral (HAO_0002152) and a ventral face (HAO_0002156) by shallow premental ditches (HAO_0002227) (**pmd**, Fig. 7B); the distal margin of the oval ventral face appears slightly truncated in ventral view (Figs. 1C, 2C); the lateral premental face bears relatively short, stout premental arms (HAO_0002155) (**pma**, Fig. 13B) as proximolateral extensions; they are connected to long crescent-shaped lateral hypopharyngeal sclerites (hypopharyngeal rods, HAO_0000408) (**hyr**, Fig. 13B), which stabilize the distal hypopharynx. The distal hypopharyngeal part (**dhy**, Fig. 7A,B) is relatively short, broad and raised high above the prementum; the lateral sclerites are anteriorly continuous with a broad, weakly sclerotized conjunctivum, which is bent downwards into the distal tip of the hypopharynx, thus forming the massive hypopharyngeal buttons (HAO_0002234) (**hyb**, Fig. 13A); these structures are ventrodistally continuous with the salivary sclerite (HAO_0001682) (**sv**, Figs. 9F, 12A). The lateral hypopharyngeal surface is mostly smooth, whereas the dorsal surface bears a dense cover of long, hair-like microtrichia (Fig. 7A,B); its anterior apical region has a scale-like surface structure with each scale bearing a single hair-like microtrichium; the distal hypopharynx is limited by the salivary opening (HAO_0000906) (**svo**, Fig. 7C); proximally it is continuous with the large, bulbous, hemispherical infrabuccal pouch (**ibp**, Figs. 7A,B,D, 11E, 12A, 13B); only a narrow opening is visible, especially when the ventral mouthparts are retracted; the upper and lower lip of the pouch opening bear minute microtrichia (Fig. 12C); the inner wall is glabrous and has a honeycombed surface (Fig. 9D); from the upper lip of the pouch opening the hypopharyngeal wall continues towards the prepharynx (described in the section “cephalic digestive tract”). The well-developed basiparaglossal brushes (HAO_0002199) (**bpb**, Fig. 7A–C) on both sides of the salivary opening consist of several rows of blunt setae which are shortest laterally; the lateral base of the brushes is covered with rows of minute finger-like microtrichia; the brushes are anteriorly continuous with membranous folds covered with spines, representing the strongly reduced paraglossae (HAO_0000686) (**pgl**, Fig. 7A,B,E). The glossa (HAO_0000376) (**glo**, Fig. 7A–C), which is inserted between these folds, is stabilized dorsally by the broad dorsal glossal sclerites (anterior glossal plate, HAO_0000112) (**glps**, Fig. 7A–C) and ventrally by the ventral glossal sclerite (posterior glossal sclerite, HAO_0000748) (**glvs**, Fig. 12A); the middle region of the latter is thick and two lateral arms project anteriorly into the ventral glossal wall; the membranous wall of the glossa is densely covered with hair-like microtrichia (Fig. 7B,C); the distal edge of the glossa (HAO_0002206) (**glam**, Fig. 7B) and of the prementum each bear rows of long setae. The four-segmented labial palps (HAO_0000450) (**plb**, Fig. 7A,B) insert immediately proximad the paraglossae; the palpomeres are similar in length and diameter, except for the slightly less wide apical palpomere; palpomere 1 is glabrous except for its distal margin, whereas the entire surface of the other palpomeres is covered with long, thin

setae; this fine pubescence is interspersed with thicker, longer, more erect hair-like sensilla on the dorsal surface of especially palpomere 3 and 4, around the distal margins of palpomeres 2 and 3 and the tip of palpomere 5; the articulatory membranes between the palpomeres are covered with small denticles.

Musculature (Figs. 9E,F, 12, 13): *M. tentoriopraementalis* (**M. 29/ 0la5**): O: posterior postgena close to posterior tentorial pit, ventrad 0hy3; I: the tendons of the paired muscle merge medially as a broad unpaired structure which extends over the dorsal margin of the hypostomal cavity and inserts on the posterior premental margin. *M. praementoparaglossalis* (**M. 31/ 0la11**): O: median premental region; I: middle region of the ventral glossal sclerite. *M. praementoglossalis* (**M. 32/ 0la12**): O: on the prementum promixad 0la11; I: base of the dorsal glossal sclerites. *M. praementopalpalis externus* (**M. 34/ 0la14**): small muscle; O: anteriorly on the premental arms; I: base of palpomere 1. *M. palpalpalis labii primus/ secundus* (**M. 35/36 0la16/ 17**): intrinsic muscles of the labial palp; O: base of palpomere 1/2; I: base of palpomere 2/3. *M. tentoriohypopharyngalis* (**M42/ 0hy3**): O: posterior postgena close to the posterior tentorial pit, dorsad 0hy3; I: with long tendon on hypopharyngeal button, close to the salivarium.

Brachyponera luteipes

The distal part of the postmentum bears only few small denticles instead of spine-like microtrichia (**psm**, Fig. 8D). The premental ditches are slightly deeper and narrower (**pmd**, Fig. 8D) than in *Formica*. The ventral premental face is more oval; (**pm**, Fig. 8D) the premental arms are thinner and rather short. The distal hypopharynx is also raised high above the prementum; the stabilizing lateral sclerites (hypopharyngeal rods) are very long and thin (**hyr**, Fig. 14C); the lateral surface of the distal hypopharynx (**dhy**, Fig. 7F) is set with long scales formed by comb-like microtrichia; the dorsal surface is covered by a complex microtrichial array; the dorsolateral margins are densely set with hair-like microtrichia; the apical part of the hypopharynx has a scale-like surface structure like in *Formica*, with each scale bearing a minute hair-like projection posteriorly; a dorsal smooth triangular depression of the hypopharynx is sparsely set with long microtrichia; they are more densely arranged proximally; the proximal region of the distal hypopharynx has a scale-like surface structure formed by combs of short microtrichia; the length of the microtrichia decreases further proximad towards the infrabuccal pouch; the membrane adjacent with the pouch is completely smooth. The salivary opening lies distally between the basiparaglossal brushes, directly behind the glossa; a stripe of cuticle with short microtrichia on its ventral side covers the opening (**svo**, Fig. 7E,G). The infrabuccal pouch is smaller than in *Formica* (**ibp**, Figs. 11H, 12B); the opening is also narrow; very distinct folds are present dorsally (similar position in all examined individuals); a strongly folded surface is displayed when the pouch is extruded, with widely opened mouthparts (Fig. 8A,C). The lateral sur-

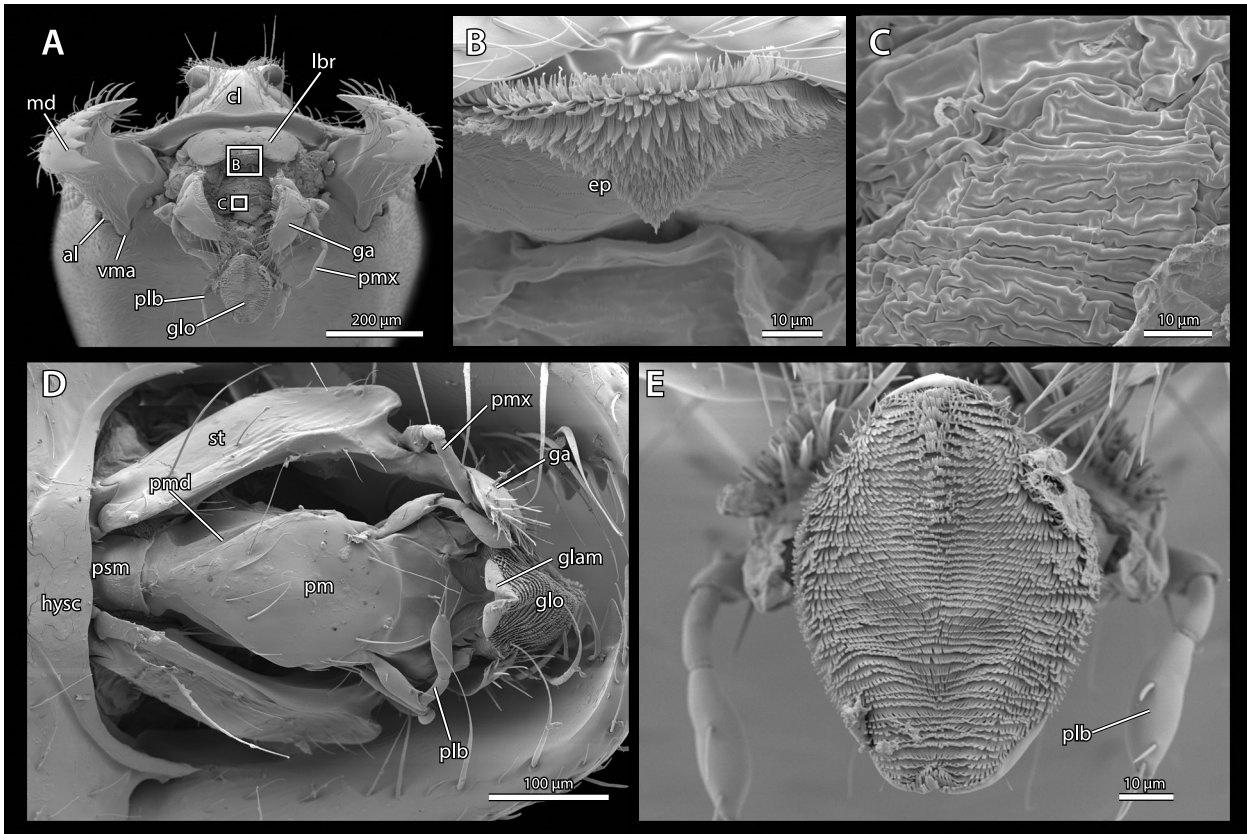


Fig. 8. SEM micrographs of the head and details of mouthparts of *Brachyponera luteipes*. **A–C,E:** Anteroventral view. **D:** Ventral view. — **Abbreviations:** al – atala; cl – clypeus; ep – epipharynx; ga – galea; glam – anterior glossal margin; glo – glossa; hysc – hypostomal carina; lbr – labrum; md – mandible; plb – palpus labialis; pm – prementum (ventral face); pmd – premental ditch; pmx – palpus maxillaris; psm – postmentum; st – stipes; vma – ventral mandibular articulation.

face of the basiparaglossal brushes is covered with rows of minute finger-like microtrichia. Reduced paraglossae are likely represented by folds of smooth cuticle with two minute distal sensilla (**pgl**, Fig. 7F,H). The broad ventral glossal sclerite is formed by a thin layer of cuticle close to the distal premental margin; it narrows towards the glossa, forming a dorsoventral flat sheet that fans out ventrally before it splits into two arms; the area between the distal premental margin and the glossa is larger than in *Formica* (Fig. 8D); most of the glossal surface is densely covered with hook-shaped microtrichia, which are thinner towards the lateral margins; the distal edge of the glossa is smooth (**glam**, Fig. 8D). The labial palps (**plb**, Figs. 7F, 8A,D) are three-segmented, with a very thin palpomere 2; the apical palpomere is club-shaped; palpomere 1 bears two ventral setae (Fig. 8D), palpomere 3 three long distal setae, a dorsal seta at about midlength, and a short terminal cone-like sensillum (Fig. 7F).

Musculature (Figs. 9G,H, 12, 14): *M. tentoriopraementalis* (M. 29/ 01a5): like in *Formica*. *M. praementopara-*

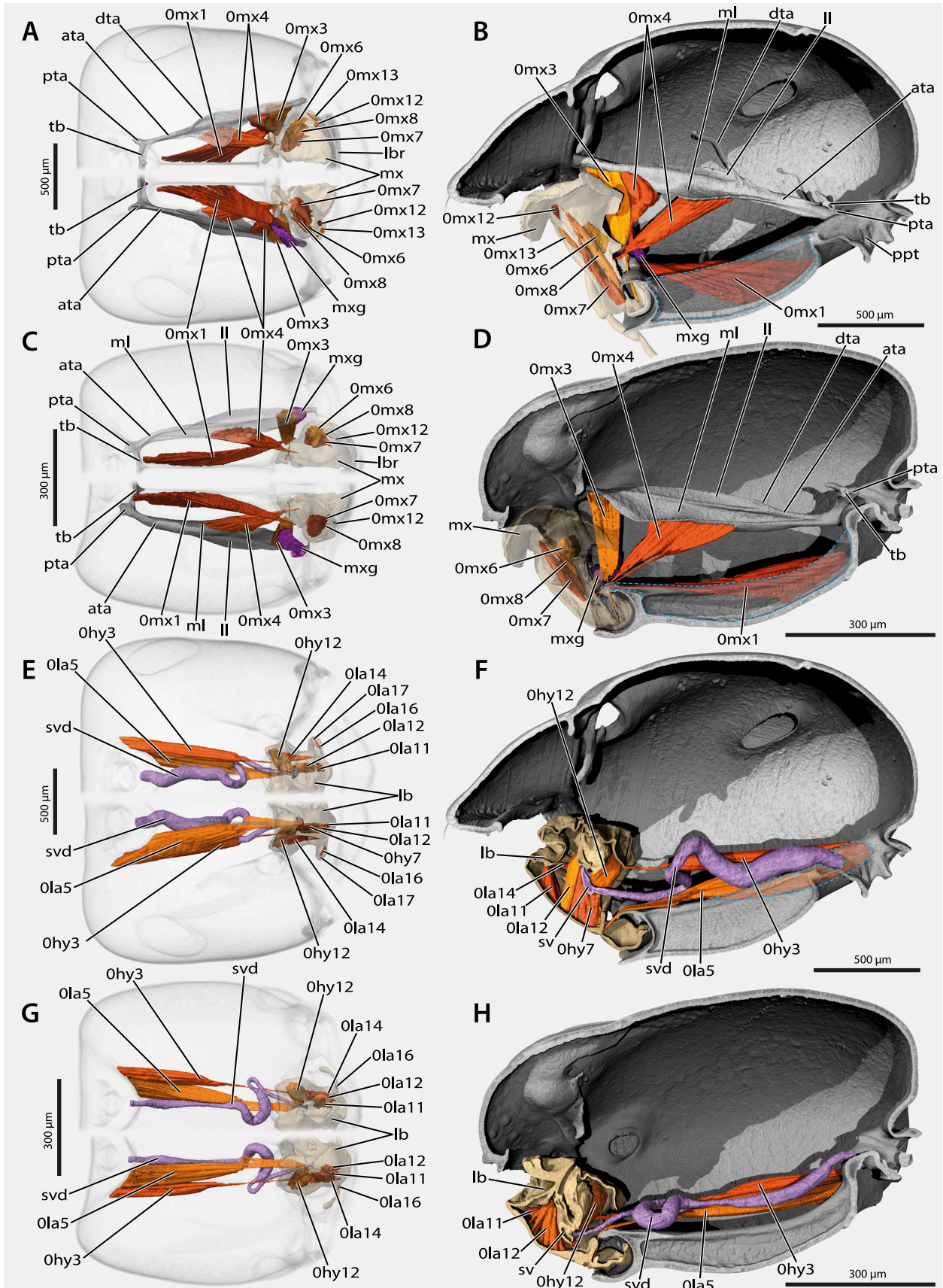
glossalis (M. 31/ 01a11): O: proximolaterally on the prementum; I: further laterad compared to *Formica*. *M. praementoglossalis* (M. 32/ 01a12): O: central premental area, distad 01a11, covering larger area of prementum than in *Formica*; I: dorsal glossal sclerites. *M. praementopalpalis externus* (M. 34/ 01a14): small muscle, very difficult to distinguish from 01a11 but otherwise like in *Formica*. *M. palpopalpalis labii primus/ secundus* (M. 35/36 01a16/ 17): only the first intrinsic muscle recognizable with the applied techniques. *M. tentoriohypopharyngalis* (M42/ 0hy3): O: very close to the posterior tentorial pit, laterad 01a5; I: hypopharyngeal button.

3.7. Salivarium and salivary duct

Formica rufa

The wall of the salivary duct (HAO_0002236) is formed by a thick layer of tissue throughout most of its length, with the diameter decreasing towards the labium (**svd**,

Fig. 9. Volume renderings of the head of *Formica rufa* (CASENT0790267: **A,B,E,F**) and *Brachyponera luteipes* (CASENT0709409: **C,D,G,H**). **A,C,E,G:** Upper part dorsal view, lower part ventral view. **B,D,F,H:** Sagittal view. **A–D:** Maxillary musculature and gland. **E–H:** Labial musculature and salivary duct. — **Abbreviations:** 0hy3 – *M. tentoriohypopharyngalis*; 0hy7 – *M. praementosalivariialis*; 0hy12 – *M. hypopharyngosalivariialis*; 01a5 – *M. tentoriopraementalis*; 01a11 – *M. praementoparaglossalis*; 01a12 – *M. praementoglossalis*; 01a14 – *M. praementopalpalis externus*; 01a16 – *M. palpopalpalis labii primus*; 01a17 – *M. palpopalpalis labii secundus*; 0mx1 – *M. cranio-*



cardinalis externus; **Omx3** – *M. tentoriocardinalis*; **Omx4** – *M. tentoriostipitalis anterior*; **Omx6** – *M. stipitolacinalis*; **Omx7** – *M. stipitogalealis*; **Omx8** – *M. stipitopalpalis externus*; **Omx12** – *M. palpopalpalis maxillae primus*; **Omx13** – *M. palpopalpalis maxillae secundus*; **ata** – anterior tentorial arm; **dta** – dorsal tentorial arm; **lb** – labium; **ll** – lateral lamella; **ml** – mesal lamella; **mx** – maxilla; **mxg** – maxillary gland; **pta** – posterior tentorial arm; **ppt** – posterior process of tentorium; **sv** – salivary sclerite; **svd** – salivary duct; **tb** – tentorial bridge. — **Colors**: beige / brown – mouthparts; grey – cuticle; orange / red – muscles; purple – glands and ducts.

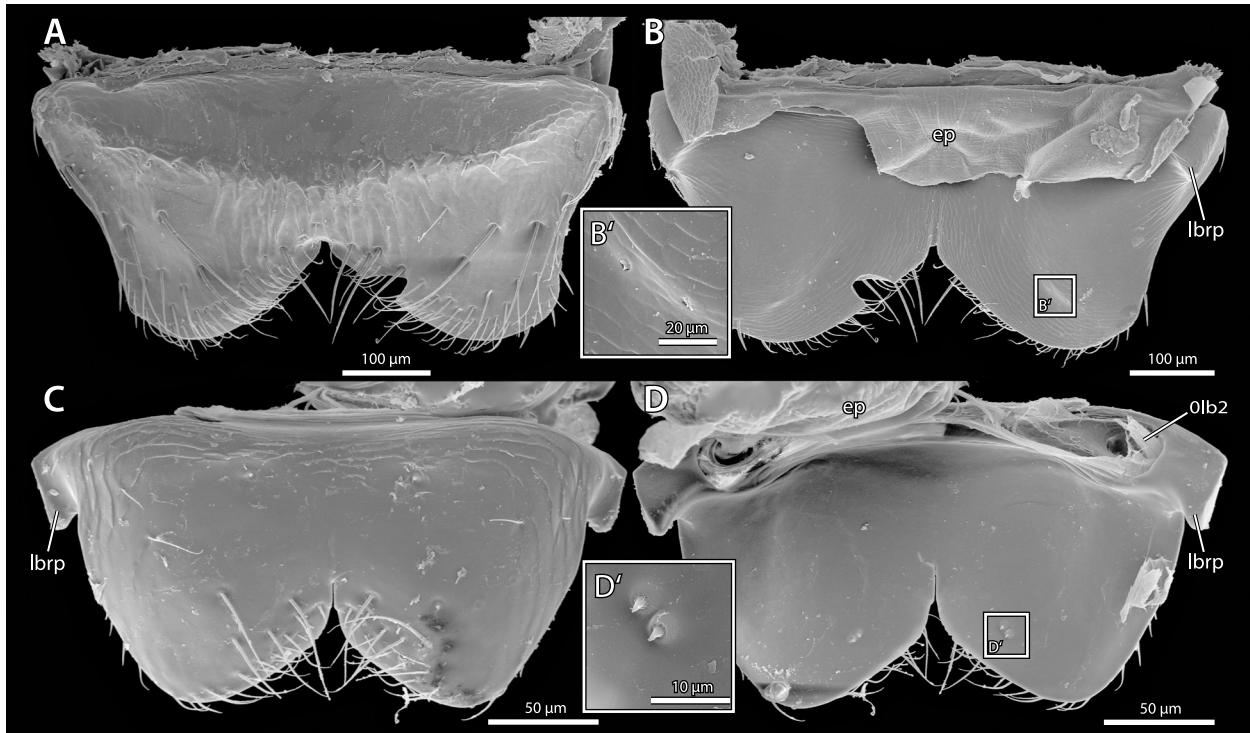


Fig. 10. SEM micrographs of the labrum of *Formica rufa* (A,B,B') and *Brachyponera luteipes*. (C,D,D'). A,B,B': Frontal view. C,D,D': Caudal view. — **Abbreviations:** ep – epipharyngeal wall; 0lb2 – *M. frontoepipharyngalis*; ep – epipharynx; lbrp – proximolateral labral processes.

Figs. 9E,F, 12A, 13E); the duct forms a loop anterior to the brain (Fig. 9E,F); it opens into the sclerotized salivarium (HAO_0000906) (sv, Figs. 9F, 13E) between the distal hypopharynx and the basiparaglossal brushes. The long, U-shaped and sclerotized salivarium encloses the salivary duct ventrally; it fuses with the hypopharyngeal button proximad its opening and to the basiparaglossal brushes distally.

Musculature (Figs. 9E,F, 12A): *M. hypopharyngosalivariialis* (M. 37/ 0hy12): two closely adjacent bundles, O: dorsolaterally from the distal hypopharynx, mostly from the stabilizing sclerites (hypopharyngeal rods); I: mesal bundle dorsally on the distal salivary duct, lateral bundle laterally on the salivarium. *M. praementosalivariialis anterior & (or) posterior* (M. 38, 39/ 0hy7): a well-developed muscle; O: prementum proximad 0la12; I: ventrally on the sclerotized salivarium, and a few fibers ventrally on the distal salivary duct.

Brachyponera luteipes

The salivary duct is also thick-walled, especially the portion forming the loop (svd, Figs. 9G,H, 12B, 14A,B), which is largely restricted to the horizontal plane in contrast to *Formica*, bending only very slightly in vertical direction (Fig. 9H). The salivarium is broader and shorter. **Musculature** (Fig. 9G,H): *M. hypopharyngosalivariialis* (M. 37/ 0hy12): like in *Formica*. *M. praementosalivariialis anterior & (or) posterior* (M. 38, 39/ 0hy7): largely reduced, no fibers originating on the prementum and inserting on the salivarium are visible in *B. luteipes* or *B. chinensis*.

3.8. Labrum

Formica rufa

The anterior surface of the trapezoid labrum (HAO_0000456) forms a distinct hump (Fig. 10A); the distal margin is bilobed, with a median notch; proximolateral processes are posteriorly directed (not visible in frontal view, lbrp, Fig. 10A,B), cone-shaped and slightly bent downwards; the bases of the maxillary palps fit below the processes when the mouthparts are retracted (Fig. S1E). The labral surface displays a scale-like cuticular surface structure, and a minute cone-shaped sensillum is inserted on the posterior surface of each distal lobe (Fig. 10B').

Musculature (Figs. 11C, 13B): *M. frontoepipharyngalis* (M. 9/ 0lb12): a moderately sized muscle; O: frontal area shortly posterad the antennal bases, laterad 0bu1; I: upon a thin, long tendon attached mesad the base of the proximolateral processes.

Brachyponera luteipes

The labrum has an even surface, without an anterior hump (Fig. 10C). The proximolateral processes are well-developed, hook-shaped and project laterad, beyond the margins of the labrum proper (lbrp, Fig. 10C,D); they fit behind the laterodistal margin of the stipes when the maxillolabial complex is retracted (Fig. S1F).

Musculature (Figs. 10D, 11F): *M. frontoepipharyngalis* (M. 9/ 0lb2): O: frontal area shortly posterad the antennal bases, laterad 0bu1, just mesad the frontal carina; I: like in *Formica*.

3.9. Distal epipharynx

Formica rufa

The distal part of the epipharyngeal wall (HAO_0000300), the unsclerotized inner wall of the labrum and the laterally free portion of the epipharyngeal wall distad the prepharynx, forms the semimembranous upper wall of the laterally open buccal cavity (**ep**, Figs. 11E, 12A,C); the surface is smooth, including the upper lip of the functional mouth opening (Fig. 12C).

Musculature: epipharyngeal muscles function as part of the cephalic digestive tract and are treated in that section.

Brachyponera luteipes

The epipharyngeal surface (**ep**, Figs. 8A,B, 11H, 12B,D) is covered with slightly wavy rows of short finger-like microtrichia; the dorsal lip of the functional mouth opening bears a brush of very long hair-like microtrichia (**white arrowhead**, Fig. 12D), expanded as a roughly triangular patch in the middle region of this structure (Fig. 8B).

Musculature: see above.

3.10. Cephalic digestive tract

Formica rufa

The cephalic digestive tract is divided into three functional subunits: the buccal cavity (HAO_0000670), the prepharynx (**pph**, Figs. 11C–E, 12A, 13A,B) (cibarium, HAO_0000201), and the pharynx (**ph**, Figs. 11A,C–E, 12A) (HAO_0001740). The buccal cavity is the space containing the mouthparts. Within this compartment, a narrow pre-oral chamber is limited by the labium and distal hypopharynx on the ventral side, the maxillae laterally, by the distal epipharynx dorsally, and by the labrum anterodorsally when the mouthparts are retracted (Fig. 11E). The distal hypopharynx posteriorly expands, forming the infrabuccal pouch (**ibp**, Figs. 11E, 12A). The lateral margins of the proximal epi- and hypopharynx fuse, thus forming an extensive prepharyngeal tube (**pph**, Figs. 11C–E, 12A, 13A,B), which anteriorly opens into the buccal cavity via the broad, fissure-shaped functional mouth (HAO_0000361) (**fmo**, Figs. 11D,E, 12B); the anteriormost section of the prepharynx, the buccal tube (**bt**, Figs. 11D,E, 12A,B), appears like a slightly flattened crescent in cross section, and is distinctly bent backwards when the mouthparts are in a retracted position (Fig. 11E); its cuticle is thick both on the anterior (epipharyngeal) and posterior (hypopharyngeal) side, and displays a peculiar banding pattern (Fig. 12A,C); the epipharyngeal side is densely covered with minute microtrichia, whereas the hypopharyngeal side display a sparse pattern of much longer hair-like microtrichia (Fig. 12C); both types of hairs are oriented towards the functional mouth; the main part of the prepharynx appears broadly crescent-shaped to oval in cross section (Fig. 13A,B); it runs parallel to the clypeus and anterior frontal region, ending posteriorly with the anatomical mouth opening (**amo**, Fig. 11E), marked by the frontal ganglion (**fg**, Fig.

11C,E) and the insertion sites of the muscles 0bu2 and 0hy1. The anterior roof of the prepharynx is sclerotized, with a broad hump (Figs. 11E, 12A), and appears fin-shaped in sagittal view (possibly representing the buccal lobe, HAO_0002412); the sclerotized prepharyngeal floor forms the sitophore plate (HAO_0000939) (**sp**, Fig. 13A); this structure bears two stabilizing elements, the oral arms (**oa**, Figs. 11C, 13B, S1G), which originate anterolaterally and are ventrally directed; they form an even curve towards the dorsal side of the prepharynx and are dorsally arranged around the anatomical mouth opening, with the dorsal portion reaching into the anterior pharynx; the posterior ends of the arms are bent outwards and form an intricate sheath-like structure which accommodates the openings of the pharyngeal gland. The pharyngeal opening, i.e. the anatomical mouth (**amo**, Fig. 11E), is not sclerotized except for the oral arms; at the level of the anatomical mouth opening the digestive tube forms an angle of about 60° (n=2), with the pharynx running straight towards the occipital foramen; its dorsal wall is deeply folded (Fig. S2C), resulting in a crescent to Y-shape in cross section. The width of the posterior pharynx decreases and it is flattened at the attachment area of 0ph2; the pharyngeal wall is finely wrinkled throughout most of its length, especially in the attachment area of 0bu2 and 0bu3 (Fig. 12A).

Musculature (Figs. 11C,E, 12, 13): *M. frontohypopharyngalis*/*M. frontooralis* (**M. 41/ 0hy1**): well-developed paired muscle (Fig. 11C,E); O: centrally on the frontal area, laterad 0bu3 (Fig. S1A); I: broadly on the posterior oral arms, on the posterior/dorsal side of the sheath surrounding the pharyngeal gland opening (Fig. 11C). *M. clypeopalatalis* (**M. 43/ 0ci1**) two subcomponents (Figs. 11E, 12A,E, 13A); M. 43a/ 0ci1a: unpaired, relatively small muscle, O: mesally on the anterior clypeus, flanked by 0ci1b (Fig. S1A); I: broadly on the anterior wall of the buccal tube, close to the functional mouth opening; M. 43b/ 0ci1b: very strongly developed paired muscle; asymmetric, with stronger bundle on one side; O: along the midline of almost the entire clypeus, intersecting with 0ci1a (Fig. S1A); I: anterior dorsal prepharyngeal wall, especially on the hump. *M. clypeobuccalis* (**M. 44/ 0bu1**): distinctly developed but much smaller than 0ci1b; paired muscle (Figs. 11E, 12A, 13B), O: posterior clypeus close to the epistomal ridge; I: dorsal prepharyngeal wall, behind the hump and anterior to the frontal ganglion. *M. frontobuccalis anterior* (**M. 45/ 0bu2**): well-developed, paired but closely adjacent along the midline (Figs. 11E, 12A), O: frontal area, distinctly posterad the supraclypeal area (Fig. S1A); I: mesally on the dorsal side of the pharynx, directly posterior to the frontal ganglion. *M. frontobuccalis posterior* (**M. 46/ 0bu3**): strongly developed, flat and unpaired muscle with two subunits (Figs. 11E, 12A), O: anterior subunit directly posterad 0bu2, posterior subunit distinctly separated from it, shortly anterad the median ocellus (Fig. S1A); I: dorsomesally on the pharynx between the dorsal longitudinal folds, posterad 0bu2. *M. frontobuccalis lateralis*/*M. tentoriooralis* (**M. 47/ 0hy2**): a relatively small,

pouch and the prepharynx (Figs. 11E, 12A, 13B), O: anterior process of the tentorial bridge with a long tendon. I: broadly on the sitophore plate. *M. tentoriopharyngalis* (M. 52/ 0ph2): relatively small, paired muscle (Fig. 11E), O: tentorial bridge and posterior tentorial arm; I: ventral side of the pharynx above and slightly posterad the suboesophageal ganglion. *M. transversalis buccae* (M. 67)/ *M. oralis transversalis* (0hy9): a well-developed layer of transverse muscles between the dorsal oral arms, directly anterior to the frontal ganglion, and an additional layer of transverse fibers connecting the arms on the ventral side posterior to the frontal ganglion (Figs. 11C,E, 12A, 12B). *M. annularis stomadaei* (M. 68/ 0st1): a thin layer of ring muscles around the pharynx behind the frontobuccal muscles. *M. longitudinalis stomadaei* (M. 69/ 0st2): weakly developed layer of longitudinal muscles below the ring musculature layer. *M. pharyngoepipharyngalis* (Mpe): very strongly developed longitudinal muscles connecting the anterior pharynx and the epipharynx: a thin unpaired median bundle on the dorsal side of the prepharynx connecting the dorsal prepharyngeal hump and the pharynx at the insertion site of 0bu3 (Mpe_d, Figs. 11C,E, 12A); paired large lateral bundles connect the posterior oral arms with the epipharynx directly before it connects with the buccal tube (Mpe_l, Figs. 11C, 13A,B).

Brachyponera luteipes

In its general features the cephalic digestive tract is similar to that of *Formica*. The bend of buccal tube is less distinct (**bt**, Fig. 11H), and almost completely straightened when the mouthparts are extruded (Fig. 12B). The lumen of the posterior prepharynx and pharynx is narrower (relative volume of cephalic digestive tract 1,2 % in *Formica*, 0,5 % in *Brachyponera*). The microtrichia on the hypopharyngeal side of the buccal tube are more densely arranged than in *Formica* (Fig. 12D). The dorsal sclerotization of the prepharynx is more pronounced and forms a short sclerotized cuticular keel on top of the more elongated prepharyngeal hump (**epk**, Figs. 11H; 12B). The oral arms (**oa**, Figs. 11F, 12B, 14B) anteriorly originate on the ventrolateral part of the sitophore plate and are bent inwards; they are not evenly curved like in *Formica* but abruptly bent in front of the frontal ganglion; their dorsal portions form nearly straight, elongate wall-like structures (Fig. S1H), which are strongly constricted at the level of the frontal ganglion (**fg**, Fig. 11F,H); posterior to this constriction, the posterior ends of the arms are strongly bent laterad and form a sheath around the openings of the pharyngeal gland as in *Formica*. The pharynx forms a slightly less distinct angle (40–50°, n=2) with the prepharynx (Fig. 11H); its lumen is very narrow and moderately flattened throughout most of its length.

Musculature (Figs. 11F,H, 12, 14): *M. frontohypopharyngalis*/ *M. frontooralis* (M. 41/ 0hy1): smaller than in *Formica* (Figs. 11F, 12B); O: centrally on the frontal area, slightly posterolaterad 0bu3 (Fig. S1B); I: narrower and concentrated on the posterior side of the short posterior end of the oral arm (Fig. 11F). *M. clypeopalata-*

lis (M. 43/ 0ci1), two components (Figs. 11H, 12B,C, 14A,D): M43a/ 0ci1a: O: similar to *Formica* (Fig. S1B), I: narrower than in *Formica*. M43b/ 0ci1b: not as asymmetric as in *Formica*; O: anterior, broad portion of the clypeus, narrowing posteriorly (Fig. S1B); I: only on the sclerotized keel of the dorsal prepharyngeal wall. *M. clypeobuccalis* (M. 44/ 0bu1): very flat but longer (and with slightly larger relative volume) than in *Formica* (Figs. 11H, 12B); O: along the thin posterior clypeal portion between the antennal sockets (Fig. S1B). I: dorsal prepharyngeal wall posterad the sclerotized keel and anterad the frontal ganglion. *M. frontobuccalis anterior* (M. 45/ 0bu2): overall similar to *Formica*, but with a different attachment angle (Fig. 11H), originating around the middle dorsal cephalic region (Fig. S1B). *M. frontobuccalis posterior* (M. 46/ 0bu3): not recognizable as a separate bundle, likely very closely adjacent to 0bu2 or reduced. *M. frontobuccalis lateralis*/ *M. tentoriooralis* (M. 47/ 0hy2): similar to that of *Formica*, but longer due to the anteriorly shifted antennal sockets (Figs. 11F, S1B); insertion area narrower due to the short posterior ends of the oral arms (Fig. 11F). *M. tentoriobuccalis anterior* (M. 48/ 0bu5) (possibly together with M.50/ 0bu6): Appears more massive, with much larger relative volume (0.9% vs. 1.7%); not constricted by the infrabuccal pouch; origin and insertion as in *Formica* (Figs. 11H, 12B, 14B). *M. tentoriopharyngalis* (M. 52/ 0ph2): very similar to that of *Formica* (Fig. 11H). *M. transversalis buccae* (M. 67)/ *M. oralis transversalis* (0hy9): a well-developed layer of transverse muscles between the straight portion of the dorsal arms of the sitophore plate, directly anterior to the frontal ganglion (Fig. 11F,H), and an additional thin layer of transverse fibers connecting the arms on the ventral side posterior to the frontal ganglion. *M. pharyngoepipharyngealis* (Mpe): very strongly developed longitudinal muscle bundles connecting the anterior pharynx and the epipharynx; the median portion of three thin dorsal bundles (Mpe_d, Figs. 11F,H, 12B) connects the posterior end of the epipharyngeal sclerotized keel with the insertion site of 0bu2; the lateral bundles attach close to the sclerotized keel; additionally, two large paired lateral bundles are present (Mpe_l, Figs. 11F, 14A), one of them originating laterally, the other one mesally on the dorsal wall formed by the oral arms; the mesal bundle inserts on the sclerotized keel and the lateral bundle on the epipharynx, where it bends into the buccal tube.

3.11. Cephalic glands

Formica rufa

The mandibular gland (HAO_0000509) (**mdg**, Figs. 5A,B, 13B) is composed of ca. 50 large cells forming a flat, cup-shaped layer, adjacent to a roughly spherical reservoir (**mdr**, Fig. 13B), which is connected to the mandalus at the dorsal mandibular base by a thin duct. From the membranous wall of the mandalus, a moderately sclerotized fold reaches towards the duct, result-

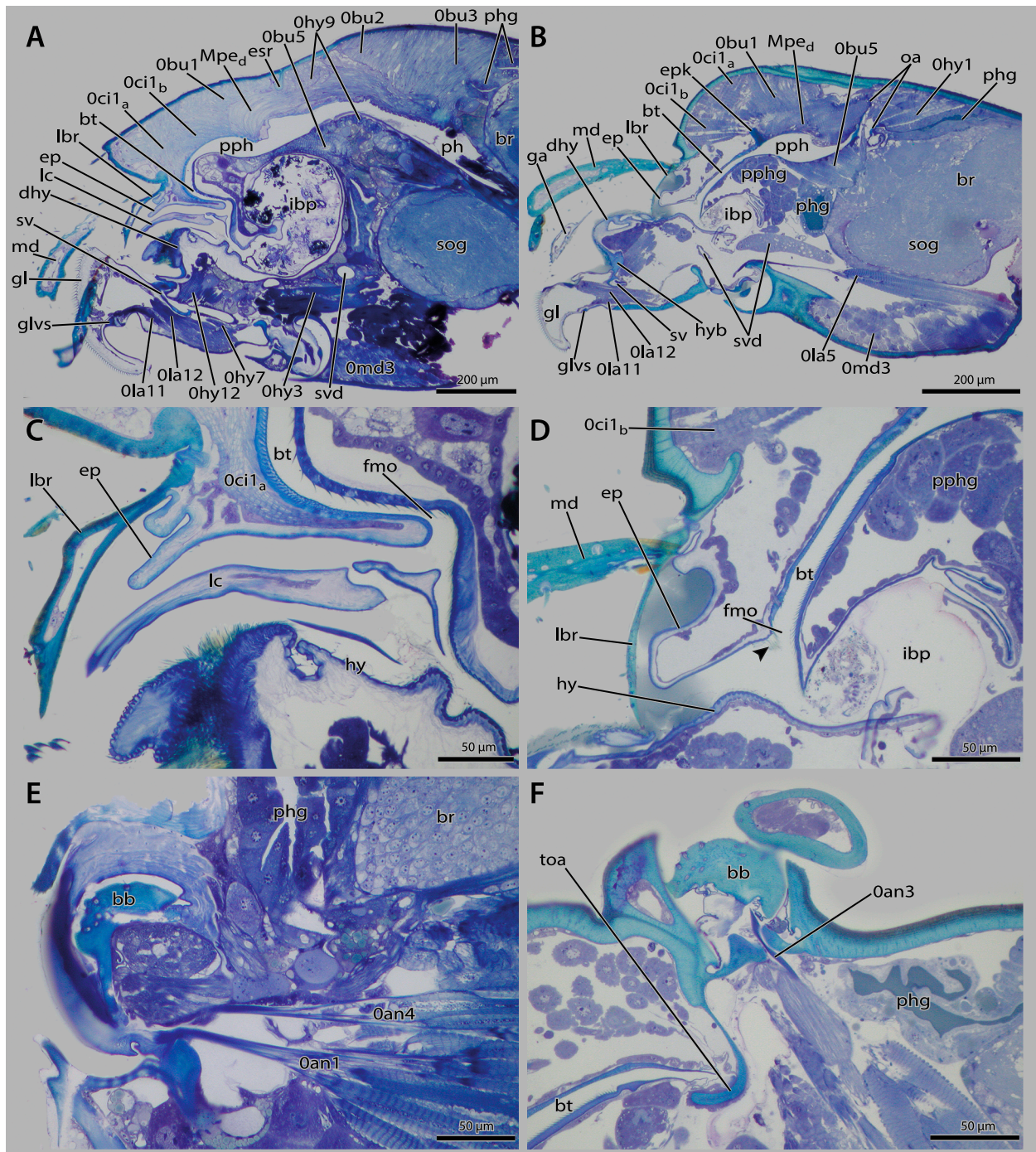


Fig. 12. Histological sections of head of *Formica rufa* (A,C,E) and *Brachyponera luteipes* (B,D,F). All sections longitudinal. **A,B:** Parasagittal region, overview. **C,D:** Parasagittal region, detail of buccal area. **E,F:** Details of antennal insertion. — **Orientation:** ← anterior region in all images except **E**: ↓ anterior region. — **Abbreviations:** **Oan1** – *M. tentorioscapalis anterior*; **Oan3** – *M. tentorioscapalis lateralis*; **Oan4** – *M. tentorioscapalis medialis*; **Obu1** – *M. clypeobuccalis*; **Obu2** – *M. frontobuccalis anterior*; **Obu3** – *M. frontobuccalis posterior*; **Obu5** – *M. tentoriobuccalis posterior*; **Oci1a** – *M. clypeopalatalis*, unpaired portion; **Oci1b** – *M. clypeopalatalis*, paired portion; **Ohy1** – *M. frontooralis*; **Ohy3** – *M. tentoriohypopharyngalis*; **Ohy7** – *M. praementosalivarialis*; **Ohy9** – *M. oralis transversalis*; **Ohy12** – *M. hypopharyngosalivarialis*; **Ola5** – *M. tentoriopraementalis*; **Ola11** – *M. praementoparaglossalis*; **Ola12** – *M. praementoglossalis*; **Omd3** – *M. cranio-mandibularis externus*; **bb** – bulbus of scapus; **br** – brain; **bt** – buccal tube; **dhy** – distal hypopharynx; **ep** – epipharynx; **epk** – epipharyngeal keel; **fmo** – functional mouth opening; **ga** – galea; **gl** – glossa; **glvs** – ventral glossal sclerite; **hyb** – hypopharyngeal button; **ibp** – infrabuccal pouch; **lb** – labium; **lbr** – labrum; **lc** – lacinia; **md** – mandible; **Mpe_a** – *M. pharyngoepipharyngalis*, dorsal portion; **oa** – oral arm; **ph** – pharynx; **phg** – pharyngeal gland; **pph** – prepharynx; **pphg** – prepharyngeal gland; **sog** – suboesophageal ganglion; **sv** – salivarium; **svd** – salivary duct; **toa** – torular apodeme. — **Symbols:** white arrow – fringe of long microtrichia along functional mouth opening.

ing in an anchor-like shape in cross-section (Fig. 13A). The flat maxillary gland (HAO_0000514) is formed by a group of about 50 slightly smaller gland cells, each

of them connected to an individual minute duct. The ducts collectively open in the membranous area laterad the cardinal base (**mxgo**, Fig. 13C). The well-developed

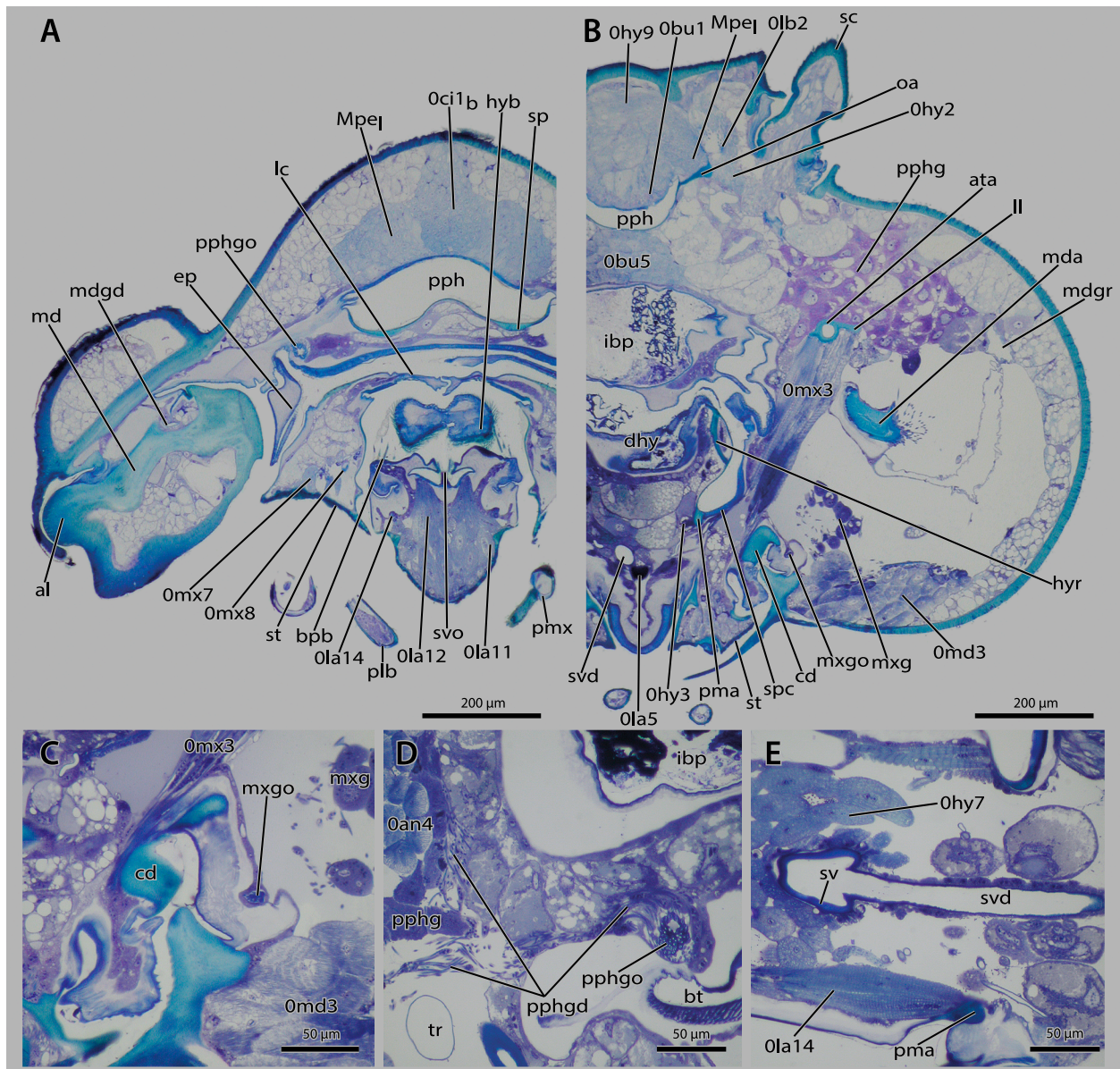


Fig. 13. Histological sections of head of *Formica rufa*. **A,B,C:** Cross sections. **D,E:** Frontal sections. — **Orientation:** **A,B,C:** ↓ ventral; **D:** ↓ anterior region; **E:** ← anterior region. — **Abbreviations:** **Oan4** – *M. tentorioscapalis medialis*; **Obu1** – *M. clypeobuccalis*; **Obu5** – *M. tentoriobuccalis posterior*; **Oci1b** – *M. clypeopalatalis*, paired portion; **Ohy2** – *M. tentoriooralis*; **Ohy3** – *M. tentoriohypopharyngalis*; **Ohy7** – *M. praementosalivarialis*; **Ohy9** – *M. oralis transversalis*; **Ola5** – *M. tentoriopraementalis*; **Ola11** – *M. praementoparaglossalis*; **Ola12** – *M. praementoglossalis*; **Ola14** – *M. praementopalpalis externus*; **Omd3** – *M. craniomandibularis externus*; **Omx3** – *M. tentoriocardinalis*; **Omx7** – *M. stiptogalealis*; **Omx8** – *M. stiptopalpalis externus*; **Ola14** – *M. praementopalpalis externus*; **al** – atala; **ata** – anterior tentorial arm; **bpb** – basiparaglossal brush; **bt** – buccal tube; **cd** – cardo; **dhy** – distal hypopharynx; **ep** – epipharynx; **hyb** – hypopharyngeal button; **hyr** – hypopharyngeal rod; **ibp** – infrabuccal pouch; **lc** – lacinia; **II** – lateral tentorial lamella; **md** – mandible; **mda** – mandibular apodeme; **mdgd** – mandibular gland duct; **mdgr** – mandibular gland reservoir; **MpeI** – *M. pharyngoepipharyngalis*, lateral portion; **mxg** – maxillary gland; **mxgo** – maxillary gland opening; **oa** – oral arm; **plb** – palpus labialis; **pma** – premental arm; **pmx** – palpus maxillaris; **pph** – prepharynx; **pphg** – prepharyngeal gland; **pphgo** – prepharyngeal gland opening; **sc** – scapus; **sp** – sitophore plate; **spc** – stipto-premental conjunctivum; **st** – stipes; **sv** – salivarium; **svd** – salivary duct; **svo** – salivary opening.

prepharyngeal (/ propharyngeal) gland laterad the prepharynx (**pphg**, Figs. 11D, 13B,D) is of rather irregular shape; mesally it extends into the space between the buccal tube and the main prepharyngeal part; it opens with numerous very thin ducts (**pphgd**, Fig. 13D) on a sieve plate at the lateral edges of the buccal tube (**pphgo**, Fig. 13A,D). The pharyngeal (“postpharyngeal”) gland (**phg**, Figs. 11A–E, 12A), by far the largest in the head (ca. 3.5% of the head volume), opens dorsolaterally into the

pharynx at the level of the anatomical mouth; its openings are stabilized by the posterior ends of the oral arms (**phgo**, Fig. S2B); it is composed of more than 40 tightly packed tubes surrounded by thick gland epithelium; it completely encloses the brain dorsally and anterolaterally; anteriorly, about four ventrally directed tubes on each side almost completely enclose the anterior pharynx; the tubes coalesce close to the openings, thus forming more extensive reservoirs.

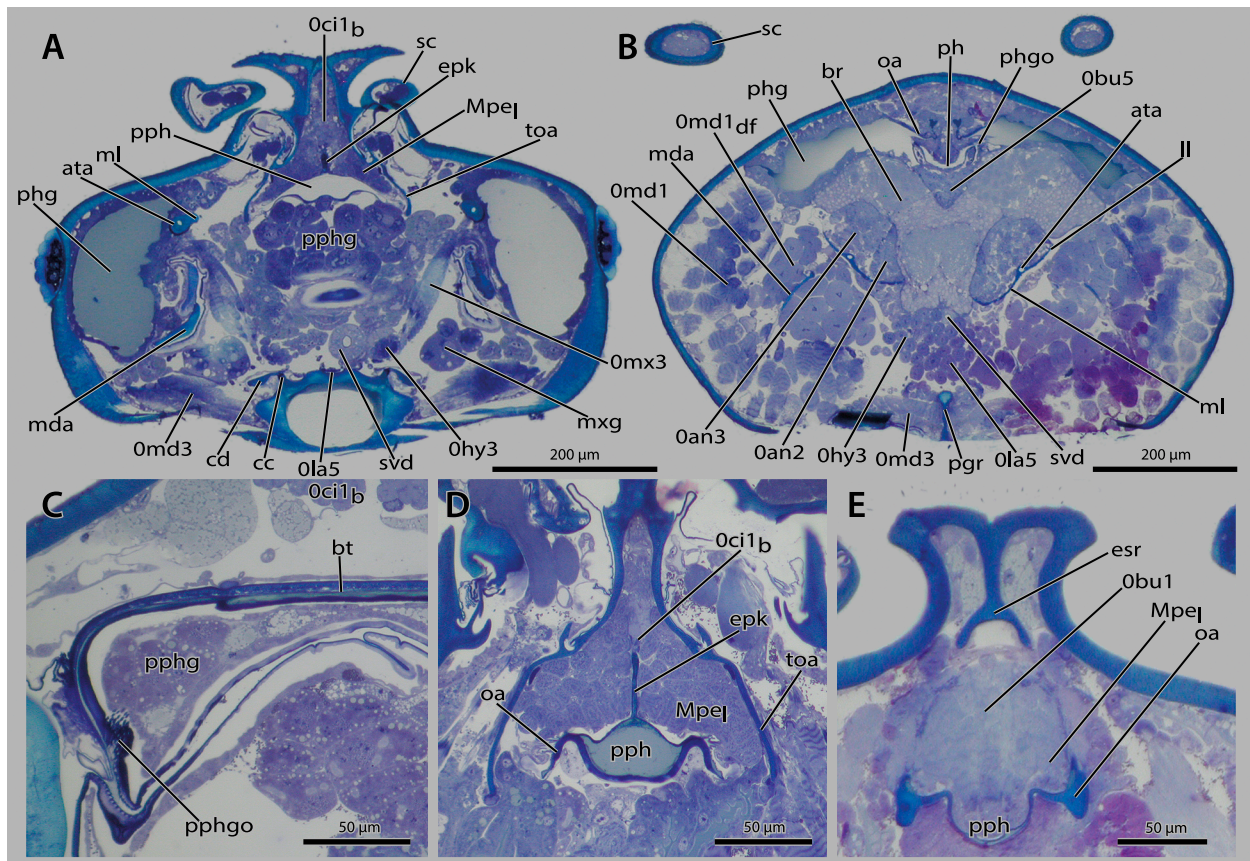


Fig. 14. Histological sections of heads of *Brachyponera luteipes* (A,B) and *Brachyponera chinensis* (D,E). All sections transverse. — **Orientation:** ↓ ventral.— **Abbreviations:** **0an2** – *M. tentorioscapalis posterior*; **0an3** – *M. tentorioscapalis lateralis*; **0bu1** – *M. clypeobuccalis*; **0bu5** – *M. tentoriobuccalis posterior*; **Oci1b** – *M. clypeopalatalis*, paired portion; **Ohy3** – *M. tentoriohypopharyngalis*; **Ola5** – *M. tentoriopraementalis*; **Omd1** – *M. craniomandibularis internus*, direct fibers; **Omd1_{df}** – *M. craniomandibularis internus*, direct fibers; **Omd3** – *M. craniomandibularis externus*; **Omx3** – *M. tentoriocardinalis*; **ata** – anterior tentorial arm; **bt** – buccal tube; **cc** – cardinal condyle; **cd** – cardo; **epk** – epipharyngeal keel; **esr** – epistomal ridge; **II** – lateral tentorial lamella; **ml** – mesal tentorial lamella; **md** – mandible; **mda** – mandibular apodeme; **Mpe_I** – *M. pharyngoepipharyngalis*, lateral portion; **mxg** – maxillary gland; **oa** – oral arm; **ph** – pharynx; **phg** – pharyngeal gland; **pgr** – postgenal ridge; **pph** – prepharynx; **pphg** – prepharyngeal gland; **pphgo** – prepharyngeal gland opening; **sc** – scapus; **svd** – salivary duct; **toa** – torular apodeme.

Brachyponera luteipes

The small mandibular gland (**mdg**, Fig. 5C,D, difficult to identify on sections) is placed more posteriorly than its equivalent in *Formica*, and the duct is slightly bent several times. The lateral mandibular pit is associated with an internal mandibular gland, represented by a thick epithelium below this concavity (**mdpg**, Fig. S2H). It is unclear whether the minute pores observed in the pit (Fig. 4F) are associated with the gland. *Brachyponera chinensis* lacks the thick epithelium observed in *B. luteipes* (Fig. S2G), even though the pit looks very similar externally. The well-developed maxillary gland is more bulbous and formed by less cells (about 35 visible on sections) (**mxg**, Figs. 9C,D, 14A). The prepharyngeal (/ propharyngeal) gland is smaller and concentrated in the space between the buccal tube and the remaining prepharynx (**pphg**, Figs. 11F–G, 12B,D, 14A,C); the cells are very densely packed. The pharyngeal (“postpharyngeal”) gland is a single sack-like structure with several flat lobes (**phg**, Figs. 11F–G, 12B, 14B); the largest, unpaired lobe reaches posterad above half of the length of the brain; smaller lobes reach anterolaterad close to the

mandibular insertions below the eyes, and small ventral lobes are present around the anterior pharynx between the brain and the infrabuccal pouch; the gland is formed by a thick epithelial layer surrounding a reservoir space; its surface is more irregular, with densely arranged small knobs reflecting the shape of the epithelial cells.

3.12. Brain and suboesophageal complex

Formica rufa

The brain (**br**, Figs. 11D,E, 12A) forms a very compact unit with the suboesophageal complex (**sog**, Figs. 11D,E, 12A), with only a narrow central passage for the pharynx; it appears small in relation to the size of the head, occupying ca. 5% of the lumen; due to the bulging mushroom bodies and large olfactory lobes it appears peanut-shaped in dorsal view. The optic lobes are well-developed, with the closely adjacent lamina, medulla and lobula forming a thick cylindrical tract connecting the brain with the compound eyes, surrounded by fibers of **Omd1**; the medulla is the largest of the optic neuropils; three thin

ocellar nerves originate on the dorsal side of the brain between the mushroom bodies (**ocn**, Fig. 11C–D). The antennal nerves extend from their origin on the anterior tips of the deutocerebral subunits (**nan**, Fig. 11C,D) through the scapus into the pedicellus and flagellum. The frontal commissures originate mesad the antennal nerves (**fc**, Fig. 11D); anterodorsally they connect with the frontal ganglion (**fg**, Fig. 11C,E), which is asymmetric: most of its mass is concentrated laterad 0bu2 rather than centrally dorsad the pharynx, where it is very thin between 0hy9 and 0bu2. Medially closely adjacent connectives link the suboesophageal complex with the prothoracic ganglion.

Brachyponera luteipes

The brain (**br**, Figs. 11F–G, 12B, 14B) fills out much more space of the cephalic lumen than in *Formica*, ca. 23% of the entire volume; its shape is elongate-rectangular and it reaches the level of the compound eyes anteriorly. The olfactory lobes and mushroom bodies are very large and similar in their general shape to the corresponding structures of *Formica* (no detailed analyses of neuroanatomy were conducted in this study). The optic lobes are less well-developed, present only as indistinct swellings of a thin optic nerve; lobula and medulla are very close to the lateral protocerebrum; the lamina is weakly developed close to the compound eye; due to the anterior placement of the eye the thin optic nerve is rather long; it curves laterad to fit through the bundles of 0md1. Ocelli and ocellar nerves are missing. Due to the location of the brain in the anterior cephalic region the antennal nerves are very short; they arise as single thick strands but divide into two branches shortly after their origin on the deutocerebrum (**nan**, Fig. 11F,G). The frontal commissures at the level of the anatomical mouth opening have a nearly vertical orientation. The frontal ganglion is placed medially above the anatomical mouth opening (**fg**, Fig. 11F,H). The suboesophageal complex appears elongated like the brain (**sog**, Figs. 11G,H, 12B).

3.13. Fat body

Both species

Fat body cells are concentrated in the anterolateral and anterior regions of the head; they also fill out most of the lumen of the mandibles and they are also present in parts of the maxillae and the labium; they are loosely arranged between other internal structures of the head.

3.14. Tracheae

Both species

The tracheae were not a special focus of this work, but from observations on the sections and μ CT-scanning data the main branching pattern appears similar to that described by RICHTER et al. (2019). Two main pairs of tracheal branches (HA_0002415) enter the head. One pair runs ventrolaterad very close to the bundles of 0md1, en-

ters the anterior head region and releases smaller antennal tracheae. The branches of the other pair split directly anterad the occipital foramen; the split branches run dorsad the brain; the main branches run below the brain.

4. Discussion

4.1. Homology based terminology for comparative anatomical studies

RICHTER et al. (2019) clarified the homology of the cephalic digestive tract in ants for the first time. This is just one example for persisting questions of the homology of morphological structures in ants. Establishing homology is an important prerequisite for any comparative anatomical work, and also for the formation of meaningful evolutionary hypotheses. Furthermore, using a consistent terminology based on a solid homology framework can help to make morphological data better suited for analyses by computer algorithms (SILVA & FEITOSA 2019). In the present work, we try to use the terminology suggested by the HAO wherever possible to support the goal of achieving a consistent terminology for all Hymenoptera and ultimately all insects. However, it should be noted that the terms in the HAO are not based on homology in the sense of structures being traced back to a common ancestor, and are thus not hypotheses of homology as applied in the present work (SELTMANN et al. 2012). Several homology issues are addressed throughout the discussion of the present study (mainly the identity of the hypostoma and the identity of several muscles associated with the cephalic digestive tract). However, a complete understanding of formicid cephalic structures linked with general insect morphology (e.g. SNODGRASS 1935; BEUTEL et al. 2014) will be a continuous process over the next years and requires more intensive anatomical investigations.

4.2. Volume measurements based on μ CT scans

μ CT-scans have a great potential for qualitative analyses of the anatomy of insects and other organisms (e.g. FRIEDRICH et al. 2014; WIPFLER et al. 2016). Moreover, they are a valuable source of quantitative data such as volumes of individual structures. This was used to great effect for instance by LILICO-OUACHOUR et al. (2018) to demonstrate specialized morphological traits in different castes of the hyperdiverse ant genus *Pheidole* Westwood, 1839. However, there are several potential technical problems with this technique that we will discuss briefly. In our case, the contrast of the used μ CT scans was not sufficient for a distinct separation of all tissues based on grey scales. Perfect manual segmentation is possible on principle, but would be extremely time consuming, and would not have been justified by the aims of the present study. The calculated volumes as such (see supplementary material

File 2) do not reflect the actual volumes of the scanned structures perfectly. Furthermore, the preparation method has a strong impact on the volume of internal structures. Different preparation methods such as fixation, staining and drying (or scanning in ethanol as was done in the present study) can influence the contrast as well as potential shrinkage, significantly influencing the resulting volumes (see e.g. SOMBKE et al. 2015; GUTIÉRREZ et al. 2018). An additional problem in the present study is that only one specimen of each *F. rufa* and *B. luteipes* were entirely segmented, thus disregarding potential intraspecific differences. An example for potential problems is the apparently non-functional “Muscle X” found in one *F. rufa* specimen. While in our case this aberrant feature could be clarified in comparison with a series of other specimens, other irregularities might be more difficult to interpret and could affect qualitative as well as quantitative morphological results. Taking all these problems into consideration, we used only very clear tendencies in the calculated volumes, also supported by visible relative size differences between the two species to draw tentative conclusions. In the previously mentioned study of LILICO-OUACHOUR et al. (2018), the authors do not give any details on how structures were segmented before volume calculation. The images (figs. 2–5) clearly show that not all muscles were reconstructed. Especially the muscles of the maxilla and labium are missing completely (intrinsic muscles) or at least partly (extrinsic muscles). While this is not necessarily a problem for the purpose of that particular study, we advocate that in the future, all aspects that can potentially influence the results of volume calculations based on μ CT-scans should be reported, to increase the comparability of the results.

4.3. The head capsule

One of the most prominent features of the ant head is its prognathism, with the mouthparts rather than the antennae placed at the forefront of the head. This was already recognized as apomorphic feature of Formicidae by BOLTON (2003), BOUDINOT (2015), RICHTER et al. (2019) and others. Among many plausible factors, prognathism is often associated with ground-dwelling and/or predacious habits (e.g. in carabid beetles, EVANS 1994) or with a preference for subcortical habitats (BEUTEL 1997). It is a feature that has evolved multiple times independently across insects with different functional and morphological backgrounds (e.g. BEUTEL et al. 2014). In contrast to other groups of Holometabola (e.g. beetles and Raphidioptera), the prognathous orientation in ants is achieved by a distinct elongation of the postgenal bridge, resulting in anteriorly directed mandibles opposite to the posteriorly directed postocciput. The exact position and angle of the occipital foramen on the back of the head is variable across Formicidae and possibly related to their specific lifestyle. The prognathous configuration also leads to far-reaching changes in the orientation of internal cephalic structures such as the tentorium, muscles, brain,

and digestive tract (see below). As in other prognathous insects, ants show a high diversity of mandibular shapes, particularly with regard to pronounced mandibular elongation (Formicidae: GOTWALD 1969; Megaloptera: CONTRERAS-RAMOS 2011; Carabidae: BALL et al. 2011). Prognathism of ants is linked to profound changes such as the shift of the origin of *M. craniomandibularis externus* Omd3 to the postgenal ridge, instead of the lateral head capsule as in other Aculeata (ZIMMERMANN & VILHELMSSEN 2016). This very unusual condition potentially facilitated the diversification of mandibular shapes in ants. The prognathous head orientation is arguably a key feature of ants and of high relevance to our understanding of their evolution. However, as pointed out above, the moderately inclined head of ants, differs distinctly from a horizontally oriented prognathous and posteriorly retracted head as found in other groups such as Coleoptera and Raphidioptera.

Several other features of the head capsule are characteristic for ants and shared among all subgroups. A concave occipital region, the lack of epicranial sutures as zones of weakness associated with ecdysis, and the inflected clypeus are ground plan features of Hymenoptera (e.g. BEUTEL & VILHELMSSEN 2007; VILHELMSSEN 1996). The general configuration of the occipital foramen is shared with many other apocritan groups (ZIMMERMANN & VILHELMSSEN 2016): it is narrow, more or less dumbbell or hourglass-shaped and enclosed by the collar-like postocciput. However, the exceptionally strong constriction of the postocciput is a potential autapomorphy of ants, further narrowing the foramen and increasing the movability of the head. In worker ants, the combination of a very narrow postocciput and large prothorax with strongly developed cervical musculature (KELLER et al. 2014; LIU et al. 2019) leads to a very flexible head-to-thorax articulation, allowing ants to lift and carry loads with their anteriorly directed mandibles (e.g. NGUYEN 2014). An aspect of ant cephalic morphology that has rarely been discussed previously is the raised middle portion of the clypeus and anterior frontal region. PRENTICE (1998) associates a strongly convex clypeus with the presence of a proboscis. This condition creates space for strongly developed muscles of the sucking pump, required for operation. As the clypeus is at least “moderately convex” in most apoid taxa (PRENTICE 1998), which also applies to *Formica*, this condition is probably generally related to the uptake of liquid food (PAUL & ROCES 2019). The very strongly raised condition in ants such as species of *Brachyponera* and other ponerines is possibly rather a side effect of the antennal approximation than an adaptation to a specific mode of food uptake.

Another insufficiently studied feature is the hypostoma. Its externally visible part, the hypostomal carina, is sometimes used as a taxonomic character (usually referred to as hypostoma, e.g. EGUCHI 2006; LUCKY & WARD 2010). The hypostoma forms the ventral margin of the oral foramen. It is distinctly concave in ants, forming a distinct emargination (**hyc**, Figs. 5F,H, 11A,B) together with the usually broad hypostomal carina (**hysc**,

Figs. 1C,F, 2C,F, 11A,B). This hypostomal cavity (**hyc**, Figs. 5F,H, 11A,B) receives and protects the base of the maxillolabial complex, mainly the cardines and the postmentum, especially when the complex is retracted (Fig. 9B,D,F,H). Another feature of the hypostoma, already described in detail for *Wasmannia affinis* (RICHTER et al. 2019), are the triangular processes (previously interpreted as part of the postgena) reaching into the oral foramen, which partially separate the mandibular cavities from the main oral foramen (**hysp**, Fig. 11A,B). In all examined species (including other aculeatans with this condition, OSTEN 1982), the lateral margins of these processes interact with the mandibular bases, stabilizing the mandibles as they operate. Their medial margins interact with the stipes when the maxillolabial complex retracts. However, among the three species examined, a distinct concavity of the process fitting with the stipes is only present in *Formica*. This interaction is probably part of a tight closing mechanism of the oral foramen (see below). The shape of the processes is highly variable across ants, with a steep lateral margin in both *Wasmannia* and *Formica*, but a much more gradually ascending margin in *Brachyponera*. *Brachyponera* is also lacking an additional smaller process bordering the pleurostomal fossa mesally, which is present in species of both other genera (white arrowhead, Fig. 11A). The differences in the shape and size of the processes may have an effect on mandibular movements likely relevant in a functional context.

The frontal carinae are almost always present in ants. They probably increase the mechanical stability of the cuticle of the frontal region, especially around the antennal foramina which sustain the forces of the usually long antennae. The antennal insertions are obviously another key feature in the evolution of ants. KELLER (2011) analyzed this character system in great detail, revealing the phylogenetic relevance of the torular or frontal lobes and the antennal acetabulum. Further analyses of this character system appear highly promising. The present study also revealed some differences in the antennal musculature. While the extrinsic antennal muscles of *Formica* are similar in size, one muscle is distinctly larger in *Brachyponera*. Moreover, all muscles are more steeply oriented in the head, related also to varying tentorial shapes. These differences are likely linked with the pattern of antennal movements. This was previously investigated by EHMER & GRONENBERG (1997) in the context of the trap-jaw mechanism of *Odontomachus*. Fast retraction of the antenna is important in this case to avoid damage of the appendage by the powerful mandibular strike. Although the authors did not homologize the muscles, they describe an enlarged “retractor” muscle which appears to correspond to the enlarged *Oan3* in *Brachyponera*. A more detailed analysis of the antennal articulation and associated musculature has certainly the potential to improve our understanding of ant evolution. The antennae of ants are not only a very important sensory organ (e.g. HASHIMOTO 1990), but also used in communication (e.g. LENOIR 1982), underscoring their importance for the evolution of social behavior.

A highly variable feature is the shape of the head. While the external contours often reflect underlying features such as specific muscular arrangements (see present work; PAUL 2001; RICHTER et al. 2019), its phylogenetic information content is questionable due to the strong adaptive aspect. Nevertheless, the highly variable and specific shapes of the head capsule often provide useful taxonomic information (e.g. BROWN 1948; LONGINO 2006). Aside from this they can be relevant in a functional and evolutionary context, as recently demonstrated by analyses of the integration of different body parts in the ant genus *Pheidole* Westwood, 1839 (FRIEDMAN et al. 2019).

One of the least studied character systems of ants is the cephalic endoskeleton. Its main functions are stabilizing the head capsule and providing space for muscle attachment (such as the antennal muscles discussed above), as it is almost always the case in insects (e.g. BEUTEL et al. 2014). The present study and the previous work on *Wasmannia* reveal some noteworthy differences. The tentorium varies considerably in shape. The general configuration with long anterior arms (**ata**, Figs. 5E–H, 11A,B, 13B, 14B, S2) with lamellar extensions (**ml**, **ll**, Figs. 5E–H, 11A,B, 13B, 14B), a short bridge (**tb**, Figs. 5E–H, 11A,B), and short posterior arms (**pta**, Fig. 5E–H) is very similar across all species and also shared by other groups of Aculeata (ZIMMERMANN & VILHELMSSEN 2016). What differs from other aculeates, however, is the frequent reduction of the dorsal arm (**dta**, Figs. 5E,F, 11A, S2F). Whereas it is distinctly developed in *Formica*, *Lasius* (KUBOTA et al. 2019), and also *Opomyrma* Yamane, Bui & Eguchi, 2008 (YAMADA et al. 2020), it is entirely missing in the myrmicines *Wasmannia* (RICHTER et al. 2019) and *Melissotarsus* Emery, 1877 (KHALIFE et al. 2018). In *Brachyponera*, a triangular base of the dorsal arm is visible at the posterior end of the lateral lamella, followed by a very thin and relatively short anteriorly directed tube. This particular configuration of the dorsal arm may be linked with the large size of the brain in *Brachyponera*, reducing the space for the dorsal arm. Other differences concern the shape and extension of the lamellae of the anterior arm. They are very strongly developed in *Brachyponera*, smaller in *Formica* and *Lasius* (KUBOTA et al. 2019), and thin but rather elongated in *Opomyrma* (YAMADA et al. 2020). The lateral lamella is completely reduced in *Wasmannia* and apparently also in *Melissotarsus* (KHALIFE et al. 2018). Interestingly, the secondary tentorial bridge (ZIMMERMANN & VILHELMSSEN 2016: figs. 1, 2, **stb**) is reduced in all investigated species except for *Melissotarsus* (KHALIFE et al. 2018), and the posterior processes in all species but *Formica*. Both structures are almost always parts of the aculeatan tentorium (ZIMMERMANN & VILHELMSSEN 2016). At present, the available information is not sufficient for a reliable evolutionary interpretation of endoskeletal character transformations across Formicidae. The structural affinities between *Wasmannia* and *Melissotarsus* on one hand, and between *Formica* and *Lasius* on the other, suggest that the tentorial shape may be generally conserved on the subfamily level.

Another structure of the cranial endoskeleton that has received little attention is the torular apodeme. This internal expansion of the antennal acetabulum was found in all species we have investigated to date, but is almost entirely neglected in the literature. It is noteworthy that it was already described for formicines by LUBBOCK (1877), but obviously forgotten afterwards. While the process is just an elongation of the acetabulum in *Wasmannia* (RICHTER et al. 2019: phragma of the acetabulum), it is a distinct, flattened process in *Brachyponera* and a distinct tubular process in *Formica*. The single obvious function of the process is that it serves as area of origin for *M. tentoriooralis* (0hy2). According to LUBBOCK (1877) its free end bends when the antenna is moved and elastically reverts to its original position, moving the entire appendage back to its resting position. However, the process is neither connected to the antennal muscles, nor directly to the antenna. It thus appears unlikely that it plays a role in antennal movements. An alternative interpretation would be that this structure stabilizes the torulus/ antennal insertion. Further investigations will be necessary to clarify the diversity and function of this remarkable structure which is apparently unique to ants. Especially the functional consequences of the shift in origin of 0hy2 should be evaluated.

4.4. The mouthparts

The mandibles apparently played a key role in ant evolution. The highly modified secondary (dorsal) mandibular joint, described in detail for *Wasmannia*, is certainly an apomorphy of Formicidae. It distinctly increases the degrees of freedom at the mandibular base and thus the flexibility of mandibular movements (B. Wipfler pers. comm.), probably contributing to the potential of these mouthparts as an all-purpose tool (GRONENBERG et al. 1997). A more detailed analysis of this specific character is currently in preparation (R. Keller and coworkers). The importance of the mandible in the evolution of Formicidae is underscored by its sheer structural diversity. The impressive spectrum of shape variations (GOTWALD 1969) includes forms with a strong degree of elongation (e.g. LATTKE et al. 2018), different trap-jaw species (LARABEE & SUAREZ 2014), and some cretaceous fossils with bizarre and highly derived mandibles (e.g. BARDEN & GRIMALDI 2016; CAO et al. 2020). Understanding the evolution of this diversity will likely lead to important insights in ant evolution in general. The mandibles of the generalist species investigated in the current work are both of the characteristic triangular, torqued form as defined by KELLER (2011). An interesting question in this context is whether this condition evolved once in the last common ancestor (with multiple secondary variations), or independently in the poneroid and formicoid clades, respectively. The latter case would imply a remarkable scenario of parallel evolution. The current study did not reveal any structural features supporting convergence. Consequently, the triangular condition is a potential

synapomorphy of the poneroid-formicoid lineage, i.e. Formicidae excl. Martialinae and Leptanillidae (B. Boudinot, pers. comm.). As a triangular mandibular shape is an isolated phenomenon in related groups (e.g. some Mutillidae and Vespidae) and narrow curved mandibles occur in different stem group ants and also in Leptanillinae and Martialinae (B. Boudinot pers. comm.; LABELING et al. 2008; CAO et al. 2020), the triangular shape is possibly not part of the formicoid groundplan. Observed differences such as the angle and length of the masticatory margin plus dentition are most likely related to dietary preferences. Further minor differences can be found in the articulatory surface, such as a deeper mandibular acetabulum. Interestingly, a specific depression anterior to the mandalus (the trulleum in *Wasmannia* and a much smaller crescent-shaped depression in *Formica*) is present in formicoid species, whereas this structural modification is completely missing in *Brachyponera*. The trulleum is likely linked with an additional stabilization of the mandible via a canthellus in some myrmicine ants (RICHTER et al. 2019). However, it cannot be excluded that a depression anterior to the mandalus is functionally associated with mandibular gland secretion. An interesting character of the mandible of *Brachyponera* is the presence of a lateral mandibular pit. This concavity is characteristic for several ponerine lineages (*Cryptopone* Emery, 1893, *Euponera* Forel, 1891, *Pseudopone* Emery, 1900; SCHMIDT & SHATTUCK 2014). It is much deeper in *B. senaarensis* than in the investigated *B. luteipes* and *B. chinensis* (BILLEN & AL-KHALIFA 2016: fig. 1c). In *B. senaarensis* and *luteipes*, the pit is associated with an intramandibular gland of unknown function. Examined serial sections of *B. chinensis* did not show an intramandibular gland (possibly an artefact of fixation), suggesting considerable intrageneric variation in this character. This underlines the necessity to investigate even closely related taxa for a reliable reconstruction of the evolutionary history of specific features.

The high diversity of mandibular shapes is also reflected by linked internal structures, especially the large apodeme of 0md1 and the three mandibular muscles. The presence of different fiber types has been investigated in detail by GRONENBERG et al. (1997), and some differences in the apodeme configuration were documented by PAUL & GRONENBERG (1999). Although our data are not sufficient to perform detailed analyses of fiber type configurations, they fit in the picture outlined in these previous works. A general feature of ants is the presence of one lateral and one mesal strand of fibers with fast contraction properties, and attached directly to the main body of the 0md1 apodeme. These are surrounded by insertion sites of fibers with different degrees of slow contraction properties, attached either directly or via thread-like extensions of the apodeme. Like GRONENBERG et al. (1997) we mainly found directly attached fibers in the ponerine *Brachyponera*, and mostly fibers attached via threads in *Formica*. The suggestion of different trends in fiber type distribution across different phylogenetic lineages thus gets new support. Concerning the apodeme confi-

guration, a tri-partition of the adductor tendon is likely a general feature in ants. However, at least one of the three branches is very small in most groups, and a clear phylogenetic pattern with respect to the length or shape of these subdivisions is presently not recognizable. An interesting feature is the presence of an accessory branch originating dorsally on the central branch, attachment site of an isolated occipital fiber bundle of Omd1. This has been found in *Wasmannia* (RICHTER et al. 2019), *Formica* and *Brachyponera*. PAUL & GRONENBERG (1999) described it only for *Diacamma* sp. and *Ectatomma ruidum* (Roger, 1860). It is conceivable that it was overlooked in other species and is in fact a very conserved feature. Further study of this character system will likely yield interesting insights into the specific functional properties of the ant mandible and potentially also phylogenetically relevant features.

Compared to the mandibles, the maxillo-labial complex of ants is clearly conserved. While different modes of proboscis formation occur in many other aculeate groups (e.g. OSTEN 1982, 1988; PRENTICE 1998; KRENN 2002), this condition is unknown in ants. While adult ants take up only liquid food (e.g. PAUL et al. 2002; PAUL & ROCES 2019) like their aculeate relatives, ant species feeding on plant sap mainly consume sugary exudates of plant sucking insects or plant sap from open “wounds”, rather than taking up nectar directly from flowers (LACH et al. 2010). Furthermore, their small body size often enables them to crawl into flowers to reach nectar. The selective pressure to reach deep into flowers with the mouthparts and to evolve a proboscis as a consequence is thus limited in ants. Another possible explanation is an ancestral soil dwelling lifestyle (LUCKY et al. 2013), making plants a much less accessible food source compared to flying insects. What can be found instead in many ant species is a tight closure of the preoral space. KELLER (2011) documented different interlocking mechanisms linking the labrum with the maxilla. This can be achieved by interaction of the labral processes with an extended distal stipital margin (as in *Brachyponera*), the flat lateral part of the stipes (as in *Wasmannia*, RICHTER et al. 2019), or with the base of the maxillary palp (as in *Formica*). Additional locking mechanisms can include stipital and premental grooves interacting with the distal labral margin (KELLER 2011; RICHTER et al. 2019). A tightly closed preoral space is probably advantageous during activities like digging in the ground (OSTEN 1982) or hunting, protecting unsclerotized elements of the mouthparts and buccal cavity.

The presence of small denticles on the surface of the cardo of ants was described by RICHTER et al. (2019) for the first time. Here we confirm that this surface sculpture also occurs in *Formica*, and that additional small setae occur in *Formica* and *Brachyponera*. Such an armature on the proximal maxillary element is apparently common in ants. While small setae may play a role as proprioceptors, the denticles possibly reduce energetic output for holding these maxillary parts in a particular conformation (B. Boudinot, pers. comm.).

Some variation in the armature of the maxillo-labial complex was already documented by GOTWALD (1969). Different specific structural elements such as a galeal crown, galeal comb, and lacinial comb are also present in other apocritan groups (e.g. POPOVICI et al. 2014). An interesting aspect is the structure of the lacinial comb. While it is usually formed by setae (e.g. in *Formica*), we observed a comb formed by thick cuticular spines without articulation in *Brachyponera*. GOTWALD (1969) did not mention unarticulated spines for any other ant species. However, illustrations of maxillae of many species now assigned to Ponerinae (e.g. *Hypoponera opacior* [Forel, 1893], *Platythyrea schultzei* Forel, 1910, *Simopelta oculata* Gotwald & Brown, 1967, *Neoponera commutata* [Roger, 1860]) show rather thick spines with a broad base. It is thus conceivable that Gotwald misinterpreted fixed spines as thickened setae, and that all these species share the condition found in *Brachyponera*. This suggests an interpretation as an apomorphy characterizing at least Ponerinae and possibly additional groups. A link with carnivorous habits is likely, as the concerned species are mostly predators (e.g. SCHMIDT & SHATTUCK 2014). A character with a certain degree of variation is the patch of microtrichia on the internal/ventral surface of the lacinia. While it is largely reduced in *Brachyponera*, there are two patches (one larger, one of moderate size) in *Formica* and one moderately sized patch in *Wasmannia*. While the microtrichial patch as such is obviously a conserved groundplan condition in ants, its specific configuration is likely correlated with functions of the lacinia, such as food uptake or cleaning the body surface.

The musculature of the maxilla is highly conserved in ants. Our findings conform with previous results such as PAUL et al. (2002) and RICHTER et al. (2019). The only distinct variation concerns Omx4, which can be undivided or composed of two separate bundles, with two tendons even in the case of a single subunit (see *Brachyponera*). However, in all cases the tendons insert on the stipes very close to each other, and they even fuse in *Formica*. Variations in size, specific shape or also sarcomere length (see PAUL et al. 2002) of the individual muscles may be interesting in a functional context. Omx1 for instance is larger in *Formica* than in *Brachyponera* (relative to head size), and an oblique Omx3 is a characteristic of *Wasmannia* (RICHTER et al. 2019).

The sensilla of the maxillary and labial palps show some variation, especially in the density of setae on the different palpomeres. Our observations suggest a trend towards reduced numbers in species with smaller body size (*Brachyponera*, *Wasmannia*, RICHTER et al. 2019), whereas setae are densely arranged on all palpomeres in larger species, as for instance in *Formica*. The sensilla of the labial palps were used for phylogenetic reconstruction by HASHIMOTO (1991). His coding of the density of setae for different subfamilies agrees with RICHTER et al. (2019) and the present study. However, our (unpublished) observations on *Acromyrmex aspersus* (F. Smith, 1858) show that this larger myrmicine has a rather dense pattern of microtrichia on its palpomere, in conflict with

HASHIMOTO's coding for the subfamily. This indicates that the character shows more variation than previously suggested.

The labial muscles are largely conserved like those of the maxilla. While *Oba5* originates on the posterior tentorium in *A. aspersus*, its usual area of origin is apparently the postgenal area close to the occipital foramen. Other differences concern mostly the size and sarcomere length (PAUL et al. 2002), potentially interesting in a functional context, but likely phylogenetically uninformative.

The infrabuccal pouch of ants has been studied with respect to its function (e.g. EISNER & HAPP 1962; QUINLAN & CHERRET 1978; FEBVAY 1981). The morphology and ultrastructure were recently investigated (WANG et al. 2019). Though some of the morphological interpretations of WANG et al. (2019) are questionable (e.g. labelling the galeolacinal complex as “hypopharyngeal plate”, fig. 3B), they provide a detailed documentation of different kinds of microtrichia and the cuticular surface structure of different areas of the pouch. The results generally conform with our observations. Groups of microtrichia on cuticular scales are visible on the surface of the distal part of the pouch, whereas honeycomb-like plates with more or less distinct folds are present proximally, with a transition area between the two patterns. While the infrabuccal pouch is usually referred to as a “filtering device”, actual filtering is achieved by microtrichia and setae of the mouthparts and on the epi- and hypopharynx (including the buccal tube), with the pouch functioning as a storage device for the processed material. WANG et al. (2019) demonstrated that the size of the pouch varies depending on the amount of material it contains. This makes comparisons between species difficult, even though distinct differences among taxa do occur. In *Formica*, for instance, the pouch is unusually large, thus displacing parts of muscle *Obu5/6*. Another interesting variation is the presence of three folds on the dorsal side of the pouch in *Brachyponera*, which were observed in all investigated species and specimens of the genus. These structures probably facilitate the enlargement of the pouch when it contains a large mass of substrate. The position of such “reserve folds” is possibly conserved, at least at species level.

A structure rarely described in detail is the salivary duct. Even though this structure is apparently rather uniform, certain differences can be found within ants. A similar condition is found in *Formica* and *Brachyponera*, where the duct runs through the ventral region of the head capsule, forming a loop anterad the brain and finally connecting to the sclerotized salivarium. The wall is formed by a thin cuticle and a layer of tissue cells with a decreasing thickness at the level of the labium. The loop is partly vertically oriented in *Formica*, which is not the case in *Brachyponera*, probably due to the limited space between the brain and infrabuccal pouch. A slightly different condition is found in *Wasmannia affinis*: the duct appears thin throughout its entire length (although different protocols for histological sections may play a role) and a loop is missing completely (RICHTER et al. 2019).

The loop probably facilitates the extension of the duct when the maxillolabial complex (including the salivarium) is protracted. However, this raises the question why it is absent in some species. Further investigations of the salivary duct may clarify functional issues and possibly provide phylogenetic information.

Another interesting structure linked with the salivarium is muscle *Ohy7*. It is generally reduced in Aculeata according to ZIMMERMANN & VILHELMESEN (2011), but a muscle originating on the prementum and inserting on the salivarium was identified in *Wasmannia* (RICHTER et al. 2019) and now also observed in *Formica*. It is missing in *Brachyponera*, but at least a very small muscle in this position is present in some other ponerines we examined. The current data suggest that this muscle may be absent in the groundplan of Aculeata, with reversal in ants. It is probably used to open the salivarium, indicating that an active opening of this cavity is important in many ant species, but apparently not in all of them (see *Brachyponera*). More work is required to assess the precise functional background of this muscle and its potential phylogenetic significance.

The labrum of ants is an interesting character complex for different reasons. In most ants it forms different interlocking mechanisms with the maxillolabial complex, and various modifications have evolved with different functional backgrounds. The rectangular, bilobed shape found in generalist species investigated here is conserved in most groups (see also GOTWALD 1969). As this shape also occurs in outgroup taxa (e.g. the crabronid *Pison spinolae* Shuckard, 1837, COWLEY 1959), it is most likely a groundplan condition. The labrum of some of the trap-jaw ants of the myrmicine Attini underwent profound transformations to act as latch mechanism for their power amplified mandible strike (e.g. GRONENBERG 1996; BOLTON 1999). Interestingly, the modifications in *Strumigenys* F. Smith, 1860 and *Daceton* Perty, 1833 were considered as homologous when these genera were still assigned to the same tribe (e.g. BOLTON 2003). However, it is now known that *Strumigenys* is not closely related to the “dacetines” (WARD et al. 2015), and closer scrutiny revealed differences in the labral modifications (J. Katzke unpubl. observation), even within the genus *Strumigenys* (E. Economo unpubl. observation). Very diverse labral shapes have evolved in the *Basiceros* genus group (e.g. LONGINO & BOUDINOT 2013), closely related to *Strumigenys* (WARD et al. 2015). This has recently been investigated in detail for *Basiceros* (PROBST et al. 2019), revealing adaptations of the labrum for prey capture and a distinct phylogenetic signal in the character system within the genus. The authors discuss the possibility of a second pair of labral muscles (“anterior frontolabral muscle”) based on the presence of a second pair of tendons on the labrum (PROBST et al. 2019: fig. 2G), without presenting direct evidence. The presence of such a muscle appears highly unlikely considering its absence in all other ants and in fact Aculeata (ZIMMERMANN & VILHELMESEN 2016; RICHTER et al. 2019). This underlines the importance and potential of detailed anatomical documentation.

Some noteworthy differences of the epipharynx were observed in the present study. In most ants the membranous main part of this structure, i.e. the part not fused to the hypopharynx to form the prepharyngeal tube, is covered with rows of minute microtrichia (see *Formica*, *Wasmannia*, RICHTER et al. 2019). Additionally, the epipharynx of *Brachyponera* bears a band of much longer microtrichia that extends along the anterior margin of the functional mouth opening and expands into a more or less triangular patch around the epipharyngeal midline. The microtrichia of the preoral cavity are usually interpreted as part of a filter apparatus preventing solid particles from entering the digestive tract (e.g. EISNER & HAPP 1962; WANG et al. 2019). A varying vestiture might thus be associated with the preferred food, which is probably mainly arthropod prey in the case of species of *Brachyponera* (SCHMIDT & SHATTUCK 2014). It is noteworthy in this context that *B. luteipes* (ZHOU et al. 2007) and also *B. senaarensis* (DEJEAN & LACHAUD 1994) belong to the few ponerine species also feeding on seeds. However, whether the specific armature of microtrichia is related to the preferred diet, cannot be clarified with the currently available data. It is also important in this context that recent studies show that ponerine ants rely more on plant materials as food than was previously assumed (HANISCH et al. 2019). Therefore, possible correlations between structures involved in feeding and carnivorous habits should be carefully considered in each case.

4.5. Cephalic digestive tract, glands and nervous system

The prepharynx of ants (**pph**, Figs. 11C–H, 12A–D, 13A,B, 14A,D,E, S1G,H, S2A,B), previously interpreted as the pharynx (**ph**, Figs. 11C–H, 12A, 14B, S1G,H, S2C), was only recently correctly homologized (RICHTER et al. 2019). Many features of this part of the digestive tract have not been investigated in detail so far. The buccal tube (**bt**, Figs. 11D,E,G,H, 12A–D, S1G,H) has been considered as a distinctive prepharyngeal subunit based on a sharp bend separating it from the remaining prepharyngeal tube. This is more strongly pronounced in ants than in other groups of Aculeata, where the anteriormost part of the cephalic digestive tract is also more or less distinctly curved (ZIMMERMANN & VILHELMSSEN 2016). It is evident, however, that the sharp bend in ants is associated with the deep retraction of the maxillolabial complex, as it almost completely disappears when this structure is in a protracted position (see Fig. 12B,D). Comparisons with other aculeates that strongly retract the maxillolabial complex (e.g. Mutillidae, OSTEN 1982) could help to clarify whether this condition is unique to ants, or whether a sharp bend in the prepharynx is generally associated with strongly retracted ventral mouthparts.

Another prepharyngeal character complex is the sclerotization pattern. The sitophore plate, the sclerotized ventral (hypopharyngeal) ventral wall of the prepharynx

(Fig. 12A,B), is a groundplan apomorphy of Hymenoptera (VILHELMSSEN 1996; BEUTEL & VILHELMSSEN 2007). However, the epipharyngeal dorsal wall of the prepharynx also displays distinct sclerotized elements in ants, just posterior to the buccal tube. In *Wasmannia* this is a simple flat sclerite. In *Brachyponera* this structure additionally bears a sclerotized keel along its midline (**epk**, Figs. 11H, 12B, 14A,D). In *Formica* this area is rather weakly sclerotized and hump-shaped. In all three species this is the insertion area of a part of *M. clypeopalatalis* (Oci1) and also of the longitudinal pharyngo-epipharyngeal muscle, which is generally very large in Hymenoptera (BEUTEL & VILHELMSSEN 2007). Even though the presently available information is insufficient for a reliable evolutionary interpretation, this character system should be carefully considered in future studies. A possible explanation for the presence of a sclerotized keel in *Brachyponera* is the strong median constriction of the clypeus, which results in a very narrow *M. clypeopalatalis* (Oci1). The keel provides additional surface for the insertion of its fibers. The most diverse sclerotized prepharyngeal structures are the oral arms (**oa**, Figs. 1C,D,F, S1G,H). These hypopharyngeal sclerites stabilize the prepharynx and their posterior parts are insertion sites of the oral muscles 0hy1 and 0hy2. Additionally, these posterior parts of the arms enclose the opening of the pharyngeal gland, indicating that the oral muscles are likely involved in opening and closing the aperture of this gland (Verhaegen unpubl. observations). The distinct differences in the shape of these arms may contain phylogenetic signal and are potentially relevant in the context of dietary specializations. The only detailed comparative study on these structures by PORTO et al. (2019) was focused on Apoidea. The authors could demonstrate that some of the changes in the shape of the oral arms (pharyngeal rods in their terminology) and the general configuration of the hypopharynx are useful characters on higher and/or lower taxonomic levels (PORTO et al. 2019).

A character system not investigated by PORTO et al. (2019) but certainly of interest in ants is the prepharyngeal and pharyngeal musculature (Figs. 11 C–H, 13, 14). In addition to minor variations in shape and size of the individual muscles, some characters may have distinct functional implications and also contain phylogenetic signal. A seemingly unusual feature of ants is the subdivision of *M. clypeopalatalis* (Oci1) into an unpaired subcomponent inserting at the functional mouth opening (part a, retractor of buccal tube of PAUL et al. 2002) and one part inserting on the epipharyngeal sclerite discussed above (part b). In other groups of Aculeata, the anterior component was interpreted as Oci1 and no posterior part was described (ZIMMERMANN & VILHELMSSEN 2016). The only muscle inserting on the dorsal prepharyngeal wall described by these authors is *M. clypeobuccalis* (Obu1), which is sometimes subdivided into two individual bundles (ZIMMERMANN & VILHELMSSEN 2016). It is conceivable that these seemingly different configurations are rather due to homologization problems than to evolutionary changes in the character system. BEUTEL & VILHELMS-

SEN (2007) described *M. clypeopalatalis* (M. 43/ 0ci1) as consisting of two subunits in basal hymenopterans, compatible with the presence of two separate bundles in most insects (v. KÉLER 1963). This suggests that our interpretation of the anterior unpaired muscle and of the anterior paired bundle as two subunits of 0ci1, and the posterior paired bundle as 0bu1 is consistent with the general interpretation in the literature (e.g. BEUTEL et al. 2014). Another interesting case is *M. tentoriooralis* (0hy2). It was previously interpreted as a subunit of *M. frontooralis* (0hy1) by RICHTER et al. (2019), even though a possible interpretation as 0hy2 (M. 47) was discussed in that study. Our investigations show that the frontoclypeal ridge, which is the area of origin of this muscle in some other aculeate groups (ZIMMERMANN & VILHELSEN 2016), is very closely adjacent (*Formica*) or even fused (*Brachyponera*) to the antennal acetabulum, which also carries the torular apodeme serving as area of origin of the muscle in question in ants. Considering this configuration, a shift from the frontoclypeal ridge to the torular apodeme, consistent with a homologization as 0hy2, is much more likely, than a shift from the middle frontal region, which would be implied by a homologization with 0hy1. It is an interesting question whether the muscle shifted its origin first and the torular apodeme evolved after this to optimize the attachment site, or whether the muscle shifted to a preformed torular apodeme, which evolved for a different reason in the first place? Comparisons with other poneroid (e.g. Amblyoponinae) or more basal formicid lineages (e.g. Leptanillinae) plus closely related aculeate groups (e.g. Scoliidae and spheciform Apoidea) will likely help to clarify the functional and evolutionary background of the involved structural transformations. A muscle affected by size reduction or even complete loss is 0bu3. It is completely reduced in *Brachyponera* and very small in *Wasmannia* and other examined ponerines. In clear contrast, it is large and subdivided into two bundles in *Formica* and also in *Lasius* (JANET 1906), suggesting that this may be an apomorphy of Formicinae. The absence of *M. verticopharyngalis* (0ph1) is very likely an apomorphy of the entire Formicidae, as this muscle is usually present in Aculeata (ZIMMERMANN & VILHELSEN 2016), but has never been found in ants so far. One possible reason for this reduction is the prognathous condition, which results in a shift of different cephalic structures. The brain usually largely fills out the posterior lumen of the head, resulting in very limited space for dorsal pharyngeal muscles in this region.

Two large glands are associated with the prepharyngeal/pharyngeal sucking pump, the prepharyngeal and the pharyngeal gland. The shape of both may be phylogenetically relevant. The prepharyngeal gland almost entirely encloses the wall of the infrabuccal cavity, whereas most cells are located behind it in the myrmicine *Monomorium pharaonis* (Linnaeus, 1758) (BOONEN & BILLEN 2016), a condition also found in the myrmicine *Wasmannia affinis* (RICHTER et al. 2019). A placement of two gland cell clusters laterad the prepharynx and infrabuccal pouch was observed in *Formica* and also in *Camponotus*

pennsylvanicus (De Geer, 1773) (FORBES et al. 1961). For ponerine species only few descriptions of this gland are available, but it is apparently concentrated in the space between the buccal tube and the remaining prepharynx in different *Brachyponera* species (BILLEN & AL-KHALIFA 2015). Different shapes and positions of the gland are likely related to the spatial configuration of internal structures, for instance the extension of the infrabuccal pouch.

The pharyngeal gland also varies considerably in shape in different groups of ants. In most described species it appears “glove-like”, with several tubes connecting to a reservoir that opens near the anatomical mouth (e.g. FORBES 1938; PEREGRINE et al. 1973; BILLEN & AL-KHALIFA 2015; BILLEN et al. 2015; RICHTER et al. 2019). This also applies to *Formica*, where the gland is formed by more than 40 individual tubes. In clear contrast to this, the gland of *Brachyponera* (including *B. sennaarensis* BILLEN & AL-KHALIFA 2015) is sack-shaped, with about five more or less separated lobes instead of individual tubes. Additionally, the epithelial cells are more globular. As this general gland shape was also observed in other ponerine species (GAMA & CRUZ LANDIM 1981; SCHÖETTERS & BILLEN 1997) (also in Pseudomyrmecinae, GAMA & CRUZ LANDIM 1981), this is arguably a plesiomorphic condition for the group. The groundplan condition of ants is most likely the glove-shaped configuration, which was also found in leptanillines (BILLEN et al. 2013) and other groups of Aculeata (e.g. HERZNER et al. 2013). Further study may reveal additional phylogenetically informative differences.

Some features of the brain are very easy to correlate with the behavior and lifestyle of the two investigated species. The large optic neuropils are certainly linked with the importance of visual orientation for *F. rufa* (e.g. NICHOLSON et al. 1999). *Brachyponera* on the other hand has about ten times less ommatidia and seems less reliant on visual cues, showing distinctly reduced optic neuropils and lacking ocelli and ocellar nerves. Interestingly, the distinct anterior shift of the eye causes the optic nerve to run at a distinct angle through the fibers of 0md1. Due to the anterior placement of the eyes, fibers of this muscle can occupy regions that are occupied by the optic lobes and the compound eye in *Formica*. This suggests a possible tradeoff between the visual sense and additional space for attachment of mandibular muscle bundles. Another interesting aspect is the general size of the brain relative to the head volume. It is well known that relative brain size increases in smaller species in ants and other groups of organisms (e.g. WEHNER et al. 2007; SEID et al. 2011; LILICO-OUACHOUR et al. 2018). The brain of *Brachyponera* looks proportionally very large, occupying most of the posterior lumen of the head. This is even more pronounced than in *Wasmannia affinis* (RICHTER et al. 2019), which is even smaller, and thus obviously not only a result of miniaturization (POLILOV 2015). Even though specific neuroanatomical features of ants were already treated in several studies (e.g. KELBER et al. 2009; MCKENZIE et al. 2016), there is probably still potential in

comparing size and shape of the brain in different ant lineages. As the brain limits the space for other head structures, its shape is also influenced by the presence and extension of other organs (see optic nerve and Omd1). Comparative studies could reveal tradeoffs between the complexity of the brain and the mechanical efficiency of different functional elements of the head.

The tracheal configuration is apparently a highly conserved character system. The general branching pattern described here was also found in *Wasmannia affinis* (RICHTER et al. 2019), *Camponotus pennsylvanicus* (KEISTER 1963) and even in representatives of the basal hymenopteran family Xyelidae (BEUTEL & VILHELMSSEN 2007).

In summary, our morphological investigations revealed a broad spectrum of characters relevant in the context of the evolution of ant head structures. Some of them have received very little attention before, like the tentorium and other endoskeletal elements, or also the salivarium and associated structures. Another neglected character system is the cephalic digestive tract, with a broad spectrum of variation likely relevant in a functional and phylogenetic context. The mandibles and the labrum have already been investigated in some detail. Nevertheless, more structural information on these key elements of the head of ants will likely lead to a better understanding of important transformations in the evolution of the group.

5. Acknowledgements

Our very great thanks are due to Brendon Boudinot (UC Davis, Department of Entomology and Nematology) for providing a very thorough and detailed review within very short time. This helped greatly to improve our study. Many helpful comments made by the editor in chief Dr. Klaus-Dieter Klass (Senckenberg Museum für Tierkunde Dresden) are also gratefully acknowledged. We also thank the OIST Imaging Section for providing access to the SEM and μ CT scanner, especially Sasaki Toshiaki who helped with sample preparation and explained the SEM facilities, and Komoto Shinya for general support with the μ CT scanner. We are grateful to An Vandoren for making the serial histological sections. We also thank Chung-Chi Lin for collecting the Taiwanese *Brachyponera* workers for histological examination and Thomas Parmentier for providing specimens of *Formica rufa*, and the Agentschap voor Natuur en Bos (Agency of Nature and Forest) for granting him permission to collect these insects. We are also thankful to James Trager for his terminological advice. This work was funded by subsidy funding to OIST, and Adrian Richter is grateful for a scholarship of the Evangelisches Studienwerk Villigst e.V.

6. References

- BALL G.E., ACORN J.H., SHPELEY D. 2011. Mandibles and labrum-epipharynx of tiger beetles: basic structure and evolution (Coleoptera, Carabidae, Cicindelidae). – *ZooKeys* **147**: 39–83.
- BARANEK B., KUBA K., BAUDER J., KRENN H. 2018. Mouthpart dimorphism in male and female wasps of *Vespula vulgaris* and *Vespula germanica* (Vespidae, Hymenoptera). – *Deutsche Entomologische Zeitschrift* **65**(1): 65–74.
- BARONI URBANI C.B., BOLTON B., WARD P.S. 1992. The internal phylogeny of ants (Hymenoptera: Formicidae). – *Systematic Entomology* **17**(4): 301–329.
- BARDEN P., GRIMALDI D. A. 2016. Adaptive radiation in socially advanced stem-group ants from the Cretaceous. – *Current Biology* **26**(4): 515–521.
- BEUTEL R.G. 1997. Über Phylogenese und Evolution der Coleoptera, insbesondere der Adephaga. – *Verhandlungen des Naturwissenschaftlichen Vereins in Hamburg NF* **31**: 1–164.
- BEUTEL R.G., FRIEDRICH F., YANG X.-K., GE S.-Q. 2014. *Insect Morphology and Phylogeny: a Textbook for Students of Entomology*. – Walter de Gruyter, Berlin.
- BEUTEL R.G., VILHELMSSEN L. 2007. Head anatomy of Xyelidae (Hemiptera: Hymenoptera) and phylogenetic implications. – *Organisms Diversity & Evolution* **7**(3): 207–230.
- BILLEN J. 1993. Morphology of the exocrine system in ants. – *Proceedings of the colloquia on social insects* 1–15. – *Socium* St. Petersburg.
- BILLEN J., AL-KHALIFA M. S. 2015. Morphology and ultrastructure of the pro- and postpharyngeal glands in workers of *Brachyponera senaarensis*. – *Sociobiology* **62**(2): 270–275.
- BILLEN J., AL-KHALIFA M. 2016. A novel intramandibular gland in the ant *Brachyponera senaarensis*. – *Insectes Sociaux* **63**(2): 321–326.
- BILLEN J., BAUWELEERS E., HASHIM R., ITO F. 2013. Survey of the exocrine system in *Protanilla wallacei* (Hymenoptera, Formicidae). – *Arthropod Structure & Development* **42**(3): 173–183.
- BILLEN J., MANDONX T., HASHIM R., ITO F. 2015. Exocrine glands of the ant *Myrmoteris iriodum*. – *Entomological Science* **18**(2): 167–173.
- BOLTON B. 1999. Ant genera of the tribe Dacetoniini (Hymenoptera: Formicidae). – *Journal of Natural History* **33**(11): 1639–1689.
- BOLTON B. 2003. Synopsis and classification of Formicidae. – *Memoirs of the American Entomological Institute* **71**: 1–370.
- BOONEN S., BILLEN J. 2016. Functional morphology of the maxillary and propharyngeal glands of *Monomorium pharaonis* (L.). – *Arthropod Structure & Development* **45**(4): 325–332.
- BOROWIEC M.L., RABELING C., BRADY S.G., FISHER B.L., SCHULTZ T.R., WARD P.S. 2019. Compositional heterogeneity and outgroup choice influence the internal phylogeny of the ants. – *Molecular Phylogenetics and Evolution* **134**: 111–121.
- BOUDINOT B. 2013. The male genitalia of ants: musculature, homology, and functional morphology (Hymenoptera, Aculeata, Formicidae). – *Journal of Hymenoptera Research* **30**: 29–49. doi: 10.3897/jhr.30.3535
- BOUDINOT B.E. 2015. Contributions to the knowledge of Formicidae (Hymenoptera, Aculeata): a new diagnosis of the family, the first global male-based key to subfamilies, and a treatment of early branching lineages. – *European Journal of Taxonomy* **120**: 1–62.
- BRANSTETTER M.G., LONGINO J.T., WARD P.S., FAIRCLOTH B.C. 2017. Enriching the ant tree of life: enhanced UCE bait set for genome-scale phylogenetics of ants and other Hymenoptera. – *Methods in Ecology and Evolution* **8**(6): 768–776.
- BROWN W.L. 1948. A preliminary generic revision of the higher Dacetini (Hymenoptera: Formicidae). – *Transactions of the American Entomological Society* (1890) **74**(2): 101–129.
- CAO H.J., PERRICHOT V., SHIH C., REN D., GAO T.P. 2020. A revision of *Haidomyrmex cerberus* Dlussky (Hymenoptera: Formicidae: Sphecomyrminae) from mid-Cretaceous Burmese amber. – *Cretaceous Research* **106**: 104226.
- CONTRERAS-RAMOS A. 2011. Phylogenetic review of dobsonflies of the subfamily Corydalinae and the genus *Corydalus* Latreille (Megaloptera: Corydalidae). – *Zootaxa* **2862**: 1–38.
- COWLEY D.R. 1959. Studies on the biology and anatomy of *Pison spinolae* Shuckard (Hymenoptera, Sphecidae). – M.Sc. Thesis, Auckland University, New Zealand.
- DÉJEAN A., LACHAUD J.-P. 1994. Ecology and behavior of the seed-eating ponerine ant *Brachyponera senaarensis* (Mayr). – *Insectes Sociaux* **41**(2): 191–210.

- DOMISCH T., FINER L., NEUVONEN S., NIEMELÄ P., RISCH A.C., KILPELÄINEN J., OHASHI M., JURGENSEN M.F. 2009. Foraging activity and dietary spectrum of wood ants (*Formica rufa* group) and their role in nutrient fluxes in boreal forests. – *Ecological Entomology* **34**(3): 369–377.
- EGUCHI K. 2006. Six new species of *Pheidole* Westwood from north Vietnam (Hymenoptera, Formicidae). – *Revue Suisse de Zoologie* **113**(1): 115–132.
- EHMER B., GRONENBERG W. 1997. Proprioceptors and fast antennal reflexes in the ant *Odontomachus* (Formicidae, Ponerinae). – *Cell and Tissue Research* **290**(1): 153–165.
- EISNER T., HAPP G. 1962. The infrabuccal pocket of a formicine ant: a social filtration device. – *Psyche* **69**(3): 107–116.
- ENGELKES K., FRIEDRICH F., HAMMEL J.U., HAAS A. 2018. A simple setup for episcopic microtomy and a digital image processing workflow to acquire high-quality volume data and 3D surface models of small vertebrates. – *Zoomorphology* **137**(1): 213–228.
- EVANS M. 1994. The carabid body plan: a functional interpretation. – *Carabid Beetles: Ecology and Evolution* 25–31. – Springer.
- FEBVAY G., KERMARREC A. 1981. Morphologie et fonctionnement du filtre infrabuccal chez une attine *Acromyrmex octospinosus* (Reich) (Hymenoptera: Formicidae): rôle de la poche infrabuccale. – *International Journal of Insect Morphology and Embryology* **10**(5–6): 441–449.
- FORBES J. 1938. Anatomy and histology of the worker of *Camponotus herculeanus pennsylvanicus* De Geer (Formicidae, Hymenoptera). – *Annals of the Entomological Society of America* **31**(2): 181–195.
- FORBES J., MCFARLANE A.M. 1961. The comparative anatomy of digestive glands in the female castes and the male of *Camponotus pennsylvanicus* De Geer (Formicidae, Hymenoptera). – *Journal of the New York Entomological Society* **69**(2): 92–103.
- FRIEDMAN N.R., BENNET B.L., FISCHER G., SARNAT E.M., HUANG J.-P., KNOWLES L.L., ECONOMO E.P. 2019. Macroevolutionary integration of phenotypes within and across ant worker castes. – bioRxiv: 604470.
- FRIEDRICH F., MATSUMURA Y., POHL H., BAI M., HÖRNSCHEMEYER T., BEUTEL R.G. 2014. Insect morphology in the age of phylogenomics: innovative techniques and its future role in systematics. – *Entomological Science* **17**(1): 1–24.
- GAMA V., DA CRUZ LANDIM C. 1982. Estudo comparativo das glândulas do sistema salivar de formigas (Hymenoptera, Formicidae). – *Naturalia* (São José do Rio Preto) **7**: 145–165.
- GOTWALD W.H. 1969. Comparative morphological studies of the ants: with particular reference to the mouthparts (Hymenoptera: Formicidae). – *Memoirs of the Cornell University Agricultural Experiment Station No.* **408**: 1–150.
- GRONENBERG W. 1996. The trap-jaw mechanism in the dacetine ants *Daceton armigerum* and *Strumigenys* sp. – *Journal of Experimental Biology* **199**(9): 2021–2033.
- GRONENBERG W., PAUL J., JUST S., HÖLDOBLER B. 1997. Mandible muscle fibers in ants: fast or powerful? – *Cell and Tissue Research* **289**(2): 347–361.
- GUÉNARD B., DUNN R.R. 2010. A new (old), invasive ant in the hardwood forests of eastern north America and its potentially widespread impacts. – *PLoS One* **5**: e11614.
- GUTIERREZ Y., OTT D., TOPPERWIEN M., SALDITT T., SCHERBER C. 2018. X-ray computed tomography and its potential in ecological research: A review of studies and optimization of specimen preparation. – *Ecology and Evolution* **8**(15): 7717–7732.
- HANISCH P.E., DRAGER K., YANG W.H., TUBARO P.L., SUAREZ A.V. 2019. Intra- and interspecific variation in trophic ecology of ‘predatory’ ants in the subfamily Ponerinae. – *Ecological Entomology*.
- HASHIMOTO Y. 1990. Unique features of sensilla on the antennae of Formicidae (Hymenoptera). – *Applied Entomology and Zoology* **25**(4): 491–501.
- HASHIMOTO Y. 1991. Phylogenetic study of the family Formicidae based on the sensillum structures on the antennae and labial palpi (Hymenoptera, Aculeata). – *Japanese Journal of Entomology* **59**(1): 125–140.
- HERMANN H.R., HUNT A.N., BUREN W.F. 1971. Mandibular gland and mandibular groove in *Polistes annularis* (L.) and *Vespula maculata* (L.) (Hymenoptera: Vespidae). – *International Journal of Insect Morphology and Embryology* **1**(1): 43–49.
- HERZNER G., KALTENPOTH M., POETTINGER T., WEISS K., KOEDAM D., KROISS J., STROHM E. 2013. Morphology, chemistry and function of the postpharyngeal gland in the south american digger wasps *Trachypus boharti* and *Trachypus elongatus*. – *PLoS One* **8**: e82780.
- JANET C. 1906. Anatomie de la tête du *Lasius niger*. – Imprimerie-Librairie Ducourtieux et Gout, Limoges, Paris.
- JANET C. 1923. Revendications à propos de ses dessins de zoologie empruntés par d’autres auteurs: Limoges: Imprimerie et Librairie Limousines Ducourtieux.
- KEISTER M. 1963. The anatomy of the tracheal system of *Camponotus pennsylvanicus* (Hymenoptera: Formicidae). – *Annals of the Entomological Society of America* **56**(3): 336–340.
- KELBER C., ROSSLER W., ROCES F., KLEINEIDAM C.J. 2009. The antennal lobes of fungus-growing ants (Attini): neuroanatomical traits and evolutionary trends. – *Brain, Behavior and Evolution* **73**(4): 273–284.
- V. KÉLER S. 1963. Entomologisches Wörterbuch. – Akademie Verlag, Berlin.
- KELLER R.A. 2011. A phylogenetic analysis of ant morphology (Hymenoptera: Formicidae) with special reference to the poneromorph subfamilies. – *Bulletin of the American Museum of Natural History* **355**: 1–90.
- KELLER R.A., PEETERS C., BELDADE P. 2014. Evolution of thorax architecture in ant castes highlights trade-off between flight and ground behaviors. – *Elife* **3**, e01539.
- KHALIFE A., KELLER R.A., BILLEN J., HITA GARCIA F., ECONOMO E.P., PEETERS C. 2018. Skeletomuscular adaptations of head and legs of *Melissotarsus* ants for tunnelling through living wood. – *Frontiers in Zoology* **15**(1): 30.
- KRENN H.W., MAUSS V., PLANT J. 2002. Evolution of the suctorial proboscis in pollen wasps (Masarinae, Vespidae). – *Arthropod Structure & Development* **31**(2): 103–120.
- KUBOTA H., YOSHIMURA J., NIITSU S., SHIMIZU A. 2019. Morphology of the tentorium in the ant genus *Lasius* Fabricius (Hymenoptera: Formicidae). – *Scientific Reports* **9**(1): 6722.
- LACH L., PARR C., ABBOTT K. 2010. *Ant Ecology*. – Oxford University Press, Oxford.
- LARABEE F.J., SUAREZ A.V. 2014. The evolution and functional morphology of trap-jaw ants (Hymenoptera: Formicidae). – *Myrmecological News* **20**: 25–36.
- LATTKE J., DELSINNE T., ALPERT G., GUERRERO R. 2018. Ants of the genus *Protalaridris* (Hymenoptera: Formicidae), more than just deadly mandibles. – *European Journal of Entomology* **115**(1): 268–295.
- LENOIR A. 1982. An informational analysis of antennal communication during trophallaxis in the ant *Myrmica rubra* L. – *Behavioural Processes* **7**(1): 27–35.
- LILICO-OUACHOUR A., METSCHER B., KAJI T., ABOUHEIF E. 2018. Internal head morphology of minor workers and soldiers in the hyperdiverse ant genus *Pheidole*. – *Canadian Journal of Zoology* **96**(5): 383–392.
- LIU S.-P., RICHTER A., STOESSEL A., BEUTEL R.G. 2019. The mesosomal anatomy of *Myrmecia nigrocincta* workers and evolutionary transformations in Formicidae (Hymenoptera). – *Arthropod Systematics and Phylogeny* **77**(1): 1–19.
- LONGINO J.T. 2006. A taxonomic review of the genus *Myrmelachista* (Hymenoptera: Formicidae) in Costa Rica. – *Zootaxa* **1141**: 1–54.
- LONGINO J.T., BOUDINOT B.E. 2013. New species of Central American *Rhopalothrix* Mayr, 1870 (Hymenoptera, Formicidae). – *Zootaxa* **3616**: 301–324.
- LÖSEL P., HEUVELINE V. 2016. Enhancing a diffusion algorithm for 4D image segmentation using local information. – *SPiE Medi-*

- cal Imaging, International Society for Optics and Photonics 97842L – 97842L.
- LUBBOCK J. 1877. On some points in the anatomy of ants. – *Journal of Microscopy* **18**(3): 120–142.
- LUCKY A., TRAUTWEIN M.D., GUENARD B.S., WEISER M.D., DUNN R.R. 2013. Tracing the rise of ants-out of the ground. – *PLoS One* **8**: e84012.
- LUCKY A., WARD P.S. 2010. Taxonomic revision of the ant genus *Leptomyrme* Mayr (Hymenoptera: Formicidae). – *Zootaxa* **2688**: 1–67.
- McKENZIE S.K., FETTER-PRUNEDA I., RUTA V., KRONAUER D.J. 2016. Transcriptomics and neuroanatomy of the clonal raider ant implicate an expanded clade of odorant receptors in chemical communication. – *Proceedings of the National Academy of Sciences* **113**(49): 14091–14096.
- MO Y. 2013. Temporal Food Preference and Effectiveness of Selected Bait Products against *Pachycondyla chinensis* (Emery) (Hymenoptera: Formicidae). – *Tigerprints All Theses*.
- NGUYEN V., LILLY B., CASTRO C. 2014. The exoskeletal structure and tensile loading behavior of an ant neck joint. – *Journal of Biomechanics* **47**(2): 497–504.
- NICHOLSON D., JUDD S., CARTWRIGHT B., COLLETT T. 1999. Learning walks and landmark guidance in wood ants (*Formica rufa*). – *Journal of Experimental Biology* **202**(13): 1831–1838.
- OSTEN T. 1982. Vergleichend-funktionsmorphologische Untersuchungen der Kopfkapsel und der Mundwerkzeuge ausgewählter „Scolioidea“ (Hymenoptera, Aculeata): mit 2 Tabellen. – *Stuttgarter Beiträge zur Naturkunde A (Biologie)* **354**: 1–60.
- OSTEN T. 1988. Die Mundwerkzeuge von *Proscolia spectator* Day (Hymenoptera: Aculeata): ein Beitrag zur Phylogenie der „Scolioidea“. – *Stuttgarter Beiträge zur Naturkunde A (Biologie)* **411**: 1–30.
- PAUL J. 2001. Mandible movements in ants. – *Comparative Biochemistry and Physiology Part A: Molecular & Integrative Physiology* **131**(1): 7–20.
- PAUL J., GRONENBERG W. 1999. Optimizing force and velocity: mandible muscle fibre attachments in ants. – *Journal of Experimental Biology* **202**(7): 797–808.
- PAUL J., ROCES F. 2019. Comparative Functional Morphology of Ant Mouthparts and Significance for Liquid Food Intake. Pp. 335–359 in Krenn, H.W. *Insect Mouthparts* – Springer, Berlin. 683 pp.
- PAUL J., ROCES F., HÖLDOBLER B. 2002. How do ants stick out their tongues? – *Journal of Morphology* **254**(1): 39–52.
- PENAGOS-ARÉVALO A.C., BILLEN J., SARMIENTO C.E. 2015. Uncovering head gland diversity in neotropical Polistinae wasps (Hymenoptera, Vespidae): comparative analysis and description of new glands. – *Arthropod Structure & Development* **44**(5): 415–425.
- PEREGRINE D., MUDD A., CHERRETT J. 1973. Anatomy and preliminary chemical analysis of the post-pharyngeal glands of the leaf-cutting ant, *Acromyrmex octospinosus* (Reich.) (Hym., Formicidae). – *Insectes Sociaux* **20**(4): 355–363.
- POHL H. 2010. A scanning electron microscopy specimen holder for viewing different angles of a single specimen. – *Microscopy Research and Technique* **73**(12): 1073–1076.
- POLILOV A.A. 2015. Small is beautiful: features of the smallest insects and limits to miniaturization. – *Annual Review of Entomology* **60**: 103–121.
- POPOVICI O., MIKO I., SELTMANN K., DEANS A. 2014. The maxillo-labial complex of *Sparasion* (Hymenoptera, Platygastridae). – *Journal of Hymenoptera Research* **37**: 77–111.
- PORTO D.S., ALMEIDA E.A. 2019. A comparative study of the pharyngeal plate of Apoidea (Hymenoptera: Aculeata), with implications for the understanding of phylogenetic relationships of bees. – *Arthropod Structure & Development* **50**: 64–77.
- PRENTICE M.A. 1998. The Comparative Morphology and Phylogeny of Apoid Wasps (Hymenoptera: Apoidea). – PhD Thesis University of California, Berkeley.
- PROBST R.S., WRAY B.D., MOREAU C.S., BRANDÃO C.R. 2019. A phylogenetic analysis of the dirt ants, *Basicros* (Formicidae: Myrmicinae): Inferring life histories through morphological convergence. – *Insect Systematics and Diversity* **3**(4): 1–12.
- QUINLAN R., CHERRETT J. 1978. Studies on the role of the infrabuccal pocket of the leaf-cutting ant *Acromyrmex octospinosus* (Reich.) (Hym., Formicidae). – *Insectes Sociaux* **25**(3): 237–245.
- RABELING C., BROWN J.M., VERHAAGH M. 2008. Newly discovered sister lineage sheds light on early ant evolution. – *Proceedings of the National Academy of Sciences* **105**(39): 14913–14917.
- RICHTER A., KELLER R.A., ROSUMEK F.B., ECONOMO E.P., HITA GARCIA F., BEUTEL R.G. 2019. The cephalic anatomy of workers of the ant species *Wasmannia affinis* (Formicidae, Hymenoptera, Insecta) and its evolutionary implications. – *Arthropod Structure & Development* **49**: 26–49.
- SCHMIDT C. A., SHATTUCK S.O. 2014. The higher classification of the ant subfamily ponerinae (Hymenoptera: Formicidae), with a review of ponerine ecology and behavior. – *Zootaxa* **3817**: 1–242.
- SCHOETERS E., BILLEN J. 1997. The post-pharyngeal gland in *Dinoponera* ants (Hymenoptera: Formicidae): unusual morphology and changes during the secretory process. – *International Journal of Insect Morphology and Embryology* **25**(4): 443–447.
- SEID M.A., CASTILLO A., WCISLO W.T. 2011. The allometry of brain miniaturization in ants. – *Brain, Behavior and Evolution* **77**(1): 5–13.
- SELTMANN K.C., YODER M., MIKO I., FORSHAGE M., BERTONE M., AGOSTI D., AUSTIN A., BALHOFF J., BOROWIEC M., BRADY S., BROAD G.R., BROTHERS D.J., BURKS R.A., BUFFINGTON M.L., CAMPBELL H., DEW K., ERNST A., FERNANDEZ-TRIANA J., GATES M.W., GIBSON G., JENNINGS J.T., JOHNSON N.F., KARLSSON D., KAWADA R., KROGMANN L., KULA R., MULLINS P.L., OHL M., RASMUSSEN C., RONQUIST F., SCHULMEISTER S., SHARKEY M., TALAMAS E.J., TUCKER E., VILHELMSSEN L., WARD P.S., WHARTON R., DEANS A.R. 2012. A hymenopterists' guide to the Hymenoptera Anatomy Ontology: utility, clarification, and future directions. – *Journal of Hymenoptera Research* **27**: 67–88.
- SIDDIQUI M. I., MASHALY A.M., AHMED A.M., AL-MEKHLAFI F.A., AL-KHALIFA M.S. 2010. Ultrastructure of antennal sensillae of the samsum ant, *Pachycondyla sennaarensis* (Hymenoptera: Formicidae). – *African Journal of Biotechnology* **9**(41): 6956–6962.
- SILVA T.S.R., FEITOSA R.M. 2019. Using controlled vocabularies in anatomical terminology: A case study with *Strumigenys* (Hymenoptera: Formicidae). – *Arthropod Structure & Development* **52**: 100877.
- SNODGRASS R.E. 1935. *Principles of Insect Morphology*. – McGraw-Hill, New York.
- SOMBKE A., LIPKE E., MICHALIK P., UHL G., HARZSCH S. 2015. Potential and limitations of X-Ray micro-computed tomography in arthropod neuroanatomy: A methodological and comparative survey. – *Journal of Comparative Neurology* **523**(8): 1281–1295.
- VILHELMSSEN L. 1996. The preoral cavity of lower Hymenoptera (Insecta): comparative morphology and phylogenetic significance. – *Zoologica Scripta* **25**(2): 143–170.
- VOGT L. 2019. Organizing phenotypic data—a semantic data model for anatomy. – *Journal of Biomedical Semantics* **10**(1): 12.
- WALTHER J.R. 1979. Morphologie und Feinstruktur der Sinnesorgane auf den Geisselantennen von *Formica rufa* L. (Hymenoptera, Formicidae). – *Verhandlungen der Deutschen Zoologischen Gesellschaft* **72**: 313.
- WANG C., BILLEN J., WEI C., HE H. 2019. Morphology and ultrastructure of the infrabuccal pocket in *Camponotus japonicus* Mayr (Hymenoptera: Formicidae). – *Insectes Sociaux* **66**(4): 637–646.
- WARD P.S., BRADY S.G., FISHER B.L., SCHULTZ T.R. 2015. The evolution of myrmicine ants: phylogeny and biogeography of a hyperdiverse ant clade (Hymenoptera: Formicidae). – *Systematic Entomology* **40**(1): 61–81.
- WEHNER R., FUKUSHI T., ISLER K. 2007. On being small: brain allometry in ants. – *Brain, Behavior and Evolution* **69**(3): 220–228.
- WIPFLER B., MACHIDA R., MÜLLER B., BEUTEL R.G. 2011. On the head morphology of Grylloblattodea (Insecta) and the systematic position of the order, with a new nomenclature for the head muscles of Dicondylia. – *Systematic Entomology* **36**(2): 241–266.
- WIPFLER B., POHL H., YAVORSKAYA M.I., BEUTEL R.G. 2016. A review of methods for analysing insect structures – the role of morphology in the age of phylogenomics. – *Current Opinion in Insect Science* **18**: 60–68.

- YAMADA A., NGUYEN D.D., EGUCHI K. 2020. Unveiling the morphology of the Oriental rare monotypic ant genus *Opamyrra* Yamane, Bui & Eguchi, 2008 (Hymenoptera: Formicidae: Leptanillinae) and its evolutionary implications, with first descriptions of the male, larva, tentorium, and sting apparatus. – *Myrmecological News* **30**:27–52.
- YODER M.J., MIKÓ I., SELTMANN K.C., BERTONE M.A., DEANS A.R. 2010. A gross anatomy ontology for Hymenoptera. – *PLoS One* **5**: e15991.
- ZHOU H., CHEN J., CHEN F. 2007. Ant-mediated seed dispersal contributes to the local spatial pattern and genetic structure of *Globba lancangensis* (Zingiberaceae). – *Journal of Heredity* **98**(4): 317–324.
- ZIMMERMANN D., VILHELMSSEN L. 2016. The sister group of Aculeata (Hymenoptera) – evidence from internal head anatomy, with emphasis on the tentorium. – *Arthropod Systematics & Phylogeny* **74**(2): 195–218.

Electronic Supplement Files

at <http://www.senckenberg.de/arthropod-systematics>

ASP_78-1_Richter_Electronic_Supplements.zip

DOI: 10.26049/ASP78-1-2020-06/1

File 1: richter&al-formicidaehead-asp2020-electronicsupplement-1.pdf. — **Fig. S1:** Volume renderings of heads of *F. rufa* (CASENT0790267: **A,C–E,G**) and *B. luteipes* (CASENT0709409: **B,F,H**). **A,B:** ventral view of the head capsule, cut open to reveal the dorsal endoskeleton and the insertions of the dorsal head muscles. **C:** posterior view, showing the functionless muscle X. **D:** lateral view of the anterior head, showing the connection of the stipito-premental conjunctivum with the maxilla and hypopharynx/infrabuccal pouch. **E,F:** lateral view of the anterior head, showing the interaction of the labrum with the maxillo-labial complex. **G,H:** lateral view of anterior cephalic digestive tract, showing the oral arms. — **Abbreviations:** **Obu1** – *M. clypeobuccalis*; **Obu2** – *M. frontobuccalis anterior*; **Obu3** – *M. frontobuccalis posterior*; **Oci1a** – *M. clypeopalatalis*, unpaired portion; **Oci1b** – *M. clypeopalatalis*, paired portion; **Ohy1** – *M. frontooralis*; **Ohy2** – *M. tentoriooralis*; **Olb2** – *M. frontoepipharyngalis*; **Omd1** – *M. craniomandibularis externus*; **Omx1** – *M. craniocardinalis externus*; **Omx3** – *M. tentoriocardinalis*; **Omx4** – *M. tentoriostipitalis anterior*; **ant** – antennifer; **bt** – buccal tube; **cd** – cardo; **epk** – epipharyngeal keel; **esr** – epistomal ridge; **ga** – galea; **lc** – lacinia; **Ibp** – infrabuccal pouch; **lbr** – labrum; **lbrp** – labral process; **MX** – functionless muscle X; **mxx** – maxillary gland; **oa** – oral arm; **ph** – pharynx; **pmx** – palpus maxillaris; **pph** – prepharynx; **spc** – stipito-premental conjunctivum; **st** – stipes — **Colors:** **beige/ brown** – mouthparts; **green** – cephalic digestive tract (prepharynx and pharynx); **grey** – cuticle; **orange/ red** – muscles; **purple** – glands. — **Fig. S2:** Histological sections of heads of *F. rufa* (**A–E**) *B. luteipes* (**F,H**) and *B. chinensis* (**G**). All sections transverse. **A:** Section at the level of the maxillo-labial complex showing especially the interaction of the stipes with the hypostomal triangular process. **B:** Section on the level of the pharyngeal gland opening. **C:** Section on the level of the eyes, showing the Y-shaped pharynx. **D,E:** Sections showing the stipito-premental-conjunctivum, D further posterior than E. **F:** Section at the level of the posterior brain, showing the tiny dorsal tentorial arm. **G,H:** Section at the level of the anterior mouthparts, showing the mandibular pit gland. — **Abbreviations:** **ata** – anterior tentorial arm; **dhy** – distal hypopharynx; **dta** – dorsal tentorial arm; **hyr** – hypopharyngeal rod; **ibp** – infrabuccal pouch; **lcs** – lacinial sclerite; **md** – mandible; **mdp** – mandibular pit; **mdpg** – mandibular pit gland; **oa** – oral arm; **ph** – pharynx; **phg** – pharyngeal gland; **phgo** – pharyngeal gland opening; **pph** – prepharynx; **pma** – premental arm; **spc** – stipito-premental conjunctivum; **stis** – stipes internal sclerite; **svd** – salivary duct; — **Symbols:** **white arrow-head** – interaction of lateral stipes with anterior concavity of hypopharyngeal triangular process.

File 2: richter&al-formicidaehead-asp2020-electronicsupplement-2.xlsx. — Volume measurements.

File 3: richter&al-formicidaehead-asp2020-electronicsupplement-3.docx. — **Table S1:** Comparison of morphological features between *B. luteipes*, *F. rufa* and *W. affinis*, data on the latter are based on RICHTER et al. (2019).

Authors' contributions

A. Richter, F. Hita Garcia, R.A. Keller, E.P. Economo and R. G. Beutel conceptualized and designed the study. A. Richter and F. Hita Garcia generated the μ CT scans; A. Richter did the 3D reconstructions, SEM images, photographs, assembled the figure plates and wrote the first draft of the manuscript. J. Billen provided the histological series and contributed important details on histological features. All authors commented on the manuscript and reviewed it together to arrive at the final version.